ผลกระทบของหน่วยแรงแบบแอนไอโซโทรปิกต่อค่าโมดูลัสเฉือนที่ความเครียดระดับต่ำของทรายโดยใช้เบนเดอร์อิลิเมนต์

นายอลิทคิง อนงค์พุท

วิทยานิพนธ์นี้เป็นส่วนหนึ่งของการศึกษาตามหลักสูตรปริญญาวิศวกรรมศาสตรมหาบัณฑิต
สาขาวิชาวิศวกรรมโยธา ภาควิชาวิศวกรรมโยธา
คณะวิศวกรรมศาสตร์ จุฬาลงกรณ์มหาวิทยาลัย
ปีการศึกษา 2549
ISBN 974-14-3511-8

EFFECT OF STRESS–INDUCED ANISOTROPY ON ELASTIC SHEAR MODULUS OF SANDS USING BENDER ELEMENTS

Mr. Alitking Anongphouth

A Thesis Submitted in Partial Fulfillment of the Requirements
for the Degree of Master of Engineering Program in Civil Engineering
Department of Civil Engineering
Faculty of Engineering
Chulalongkorn University
Academic Year 2006
ISBN: 974-14-3511-8

Thesis Title	EFFECT OF STRESS-INDUCED ANISOTROPY ON ELASTIS SHEAR MODULUS OF SANDS USING BENDER ELEMENTS
By	Mr. Alitking Anongphouth
Field of Study	Civil Engineering
Thesis Advisor	Associate Professor Supot Teachavorasinskun, D.Eng

---

Accepted by the Faculty of Engineering, Chulalongkorn University in Partial Fulfillment of the Requirements for the Master's Degree

.....Dean of the Faculty of Engineering
(Professor Direk Lavansiri, Ph.D.)

THESIS COMMITTEE

..... Chairman
(Assistant Professor Thavee Thanacharoengit, Dr.Ing)

..... Thesis Advisor
(Associate Professor Supot Teachavorasinskun, D.Eng)

..... Member
(Assistant Professor Tirawat Boonyatee, D.Eng)

..... Member
(Suched Likitlersuang, D. Phil.)

Alitking Anongphouth: ผลกระทบของหน่วยแรงแบบแอนไอโซโทรปิกต่อค่าโมดูลัสเฉือนที่ความเครียดระดับต่ำของทรายโดยใช้เบนเดอร์อิลิเมนต์ (Effect of Stress-induced Anisotropy on Elastic Shear Modulus of Sands using Bender Elements) อาจารย์ที่ปรึกษา: รศ.ดร.สุพจน์ เตชวรสินสกุล 88 หน้า ISBN 974-14-3511-8.

โมดูลัสเฉือนของดินที่ความเครียดระดับต่ำๆ มีความสำคัญเป็นอย่างยิ่งในทางวิศวกรรมปฐพี โดยเฉพาะในการวิเคราะห์ทางด้านพลศาสตร์ของดินและพฤติกรรมของดินที่ความเครียดระดับต่ำๆ ดังนั้นในงานวิจัยนี้จึงมีวัตถุประสงค์ที่จะศึกษาผลกระทบของหน่วยแรงแบบไอโซโทรปิกที่มีต่อค่าโมดูลัสเฉือนโดยวิธีการตรวจวัดด้วยเบนเดอร์อิลิเมนต์ การทดสอบกระทำในเครื่องมือทดสอบแรงอัดสามแกนที่ได้ติดตั้งเบนเดอร์อิลิเมนต์ที่แท่นบนและฐานวางตัวอย่างดินและคำนวณค่าโมดูลัสเฉือนจากวัดเวลาการเดินทางของคลื่นแรงเฉือนที่ส่งผ่านตัวอย่างดินโดยเบนเดอร์อิลิเมนต์ ตัวอย่างทรายที่นำมาทดสอบประกอบด้วย 2 ชนิด คือ ตัวอย่างทรายหลวมและแน่นที่ได้จากการเตรียมโดยวิธี Air-Pluviation และการวัดคลื่นแรงเฉือนจะกระทำในช่วงการบีบอัดตัวคายน้ำแบบไอโซโทรปิก แบบแอนไอโซโทรปิก และในช่วงการเฉือนตัวอย่างดินแบบระบายน้ำ จากการศึกษาพบว่า โดยส่วนใหญ่ค่าโมดูลัสเฉือนของทรายมักขึ้นอยู่กับหน่วยแรงประสิทธิผลเฉลี่ยและอัตราส่วนช่องว่าง นอกจากนั้นยังพบว่าค่าโมดูลัสเฉือนที่ได้จากผลการทดลองแบบไอโซโทรปิกและแอนไอโซโทรปิกมีค่าแตกต่างกันเพียงเล็กน้อย นั่นหมายความว่าผลกระทบจากแรงแบบแอนไอโซโทรปิกมีน้อย เส้นทางการเคลื่อนที่ของ $G_{max} - p'$ ในช่วงการเฉือนตัวอย่างดินแบบระบายน้ำมีแนวโน้มคล้ายกันช่วงการบีบอัดตัวคายน้ำ ด้วยเหตุนี้จึงสามารถสรุปได้ว่าหน่วยแรงประสิทธิผลเฉลี่ยมีอิทธิพลอย่างมากต่อค่าโมดูลัสเฉือนของดิน แต่ในทางตรงกันข้ามหน่วยแรงเฉือนกลับมีผลกระทบต่อค่าโมดูลัสเฉือนน้อย จากผลการทดลองดังกล่าวได้มีการเสนอสมการที่แสดงถึงความสัมพันธ์ระหว่างค่าโมดูลัสเฉือนและหน่วยแรงประสิทธิผลเฉลี่ยของทรายที่นำมาทดสอบ.

ภาควิชา วิศวกรรมโยธา ลายมือชื่อนิสิต.....

สาขาวิชา วิศวกรรมโยธา ลายมือชื่ออาจารย์ที่ปรึกษา.....

ปีการศึกษา 2549

4770690221: MAJOR CIVIL ENGINEERING
KEY WORD: STRESS-INDUCED ANISOTROPY / MEAN EFFECTIVE STRESS / DEVIATOR STRESS / SHEAR WAVE VELOCITY / ELASTIC SHEAR MODULUS / SAND / BENDER ELEMENTS.

ALITKING ANONGPHOUTH: THESIS TITLE: EFFECT OF STRESS INDUCED ANISOTROPY ON ELASTIC SHEAR MODULUS OF SANDS USING BENDER ELEMENTS. THESIS ADVISOR: ASSOC. PROF. SUPOT TEACHAVORASINSKUN, D.Eng. 88 pp. ISBN: 974-14-3511-8.

The elastic shear modulus G_{max} is a required parameter for analyses of the dynamic and small strain geotechnical problems. The objective of this research was to evaluate the effect of stress-induced anisotropy on elastic shear modulus of a sand specimen by using bender element technique. A number of isotropically and anisotropically consolidated drained triaxial compression tests were conducted on loose and dense sand specimens. These specimens were prepared by Air- pluviation method. In this study, the measurement of shear wave velocity was performed in two phases, i.e., during consolidation and shearing. It was found that the elastic shear modulus mainly depended on the mean effective stress and void ratio and rather independent of the level of the deviator stress. The elastic shear modulus was affected by consolidation stress ratio K (stress-induced anisotropy) slightly. This was observed for both loose and dense specimens. The results also showed that the paths of $G_{max} - p'$ during shearing were almost similar to the one that was obtained during consolidation in both isotropic and anisotropic tests. Based on this experimental data, the empirical equation was proposed to express G_{max} as a function of the void ratio and the mean effective stress p' for the sand tested.

Department	Civil Engineering	Student's signature.....
Field of study	Civil Engineering	Advisor's signature.....
Academic year	2006	

ACKNOWLEDGEMENTS

My first thanks must go to my advisor, Assoc. Prof. Dr. Supot Teachavorasinskun. His patience and dedication to this work knew no bounds during the completion of this thesis. Thanks for giving me this chance and always guiding me in the right direction. It has been a great experience working and lessons with him. I have learned that will stay with me throughout my career. I also would like to thank my co-advisor Assoc. Prof. Dr. Tanaka Hiroyuki, Hokkaido University for his useful suggestions. Thank you for the constant inspiration and encouragement throughout this difficult thesis.

My thankfulness goes to all my thesis committee members. The committee Chairman Asst. Prof. Dr. Thavee Thanacharoengit, and committee members Asst. Prof. Dr. Tirawat Boonyatee, and Dr. Suched Likitlersuang for their kindness to spend their time to review my thesis and give some valuable comments. I really would like to thanks to AUN Seed-Net and JICA for the scholarship and financial support for this research.

I would like to thank all Civil Engineering's staff, technicians, and students, in Chulalongkorn University who made this enjoyable experience. I also thank all my fellow students at the Geotechnical Engineering Division, and all of my friends under AUN / SEED-Net Scholarship for their help, support, discussion and good friendship. Special thanks to Ms. Irene Olivia Ubay for being my editor for this thesis.

In addition, I would like to thank all of my teachers at Department of Civil Engineering, Faculty of Engineering, National University of Laos, and also my Lao friends, for their kindness and support for this matter.

Finally, I am deeply grateful to my supportive family who constantly give me the strength to achieve my goals. Even in trials and tribulations, their words give me comfort and newfound confidence that I can indeed fulfill my dreams. I dedicate my success to them.

CONTENTS

Page

LIST OF TABLES

LIST OF FIGURES

Page

Page

Page

Page

CHAPTER I

INTRODUCTION

1.1. Introduction

The measurement of dynamic shear modulus is increasingly important with regards to the investigation of dynamic properties of the subsoil, especially in the case when buildings have to resist vibrations. Elastic shear modulus G_{max}, also known as initial shear modulus or shear modulus at very small strain level, is one of the required parameters for a variety of geotechnical problems and design applications including tunneling, deep excavation, foundations subjected to dynamic loading, prediction of soil behavior or soil structure interaction during earthquakes, explosions, or machine and traffic vibrations.

In general, the strains in the ground around engineering structures are in the small and very small strain regions (Berland 1989). Therefore, it is important to measure soil stiffness at small strain levels. It is well known that the behavior of stiffness–strain relationship is continuously non-linear with an increase in strain level (Atkinson & Sallfors 1991, Mair 1993). However, at very small strain of about 10^{-3} % or less, the value of modulus is at maximum and is nearly constant. For this reason, elastic constants such as Young's modulus, Shear modulus, Bulk modulus and Poisson's ratio can be used to represent small strain soil behavior.

The bender element technique experienced an ongoing progress in the last two decades. It is now frequently associated with the triaxial apparatus in order to determine the elastic properties of soils such as sands, gravels, clays, etc. For instance, many theoretical works (Bates 1989, Viggiani & Atkinson 1995, Brignoli *et al* 1996, Jovicic *et al* 1996, Blewett *et al* 2000) have led to a more accurate measurement of the velocity of the shear waves generated by these piezoelectric transducers. A large quantity of experimental results was also published in the literature.

Soils in its natural state are non-homogenous and anisotropic. There are two types of anisotropy in soils. One is due to anisotropic fabric (inherent anisotropy), and the other due to anisotropic loading. Under anisotropic loading, a homogeneous and fabric isotropic soil can behave anisotropically which is called stress-induced anisotropy (Zeng & Ni, 1999). The effects of the stress state on the elastic shear modulus of soils have been extensively studied in the past decades (Roesler 1979, Yu & Richart 1984, Zeng & Ni 1999, Yamashita & Suzuki 2001, Zhou & Chen 2005, and other researchers).

Most of the previous studies usually stated the influences of states of consolidations, i.e. isotropic and anisotropic stress consolidations. However, there are very little data about the behavior of elastic shear modulus during drained shearing of triaxial tests on sands. Therefore, the objective of this study is to evaluate the variation of elastic shear modulus and shear wave velocity of saturated sands during isotropic and anisotropic consolidations, and also during drained shearing by using bender elements equipped with triaxial apparatus.

1.2. Objectives of the Research

The primary objective of this research is to study the effect of stress-induced anisotropy on elastic shear modulus of saturated sands by using bender elements. The main parameters that can be obtained in this study are the shear wave velocity and the elastic shear modulus from different stress state conditions. This experimental study will be conducted to study the following:

1. To study the variation of elastic shear modulus of saturated sand under different effective stress states during isotropic and anisotropic consolidations, and during drained shearing of triaxial compression tests to evaluate the effect of stress-induced anisotropy on elastic shear modulus of sands.
2. To study the variation of shear wave velocity and elastic shear modulus of saturated sand with different densities, i.e., loose and dense conditions.

1.3. Scope of the Research

This research will study the dynamic properties of Ping river sand, located at Chiang Mai province in the northern part of Thailand, using the triaxial apparatus equipped with bender elements at the top cap and pedestal. The testing procedure is limited as follows:

1. Preparation of specimens using two conditions: loose condition with initial relative density $D_r \approx 30\%$; and dense condition with initial relative density $D_r \approx 70\%$.
2. Measurement of shear wave velocity during isotropic and anisotropic consolidations (K= 1; 0.8; 0.6) under different effective confining pressures ranging from 30 – 300 Kpa.
3. Measurement of shear wave velocity during drained shearing of triaxial compression tests. These phases will be conducted at final confining stresses: 100; 200; and 300 Kpa.

1.4. Significance of the Research

This research is an experimental study on the dynamic properties of saturated sands, and the expected contributions of this study would be the following:

1. Findings of this research might be used in the soil dynamic analyses and design such as soil modeling, foundations subjected to dynamic loading, prediction of soil behavior or soil structure interaction during earthquakes, explosions, or machine and traffic vibrations.
2. Findings of this research might be an important piece of information of soil dynamic properties of sands, especially in the northern part of Thailand. The occurrence of earthquakes in this area suggests the need to study the dynamic properties of soil to be used in proper design, and possible predictive and preventive measures against possible deterioration of structures (due to instability or lack of durability).

CHAPTER II

LITERATURE REVIEW

2.1. Introduction

Knowledge of soil stiffness has great importance for calculating ground movements and obtains solutions to problems of soil-structure interaction. Stiffness relates increments of stress and increments of strain; an increase in shear strains tend to lead to a decrease in G and E while an increase in the volumetric strains would lead to a decrease in K. It is customary to identify three regions of soil stiffness based on the level of applied shear strain. At very small shear strain ($\gamma < 0.001\%$), the soil stiffness is approximately constant and the soil behaves like a linearly elastic material (Figure 2.1). At small shear strain level ($0.001\% < \gamma < 1\%$), the soil stiffness decreases significantly and the soil behavior is non-linear. At large strain ($\gamma > 1\%$), the soil stiffness decreases slowly to an approximately constant value as it approaches the critical state and the soil behaves like a viscous fluid.

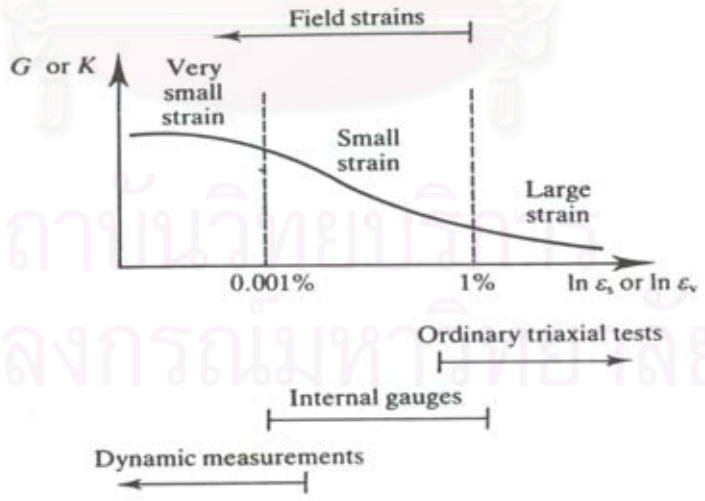

Figure 2.1: Characteristic ranges of stiffness in the field and in laboratory tests (After Atkinson 1993)

In conventional laboratory tests, it is not practical to determine the soil stiffness at shear strain less than 0.001 % because of inaccuracies in the measurement of soil displacements due to the displacements of the apparatuses themselves. The soil stiffness at small strains can be determined in the field using wave propagation techniques. In the laboratory, the shear modulus at small strain can be determined using resonant column test, cyclic test, *etc.* Recently, the new lab-technique called "bender element" is widely used to measure the shear modulus at small strain level because it is non-destructive, relatively simple to use, and allows for unlimited number of tests during the experiment. This bender element was first introduced to soil testing by Shirley & Hampton (1978), and developed by Dyvik & Madshus (1985).

The previously mentioned transducers can be used to transmit and receive shear waves only. However, a new transducer called bender-extender element can transmit and receive both compression wave (P- wave) and shear wave (S- wave). Consequently, these elements can be used easily to identify the Young's modulus E_{max}, and the shear modulus G_{max} in the small strain domain simultaneously (Lings & Greening 2001, Dano *et al* 2003).

2.2. Definition and Origin of Anisotropy

The literature review indicated that anisotropy in soils results from essentially two causes:

(a) The manner in which the soil is deposited. This is called structural anisotropy and it is the result of the kind of soil fabric that is formed during deposition. The structural anisotropy is related to the history of the environment in which the soil is formed. For example, when a river deposits sand grains, there is a tendency for more coarse grains to settle when the flow rate is high, and more fine grains to settle at low flow rates. Seasonal changes in the river flow thus result in a micro-lamination of deposited sand (Figure 2.2 illustrates some sources of inherent anisotropy). A special form of structural anisotropy occurs when the horizontal plane is

a plane of isotropy. This form of structural anisotropy is called transverse anisotropy.

(b) The difference in stresses in the different directions. This is known as stress-induced anisotropy.

Transverse anisotropy, also called cross-anisotropy, is the most prevalent type of anisotropy in soils. If we were to load in the vertical direction (Z-direction) and repeat the same loading in the horizontal direction, say, the X- direction, the soil will respond differently; its stress-strain characteristics and strength would be different in these directions. However, if we were to load the soil in the Y-direction, the response of soil would be similar to the response obtained in the X-direction. In general, the implication is that a soil mass will respond differently depending on the different of the load. For transverse anisotropy, the elastic properties are the same in the lateral directions (X and Y directions), but different from the vertical direction. Because of those reasons, the effect of inherent anisotropy and stress-induced anisotropy on stiffness of soil should be considered when measuring the soil stiffness.

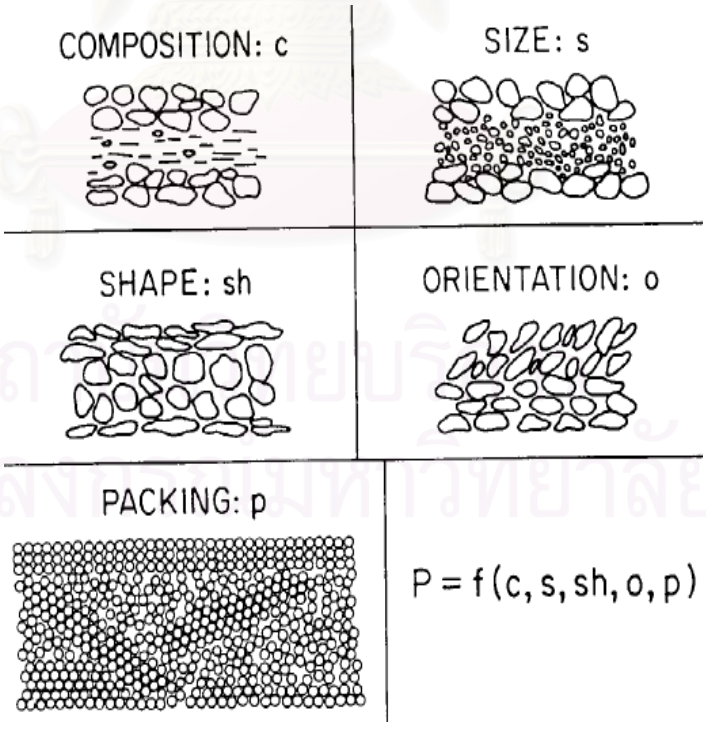

Figure 2.2: Different lithological factors that may affect anisotropy

(After Holt, 2000)

2.3. Some of the Previous Works on Elastic Shear Modulus

Most determinations of G_{max} are obtained by using vertical transmission of shear waves with horizontal polarization through the soil specimen produced by bender elements embedded in the end platens of a triaxial apparatus. Once the shear wave velocity is measured, the shear modulus of the soil specimen in the vertical plane, G_{vh}, can be calculated. Recent advances in laboratory techniques, however, enable accurate measurements of the horizontal transmission of shear wave velocity, with either horizontal or vertical polarization, through the soil specimen in oedometer or triaxial tests (Vigginia & Atkinson 1995, Jovicic *et al* 1996, Bellotti *et al* 1996, Zeng & Ni 1999, Fioravante 2001, Yamashita & Suzuki 2001, Callisto & Rampello 2002, Kuwano & Jardine 2002, Ng *et al* 2004, and other researchers). This technique involves inserting two pairs of orthogonal bender elements diametrically across a soil specimen, allowing the measurements of shear wave velocities $V_{s(hh)}$ and $V_{s(hv)}$, and then the value of shear moduli in the horizontal planes, G_{hh} and G_{hv}, can be obtained respectively.

2.4. Factors Affecting Elastic Shear Modulus

Many experimental investigations carried out on sandy soils through resonant column test or improved triaxial test in early study (Hardin and Richart 1963; Hardin and Black 1968; Drnevich and Rechart 1970; Seed and Idriss 1971; Kokusho 1980) were quoted from the paper by Zhou & Chen 2005. It showed that the small strain shear modulus $G_{\max}$ ($\gamma < 10^{-5}$) of soil was basically related to the mean effective principal stress (p') and void ratio (e) of the soil, and even overconsolidation ratio, OCR, for cohesive soil. This was expressed by the well known Hardin and Richart equation taking a general form as shown in Equation 2.1. The previous experimental data also showed that the stiffness of sands at very small strain under dynamic and static conditions tests is independent of the rate of loading.

$$G_{\max} = A\,F(e)\,(p')^{n}\,OCR^{k} \tag{2.1}$$

where, A = the empirical constant reflecting soil fabric formed through various stress and strain histories.

n = the empirical determined exponent, approximately equal to 0.5.

p' = the mean effective confining pressure $p' = (\sigma_v' + 2\sigma_h')/3$ where σ_v' = vertical effective consolidation stress, and σ_h' = horizontal effective consolidation stress.

$F(e)$ = the void ratio function, $F(e) = (2.973 - e)^2/(1 + e)$ for angular grain sands, and for round grain sands $F(e) = (2.17 - e)^2/(1 + e)$.

k = the exponent of OCR that depends on plasticity index

In the case of cohesiveless soils, OCR has no effect on G_{max} .Therefore; the Equation (2.1) can be reduced into the new form as below:

$$G_{max} = A\,F(e)\,(p')^n \tag{2.2}$$

The interpretation of shear modulus by using the void ratio function, *F(e)*, at different effective stress state conditions has been widely accepted. Kokusho (1980) evaluated the value of shear modulus of Toyoura sand using Cyclic test wherein the sand specimen was saturated with a Poisson's ratio of 0.5. Results have shown that the shear modulus tend to increase linearly with the increase of mean effective stress. These results were similar to a previous study done by Hardin and Richart (1963) as shown in Figure 2.3. He recommended that the empirical relationship between shear modulus and effective stress for Toyoura sand at small shear strain ($\gamma = 10^{-5}$) would be expressed as:

$$G_{max} = 8400\frac{(2.17 - e)^2}{(1 + e)}(p')^{0.5} \tag{2.3}$$

The Equation (2.3) can be applied to any sand specimen. However, the value of *A* and *n* would differ depending on the type of sand as summarized in Table 2.1.

Table 2.1 The values of *A*, *n*, and *F (e)* for equation (2.3) (After Koshuko, 1987), quoted from Amornwithayarax (2000)

References	*A*	*n*	*F(e)*	Materials
Hardin & Rechart (1963)	7000	0.5	$(2.17\text{-}e)^2/(1+e)$	Round grained Ottawa sand
	3300	0.5	$(2.97\text{-}e)^2/(1+e)$	Angular grained crushed quart
Shibata – Soelarno (1975)	42000	0.5	$(0.67\text{-}e)^2/(1+e)$	Clean sand
Shibata – Soelarno (1975)	9000	0.38	$(2.17\text{-}e)^2/(1+e)$	Clean sand
Kokusho (1980)	8400	0.5	$(2.17\text{-}e)^2/(1+e)$	Toyoura sand
Yu & Rechart (1984)	7000	0.5	$(2.17\text{-}e)^2/(1+e)$	Clean sand

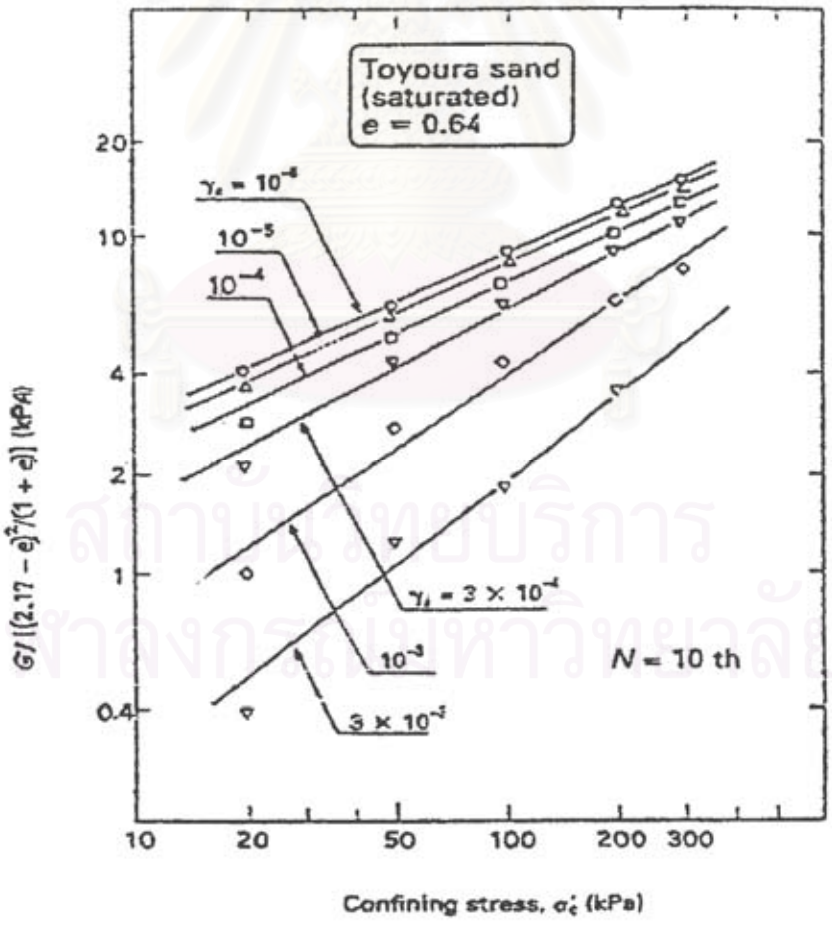

Figure 2.3: Effect of effective confining stress on shear modulus (Kokusho, 1980)

To study the effect of stress ratio on shear modulus, Yu and Richart (1984) performed cyclic tensional shear and resonant column tests of Ottawa sand. They observed that a reduction of G_{max} by about 20% where $K < 0.5$ or $K > 2$ for compression and extension consolidation stress paths respectively. Bellotti *et al* (1996) studied anisotropy of small strain stiffness in Ticino sand by performing comprehensive tests in a large calibration chamber. Several tests were performed over a range of values of consolidation stress ratio. The ranges of K studied were from 0.33 to 2 for medium dense specimens and from 0.5 to 1.5 for very dense specimens. The results of seismic tests performed on anisotropically consolidated specimens showed that the velocities of seismic shear waves polarized and propagated on the horizontal plane were not affected by the magnitude of *K*. On the other hand, the velocities of the shear wave in the vertical plane were affected by *K* when $K \leq 0.5$ as shown in Figure 2.4. In here, $\sigma_a^{'}$ is the principal effective stress along the direction of wave propagation and $\sigma_b^{'}$ is the principal effective stress in the direction of particle motion.

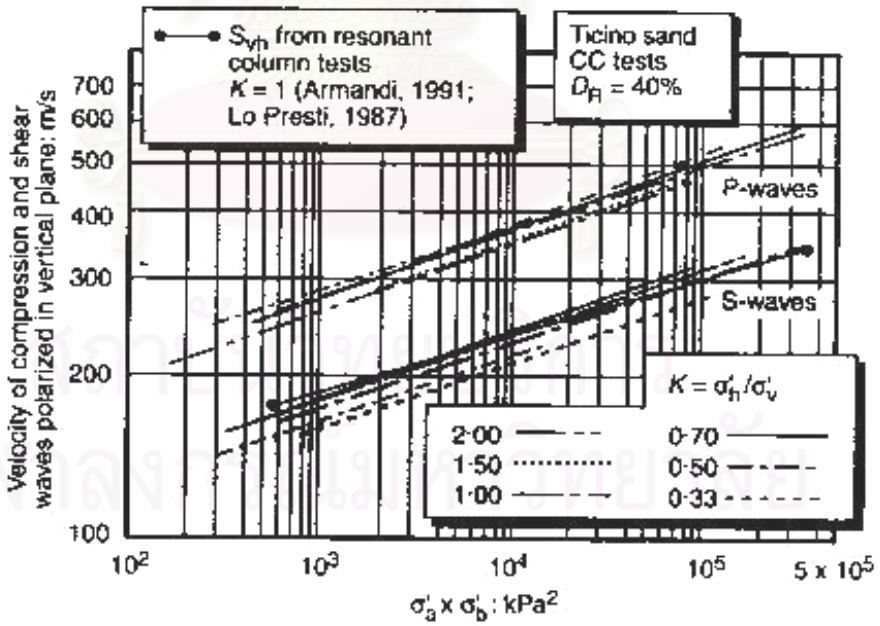

Figure 2.4: Influence of consolidation stress ratio on seismic wave velocities in medium dense sand in vertical plane (Bellotti *et al*, 1996)

Dano and Hicher (2002) studied the elastic shear modulus in granular materials along isotropic and deviatoric stress paths as shown in Fig 2.6 by using triaxial tests which were carried out on three unbound granular materials and the shear modulus was continuously measured using piezoelectric transducers. This experimental study shows that the power laws, usually considered to describe the effect of the mean effective stress on the shear modulus, are suitable only along isotropic stress paths and along deviatoric stress paths as long as the volumetric behavior is contracting. Indeed, when dilation appears, the shear modulus G_{max} gradually decreases during shearing. The empirical relations of G_{max} that they suggested were similar to those presented in previous researches (Hardin & Richart 1963, Iwasaki & Tatsuoka 1977, Hicher 1996, Lo Presti *et al* 1997) as shown in general form:

$$G_{vh\max}(MN/m^2) = \frac{K}{F(e)} \times P'^{n}(KN/m^2) \qquad (2.4)$$

Where, K and n are material constants, P'^{n} is the mean effective stress, and $F(e)$ is a function of void ratio. Fig 2.5 represents a non-exhaustive compilation of experimental data relative to sands and gravels found in the literature.

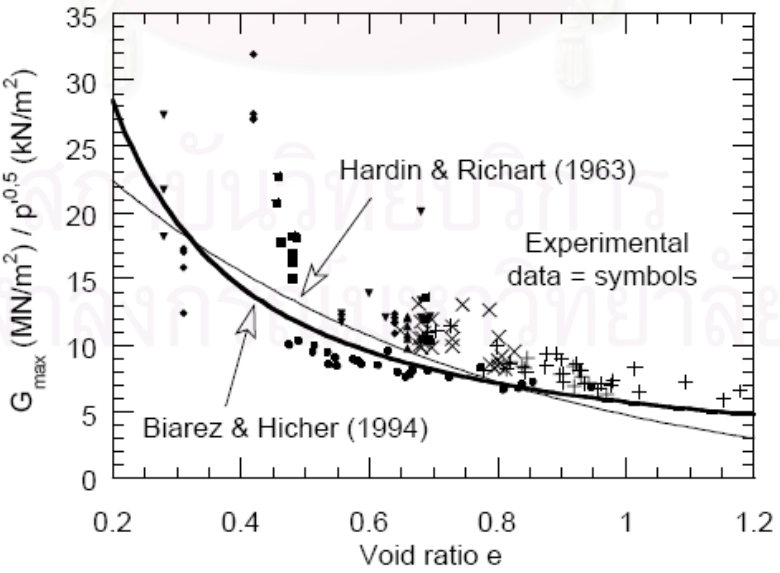

Figure 2.5: Relation between G_{max} and void ratio e

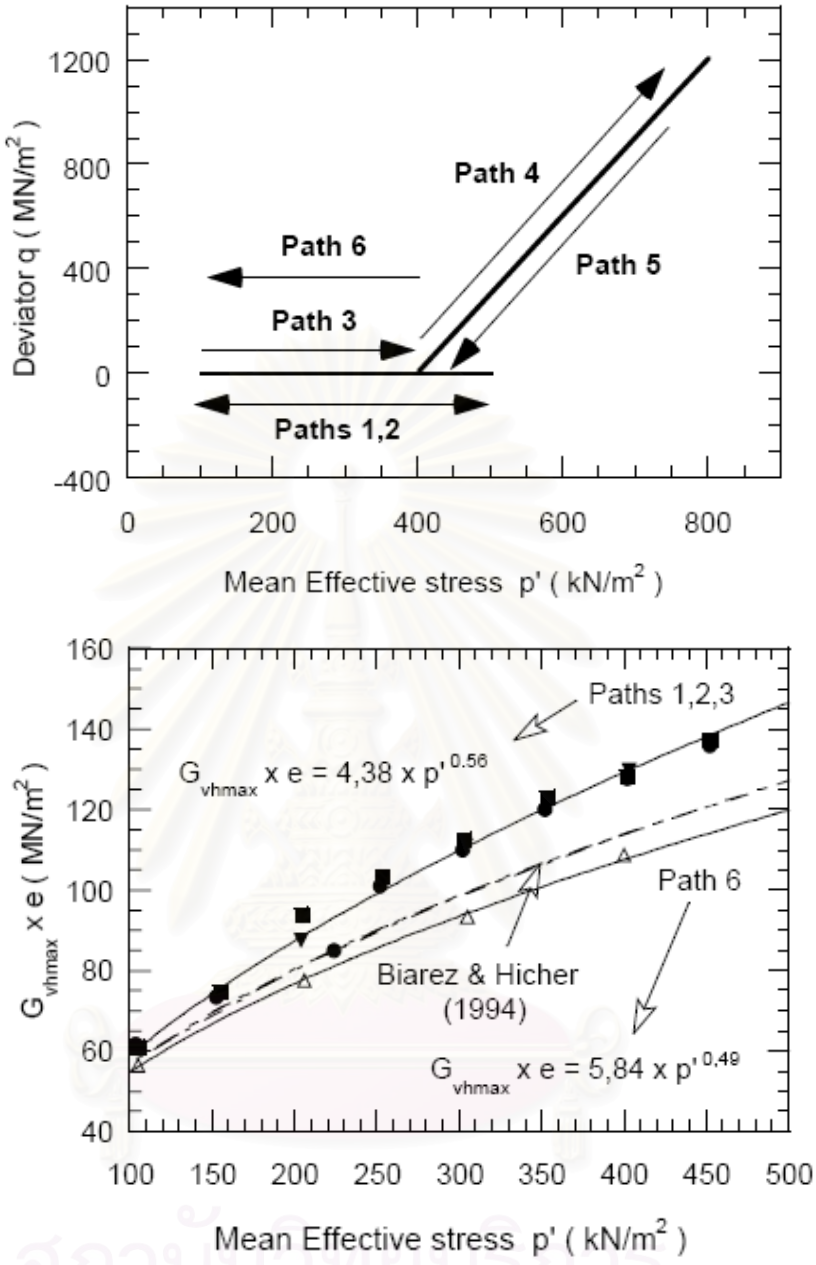

Figure 2.6: Evaluation of $G_{vh\max}$ along isotropic stress paths (Dano & Hicher, 2002)

To investigate the effect of fabric anisotropic of sand specimens on small strain stiffness, Yamashita & Suzuki (2001) performed the tests using triaxial apparatus and bender element method. The sand specimens were prepared by air-pluviation method, and shear wave velocities were measured in three different directions (VH, HH, HV- wave). The results showed that shear waves propagate faster in the plane parallel to the bedding plane than in the normal one. The V_{HH*} is

higher than the V_{VH*} with an average value of $V_{HH*}/(V_{VH*}=V_{HV*})=1.05$ on Toyoura sand and 1.13 on Kussharo sand. The V_{VH*} was equal to V_{HV*} irrespective of the inherent anisotropy and the kind of sand. These results were similar to the one that presented by Fioravante (2000). He reported that air-pluviated dry Ticino sand and Kenya sand under anisotropic stress state exhibited slight inherent anisotropy, with shear wave velocity ratios, $V_{S(HH)}/V_{S(HV)}$, of 1.05 and 1.11 respectively (where $V_{S(HH)}$ and $V_{S(HV)}$ are the velocities of horizontal transmitted shear waves with horizontal and vertical polarizations, respectively). These results imply that shear stiffness ratios, G_{HH}/G_{HV} for Ticino sand and Kenya sand were 1.1 and 1.2, respectively.

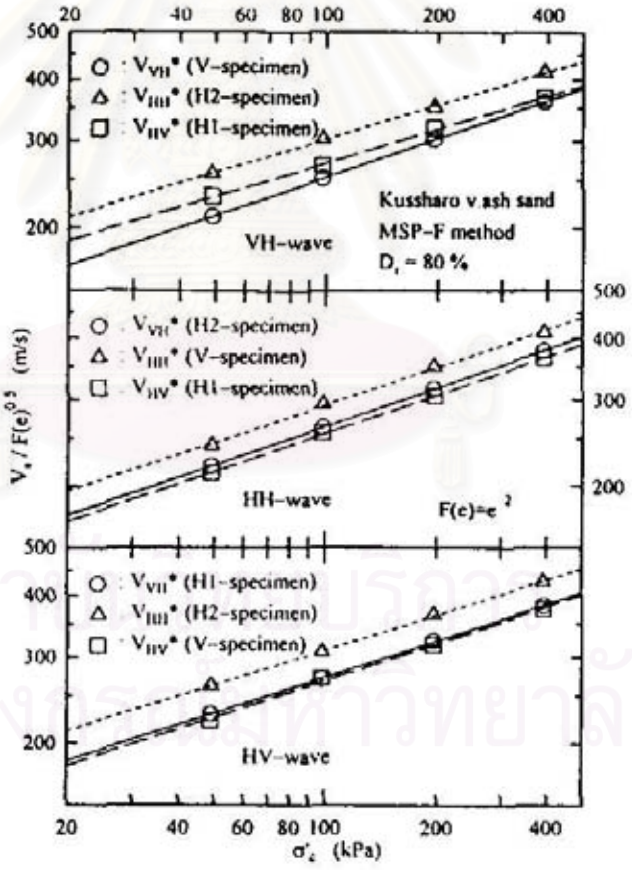

Figure 2.7: Effect of fabric anisotropy on the shear wave
(Yamashita & Suzuki, 2001)

Teachavorasinsakun and Amornwithayalax (2002) have studied the elastic shear modulus of Bangkok clay during undrained triaxial compression tests. Results of this study showed that the effect of the deviator stress was very small. However, there was a sudden drop in elastic shear modulus when the peak deviator stress was attained. This was believed to be the result of some permanent changes induced inside the sample (See Figure 2.8).

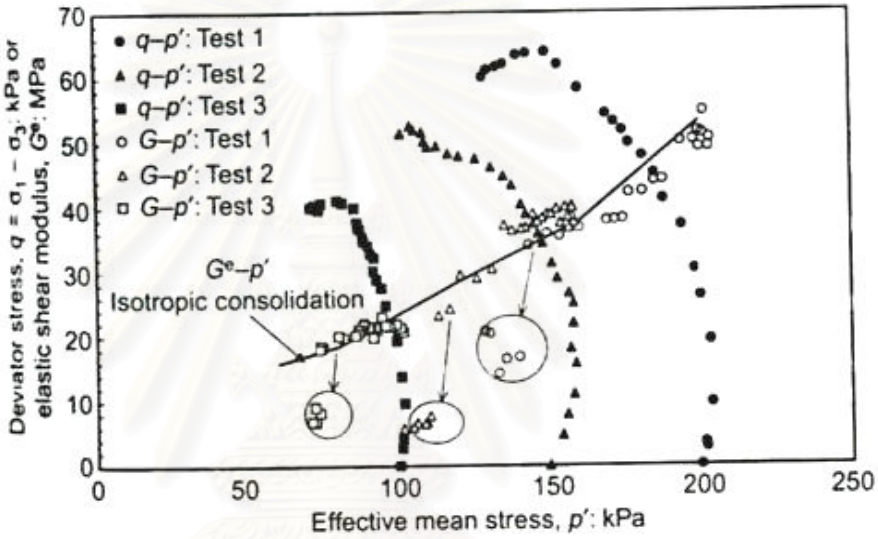

Figure 2.8: Variation of elastic shear modulus during undrained shearing

The relationships between the shear modulus and the mean effective stress called Elastic shear modulus paths of Bangkok clays were also studied by Teachavorasinsakun and Akkarakun (2004). The results showed that the deviator stress applied during shearing significantly influenced the elastic shear modulus of OC clay, whereas it plays a minor role in the elastic shear modulus of NC clay. It is believed that the stiffer structures during isotropic unloading of OC samples might be destroyed during shearing.

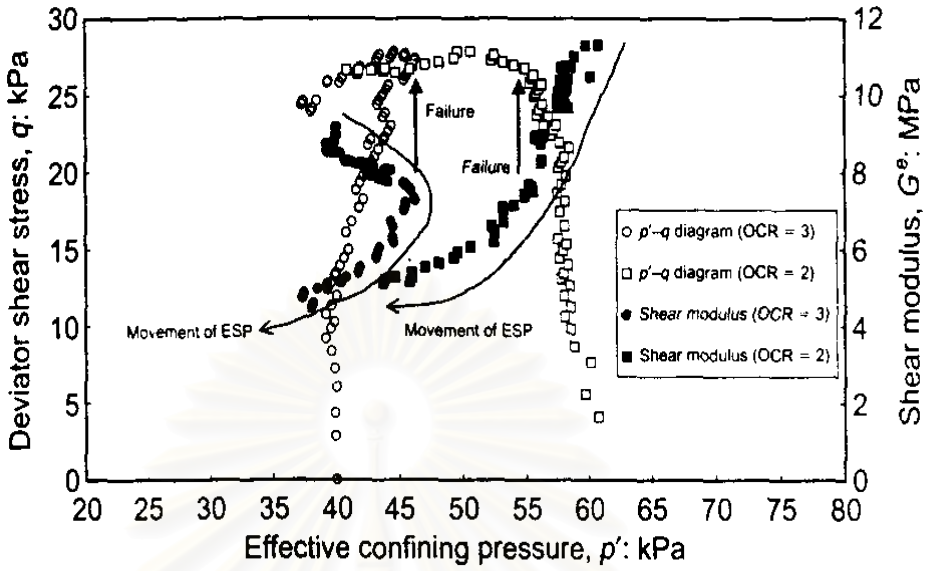

Figure 2.9: Effect of stress path and ESP of OC sample

In recent years, the study by Zhou & Chen (2005) also indicated that the shear modulus is a function of void ratio and effective principal stress. The original test data of G_{max} versus effective confining pressure $\sigma_m^{'}$ (p') of two sands are plotted in Figure 2.10 (a). To eliminate the effect of void ratio non-uniformity, G_{max} was further divided by $F(e) = (2.973 - e)^2 /(1 + e)$, and the results were plotted in Figure 2.10 (b), where e is void ratio corresponding to G_{max} at a given loading. As shown in Figure 2.10 (b) if divided by $F(e)$, the data points of the two ways of tests were almost identical and the small strain shear modulus was well correlated with the effective stress $\sigma_m^{'}$ (p') regardless of the void ratio. Then the following approximation for G_{max} can be fitted:

$$G_{max} = 2.121 F(e)\ (p')^{0.505} \qquad \text{(For medium sand)} \qquad (2.5)$$

$$G_{max} = 2.227 F(e)\ (p')^{0.510} \qquad \text{(For fine sand)} \qquad (2.6)$$

Note that $G_{\max}$ and $\sigma_m^{'}$ (p') are expressed in Mpa and Kpa, respectively.

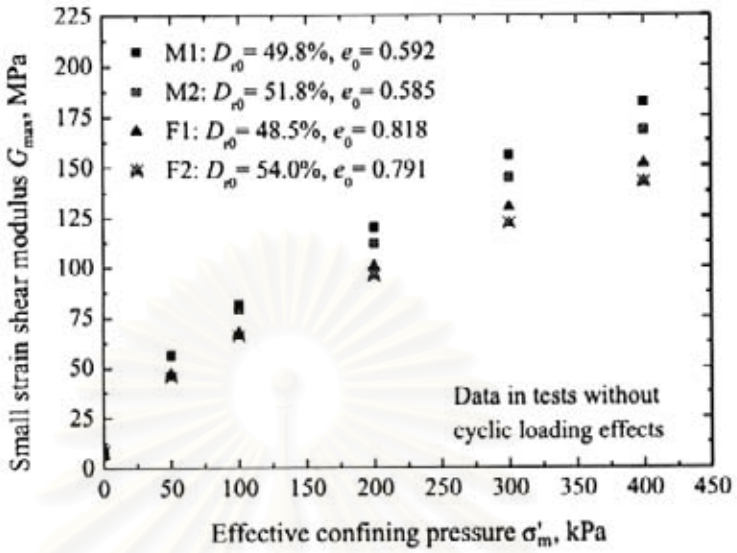

(a)

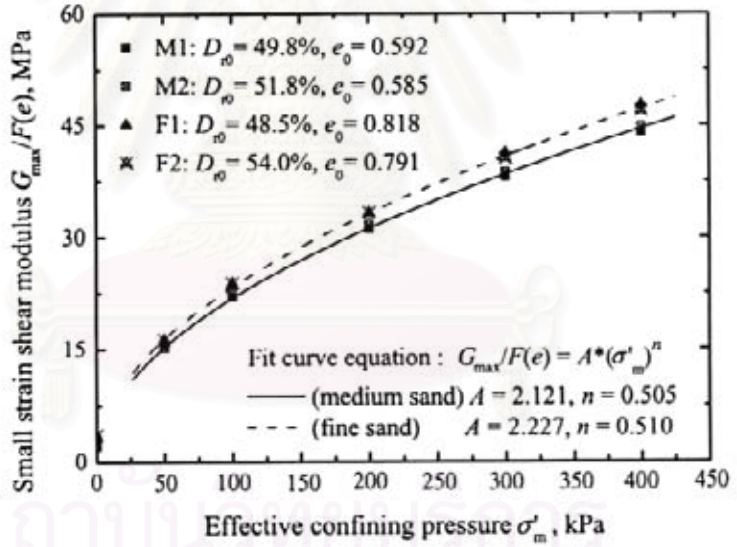

(b)

Figure2.10: (a) Dependence of $G_{\max}$ on void ratio and confining pressure $\sigma_m^{'}$ (p'), Kpa

(b) Dependence of $G_{\max} / F(e)$ on confining pressure $\sigma_m^{'}$, Kpa

According to the literature review, most of the previous researches have been determined the behavior of elastic shear modulus of sands during the consolidation phases. However, there are a little data about elastic shear modulus during drained shearing of triaxial compression tests.

In Thailand, the determination of dynamic properties of Bangkok clays has been done by many researchers. On the other hand, there were only a few investigations about the dynamic properties of sands in Thailand Because of this, the writer intends to carry out the experimental study for evaluation of the elastic shear modulus of sands along isotropic, anisotropic and deviator stress paths using bender elements equipped with triaxial apparatus. Then the behavior of saturated sands during isotropic, anisotropic consolidations and during drained triaxial compression tests will be explained, and finally the effect of stress-induced anisotropy on elastic shear modulus of sands will be discussed.

2.5. Methods to Determine Shear Modulus

The deformations and modulus of the soil at each strain level can be determined by using different methods to fit in the practical conditions. Large strain conditions may be better represented by conventional tests such as triaxial, direct shear, and unconfined compression tests, whereas dynamic loading cases and small strain cases are represented by the small strain tests as field methods such as seismic cone, down-hole, cross-hole and other seismic tests, or laboratory methods such as resonant column test, cyclic triaxial test, and torsional shear test. However, the new lab-technique called bender element is an easy technique to measure shear modulus at very small strain level. This bender element can be attached to numerous apparatus such as triaxial, oedometer, direct simple shear apparatuses, and so on.

As explained above, there are many methods to determine the shear modulus. Nevertheless, only the details of the bender element test will be explained here.

2.5.1. Bender Elements

2.5.1.1. Interpretation of Bender Elements

The bender element method, developed by Shirley & Hampton (1978), is a simple technique to measure the very small strain shear modulus of soil, G_{max}, by measuring the velocity of the propagation of a shear wave though a speciemn (Viggiani & Atkinson, 1995; Jovicic et al,1996).

The bender element consists of two sheets of piezoelectric ceramic material such as barium titanate, or lead titanate sandwiching a center shim of brass, stainless steel, or other ferrous nickel alloys to add strain to it (Leong et al, 2005). The bender element is an electromechanical transducer capable of converting mechanical energy into electrical energy and vice versa. When a driving voltage is applied to the bender element, the polarization will cause a bending displacement, then the bender element acts as a signal generator. When the element is forced to bend, voltage is generated, thus, the bender element can act as a receiver. Bender element systems can be set up in most laboratory apparatus, but are particularly versatile when used in the triaxial test as described by Dyvik & Madshus (1985) quoted from Jovicic et al (1996).

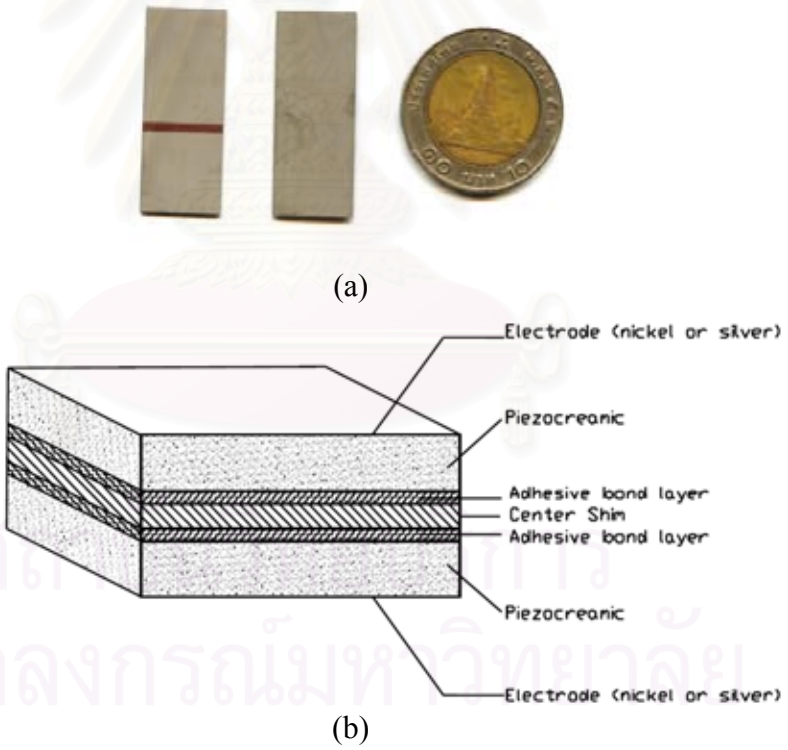

Figure 2.11: (a) Bender Elements, (b) its structure (Source: Piezo System, Inc)

2.5.1.2. Types of Bender Elements

Depending on the polarization, there are two types of bender elements: X-poled and Y-poled as shown in (Figure 2.12). From the energy point of view, there is no difference between X-poled and Y-poled bender elements. Both X-poled and Y-poled bender elements act similarly when connected in a series connection and a parallel connection, respectively. The important parameters of a transmitter bender element are the free deflection x_f and the maximum force generated $F_{\max}$. For the receiver bender element, the important parameter is the voltage generated V_0. The Y-poled bender element in parallel connection is more suited as a transmitter as it needs lower voltage to generate motion compared to the X-poled bender element in series connection. Whereas, the X-poled bender element in series connection is more suitable as a receiver as it generates higher output voltage per unit force applied to the tip of bender element (Leong et al, 2005).

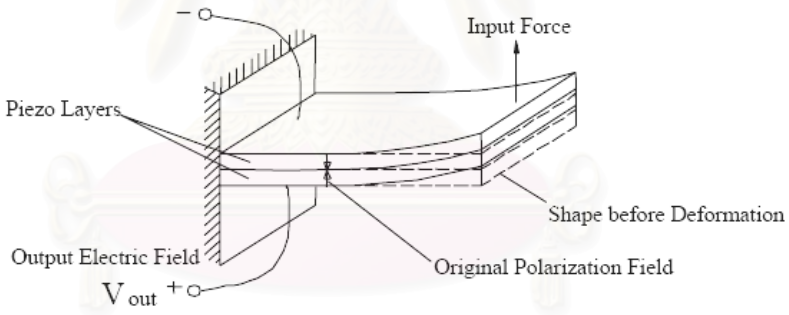

(a)

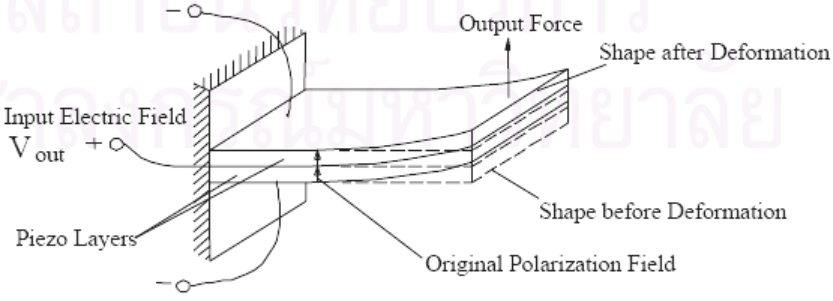

(b)

Figure 2.12: (a) X-poled bender Element Poled for Series Operation (2 wires)
(b) Y-poled bender Element Poled for Parallel Operation (3 wires)
(Source: Piezo System, Inc)

2.6. Principles and Sources of Errors in Bender Element Tests

In the bender element test for measurement of shear wave velocity, at least a pair of bender element is used whereby one of the bender element acts as the shear wave transmitter and the other bender element acts as a receiver. By measuring the travel time of the wave, the wave velocity V_s is determined as follows (Dyvik and Mashus 1985; Brignoli et all 1996; Viggiani and Atkinson 1995; Jovicic et al 1996):

$$V_s = \frac{L_{tt}}{t} \tag{2.7}$$

where, L_{tt} = the tip to tip distance between transmitter and receiver bender elements.

t = the travel time of the wave from the transmitter and the receiver.

From shear wave velocity, the shear stiffness $G_{\max}$ can be calculated from the elastic wave propagation theory as this equation:

$$G_{\max} = \rho V_s^2 \tag{2.8}$$

where, ρ = the total density of the soil specimen.

The density of the cylindrical soil specimen can be determined correctly by direct measurement, but it is not easy to determined L and t.

2.6.1. Determination of Effective Length

Viggiani and Atkinson, 1995 conducted the tests on a set of reconstituted samples of kaolin of different lengths, and the bender elements were protruded 3 mm into each end of the specimen. They plotted the travel times against the overall length of the specimen for tests with different stress states as shown in Figure 2.13. The test data fall on straight lines, each with an intercept of about 6 mm on the vertical axis, which conforms that L should be taken as the distance between the tips of bender elements rather than the whole length of the specimen.

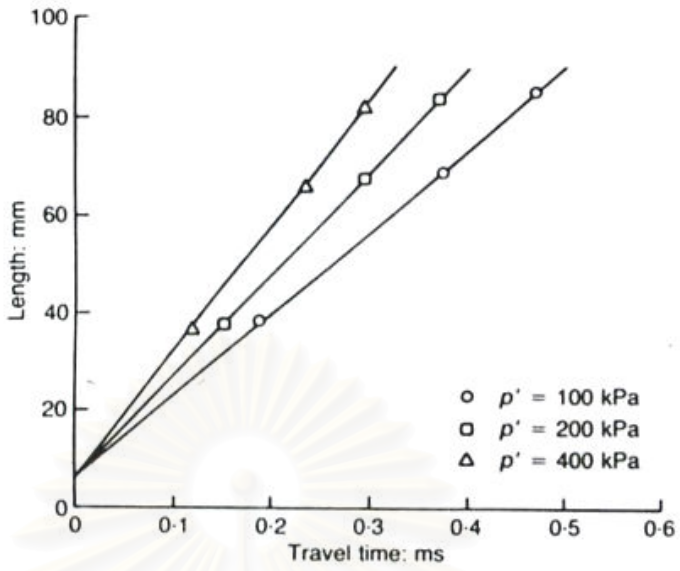

Figure 2.13: Relationship between travel time and specimen length (Viggiani & Atkinson, 1995)

2.6.2. Determination of Travel Time

It is common practice to locate the first arrival of the shear wave at the point of first deflection of the received signal at the point 0. Reversal of the polarity of the received signal as the polarity of the input signal is reversed is usually taken as demonstration that the point 0 actually corresponds to the first arrival of the shear wave (Abbiss, 1981). However, a theoretical study by Salinero et al (1986) showed that the first deflection of the signal may not respond to the arrival of the shear wave, but to the arrival of the so-called near-field component which travels with the velocity of a compression wave. Brignoli & Gotti (1992) found the evidence for the existence of near field components in bender element tests.

Results of the numerical analyses signals from the bender element tests on a reconstituted boulder clay specimen (Viggiani & Atkinson, 1995) shows that the travel time should not be taken as the time corresponding to the first deflection of the received signal as in point 0. The first arrival of the shear wave, for simple analyses, can be taken as the point of the first inversion of the received signal at point 1 (Figure 2.14) which could lead to overestimation of the shear modulus to about 14%.

This is in agreement with Jovicic et al, 1996. They suggested that for the square wave in Figure 2.14, the first reversal point (1) is close to the correct arrival time of the shear wave as proposed by Dyvik & Madshus (1985). They also said that the part of the trace between point 0 and 1 represents the near-field effect.

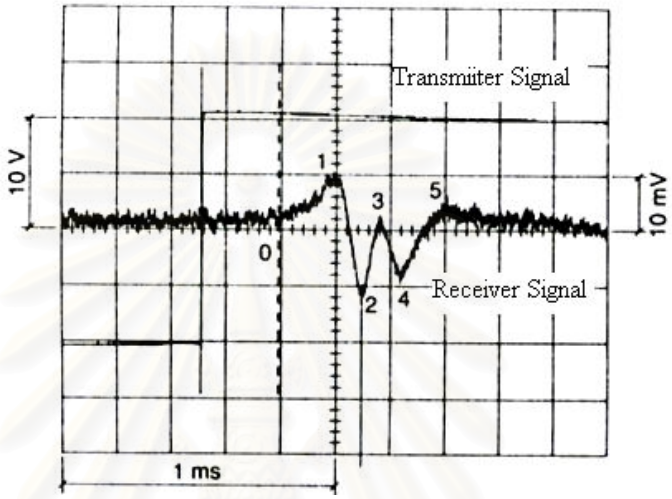

(a)

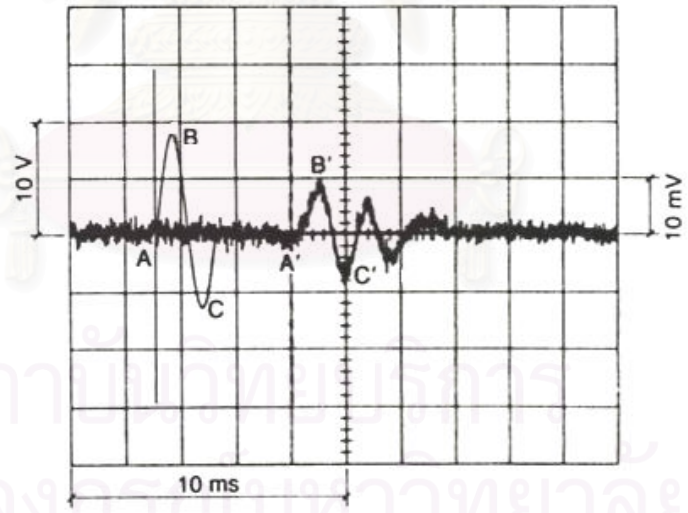

(b)

Figure 2.14: (a) Typical oscilloscope signal from a bender element test with Square pulse excitation

(b) Typical oscilloscope signal from a bender element test with Sine pulse excitation

(Viggiani & Atkinson, 1995)

The input and output signals for sine pulse wave as shown Figure 2.13 (b). Several options for the measurement of the travel time have been suggested in the literature. the suggestions were the measurement between: A - A', B – B', C – C'. Therefore, the location of the arrival signal still needs engineering judgment.

2.6.3. Driving Waveform

The receiver bender element signal is dependent on the voltage applied to the transmitter bender element and the soil types. The applied voltage has three parameters: waveform, magnitude, and frequency. Three types of waveforms are commonly used: square pulse, sine pulse, and continuous sine wave as shown in Figure 2.15. Those waveforms were used in bender element tests on soil specimens. However, square wave will be adopted in this study because it is relatively easy to operate. Table 2.2 summarizes the wave form, magnitude, and frequency of applied voltage and soil types tested by the previous researchers.

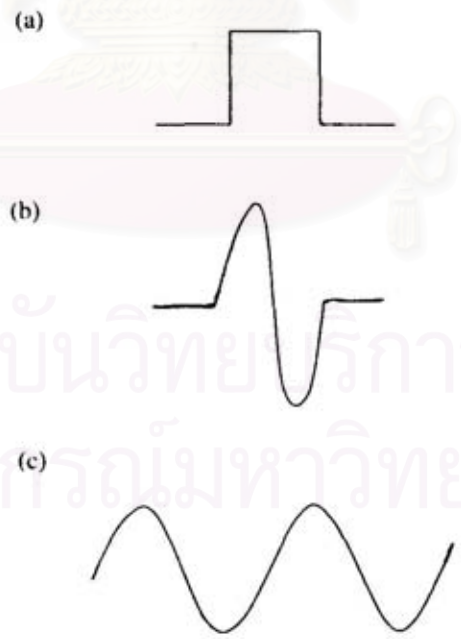

Figure 2.15: (a) square pulse, (b) sine pulse, and (c) continuous sine wave (Blewett *et al*, 2000)

Table 2.2 Summary of waveform, magnitude, and frequency of applied voltage and soil type used by previous researchers (After Leong *et al*, 2005)

Reference	Voltage Applied			Soil Type	Method of Interpretation
	Waveform	Magnitude (V_{pp})	Frequency (Hz)		
Dyvik and Madshus (1985)	Square	20	5–100	Clay	First arrival (first reversal)
Bates (1989)	Square	10	2	Sand	First arrival (?*)
Argawal and Ishibashi (1991)	Sine	100–600	13 560	Glass spheres	First arrival (?)
					First arrival (first deflection, first reversal)
Viggiani and Atkinson (1995)	Square	20	50	Clay	Characteristics points
	Sine		1000–10 000		Cross correlation
					Cross power
Brignoli et al. (1996)	Sine	20	3000–10 000	Clay	First arrival (first reversal)
				Sand	
Gajo et al. (1997)	Square	150	10 000	Sand	First arrival (first deflection)
	Sine				
					First arrival (?)
Arulnathan et al. (1998)	Sine	20	900–4,500	Organic soil	Characteristics points
					Cross correlation
					Cross power
Lohani et al. (1999)	Square	20	50	Clay	First arrival (first reversal)
Blewett et al. (2000)	Sine	—	200–10 000	Sand	—
Diaz-Rodriguez et al. (2001)	Square	20	7	Silty clay	First peak
Kawaguchi et al. (2001)	Square	20	100	Clay	First arrival (average of first rise and first peak)
	Sine		1,2,4,8		
Pennington et al. (2001)	Sine	20	8000–25 000	Clay	First arrival (first deflection)
Callisto and Rampello (2002)	Square	20	50	Clay	Average of first deflection and reversal point
	Sine		10 000		Characteristics peaks

* Not specified.

CHAPTER III

RESEARCH METHODOLOGY

3.1. Location and Method of Sampling

The sample used in this study was Ping river sand located at Chiang Mai province in the northern area of Thailand. There is a need to investigate the dynamic properties of soils in this area given that the probability of earthquake is quite high.

Generally speaking, it is difficult to obtain undisturbed sample of the cohesiveless soils (sands), especially in the deep layer. However, the undisturbed sample can be obtained by using advanced techniques such as soil freezing method, chemical grouting, *etc.* on the other hand, these methods are not economical. Therefore, in this study the disturbed sand sample was used. Approximately 50 Kg of the sand sample was taken from the Ping river bank.

3.2. Testing Apparatus

In this study, the laboratory tests were carried out in a computer-controlled hydraulic triaxial cell made by ELE international. The equipment consists of six main components as follows:

1. Triaxial machine and accessories:
   - Axial loading device, triaxial cell (chamber), de-aired water apparatus
   - Oil/water constant pressure system
   - Axial force transducer, axial displacement transducer, pressure transducers, and volume change transducer.
   - Split mold, funnel, rubber membrane, vacuum pump, calipers, etc.
2. Bender Elements
3. Digital Oscilloscope
4. Function generator
5. Computer for data processing

3.3. Bender Element Set-Up and Operation

The mode of operation of bender elements based on Dyvik & Madshus (1985) in Figure 3.1 shows the three- wire parallel connection and same-sense polarization needed for a typical transmitter element. Receiver elements have a two-wire series connection and opposite-sense polarization. In both cases, only two-wire cabling to the instrumentation are required. The key is to match the wiring and polarization. Therefore, the largest displacements and largest voltage are created at the transmitter and receiver respectively.

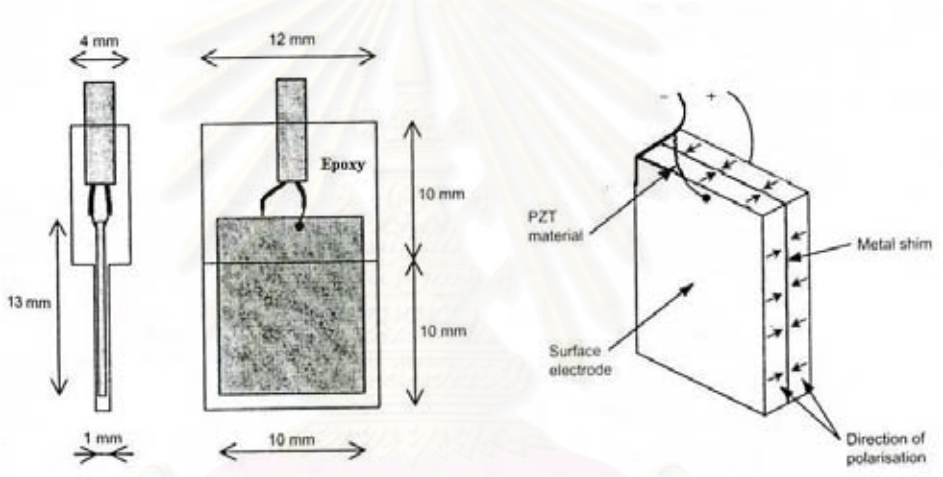

(a)

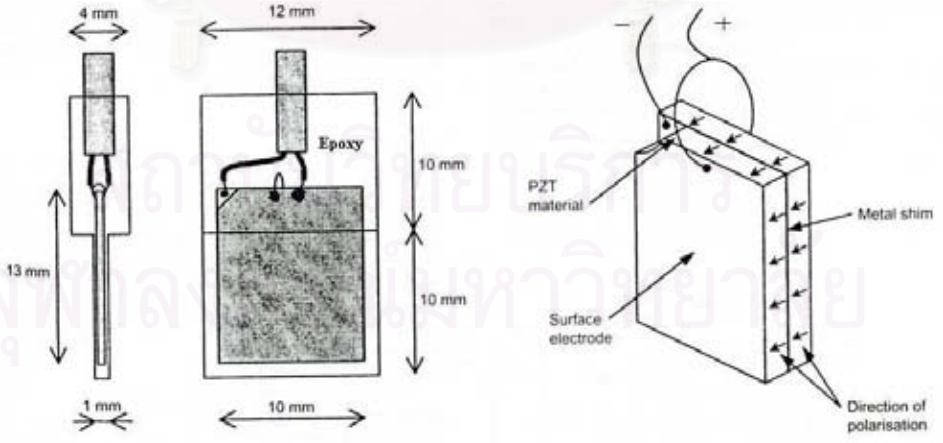

(b)

Figure 3.1: Wiring and coating of bender elements (a) Receiver (b) Transmitter (Lings & Greening, 2001)

The bender element types T 224- A4SS -303Y (Transmitter) and T 224- A4SS -303X (Receiver) with dimensions of 34.7 × 12.7 × 0.66 mm (length × width × thickness) were used in this experimental study. These bender elements were produced by Piezo System, Inc. At first, the series and parallel connections were employed for the X-poled and Y-poled respectively, as shown in Figure 3.1. Before installation in the triaxial apparatus, these bender elements had to be coated with the waterproof epoxy resin in order to prevent them from short-circuiting when in contact with water. Then, the bender elements, which placed in the slots provided at the top cap (receiver) and pedestal (transmitter) of the triaxial cell, were sealed in place by epoxy. Keeping in mind that the alignment of the bender relative to the caps was also important; a perfectly vertical bender element would generate the most energy in the preferred direction as well as reduce the reflection from membrane. The tips of bender elements should be projected in the distance of about 3 mm from the porous stone surfaces. The porous stones with corresponding (larger) slots were placed in the platens. The gaps between porous stones and the bender elements were filled with silicone rubbers so as to prevent any soil from jumping into the gaps as well as permit the free movement of the bender elements.

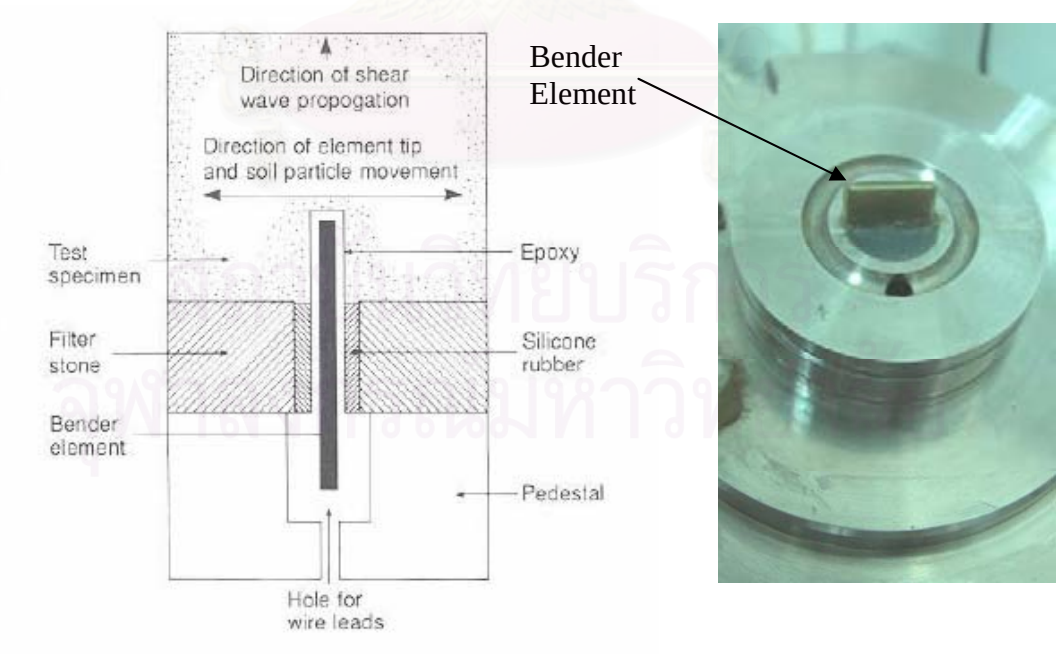

Figure 3.2: Detail of bender element fixing to pedestal and connecting to soil specimen

The other components of the test set-up were a function generator, digital oscilloscope, and computer for data processing. The function generator was used to supply the transmitter with the driving voltage. This normally consisted of a square wave with a frequency of 50 Hz and amplitude of 10 V (20 V peak to peak) as described by Viggiani & Atkinson, 1995. The excitation voltage which produced by function generator was applied to the transmitter bender element in the bottom pedestal and caused it to bend or vibrate, generating the shear wave which propagated through the soil specimen. The wave traveling through the soil specimen would be received by the receiver bender element in the top cap. Both the applied voltage and the receiver signal were recorded in the digital oscilloscope. Then the data recorded by the digital oscilloscope were directly transferred to a computer for further signal processing. The difference between the arrival of the transmitter signal and the receiver signal is called travel time. Figure 3.3 shows the schematic diagram of the connection of equipments set-up in bender element test.

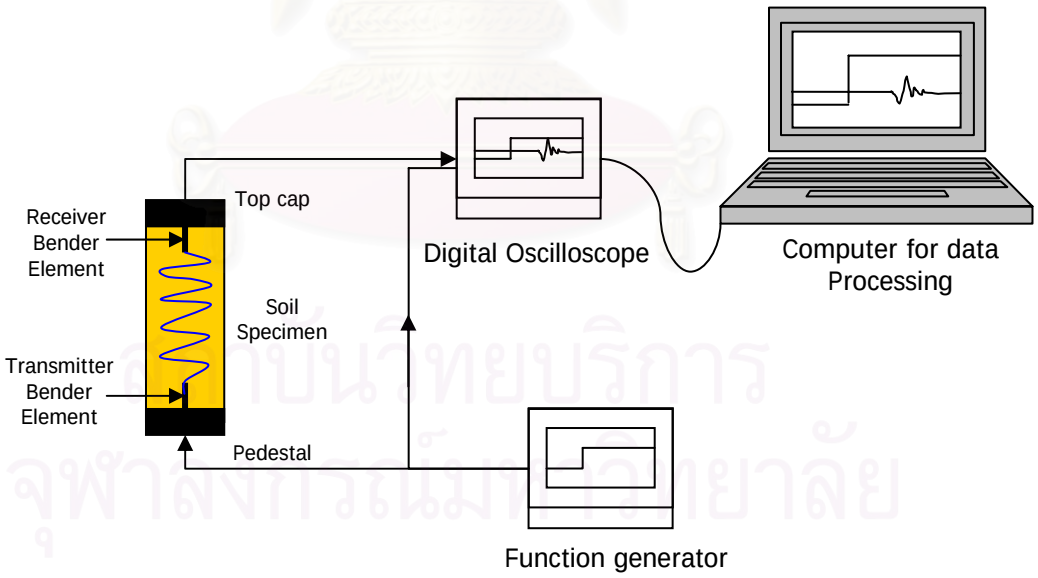

Figure 3.3: Bender element tests set-up

3.4. Testing Procedure

3.4.1. Preparation of Specimens

The sand specimens of about 50 mm in diameter and 100 mm in height were tested in a triaxial machine. The preparation of sand specimens was done using two conditions: loose condition with initial void ratio (e_o) ranging from 0.74 to 0.79 and D_r of 20.8% to 35.4%; and dense condition with e_o ranging from 0.60 to 0.63 and relative density (D_r) of 69.4% to 77.6%. These specimens were prepared by using the air- pluviation method.

Air-pluviation Method:

A split former (mold) is used for preparation of sand specimen, but since there is no water pressure to press the membrane in contact with the mold, the correct initial size of the membrane is more important. Therefore, the section between the former and membrane is used. Loose specimens are placed by running the dry sand continuously and rapidly from a funnel using a constant height of drop. Dense specimens can be obtained by subsequent vibration. Alternatively, a uniform material can be poured at a slower rate, using a larger drop. Homogenous specimens can be obtained by this manner. The specimens can be tamped in thin layers, though this may lead to holes in the rubber membrane (Bishop & Henkel, 1982). The specimen preparation will be explained in details as follows:

1. Obtain the thickness of the membrane. This thickness is best obtained by measuring the membrane doubled and then halving the measurement.
2. Place a porous stone and filter paper on the bottom platen.
3. Attach a rubber membrane of the proper diameter to the bottom platen with rubber "O" rings. The membrane should overlap the platen at least 1/2". (In this study two layers of membranes were used to prevent leaking).
4. Weigh a dish of dry sand which is to be tested. An amount of sand should be slightly larger than the one to be used for the test specimen.

5. Place a split mold around the rubber membrane. Fold the top portion of the membrane down over the mold, taking care that the membrane is not twisted or pinched.
6. Apply a vacuum (around 20-30 Kpa) to a hole at the side of the mold in order to pull the membrane against the side of the mold.
7. Place the dry sand in the membrane and mold by pouring the sand form a funnel. Loose sample are place running the sand continuously and rapidly from the funnel using a constant height of drop. Dense samples can be obtained by subsequent vibration. Alternatively, the material (particularly if uniform) can be poured at a slower rate, using a larger drop. The homogenous samples can be obtained by this means.
8. Level and smooth the final top surface of specimen by scraping with a thin plate having a straight edge.
9. Again, weigh the dish of sand. The difference in masses is the mass of sand used.
10. Place a porous stone and then the top platen onto the sand. It may also be necessary to coat the outer rim of the top platen with silicone grease to make a good, leak-proof seal at the top. Roll the membrane off the mold and onto the top platen and seal it to the platen with rubber "O-ring". Take a small level and level the top platen.
11. Release the vacuum to the side of the mold.
12. Apply the vacuum of about - 30 Kpa to the drainage line to the lower platen, and the line from the top platen instead.
13. Now remove the spilt mold and observe the membrane for holes and obvious leaks. If any are found, the sample must be rebuilt using a new membrane.
14. Obtain four height measurements approximately 90° apart and use the average value for the initial specimen height L_o. Take two diameter readings 90° apart at the top, at mid-height, and at the base using a pair of calipers. Take these measurements to the nearest 0.1 cm. Compute the average diameter of the specimen at each height location and then compute a final average specimen diameter as

$$d_{avg} = (d_t + 2d_m + d_b)/4$$

where, d_t is the average diameter based on the two top measurements and taking into account membrane thickness, etc. Compute the corresponding value of initial specimen area A_o using the average diameter just computed.

15. Place the cell chamber on the cell base. Be sure the base is free of soil grains so that an airtight seal can be obtained (It may needs to put some silicon grease on cell base). Then place the cell in the compression machine.
16. Fill the chamber with water through the cell chamber line with the bleed off valve at the top of the chamber open.
17. Attach pressure line to the cell chamber line and slowly apply a cell pressure of 30 Kpa while slowly decreasing the vacuum. While the cell pressure is equal 30 Kpa and vacuum pressure is equal to 0 Kpa, disconnect the bottom and top specimen drainage line from the vacuum.

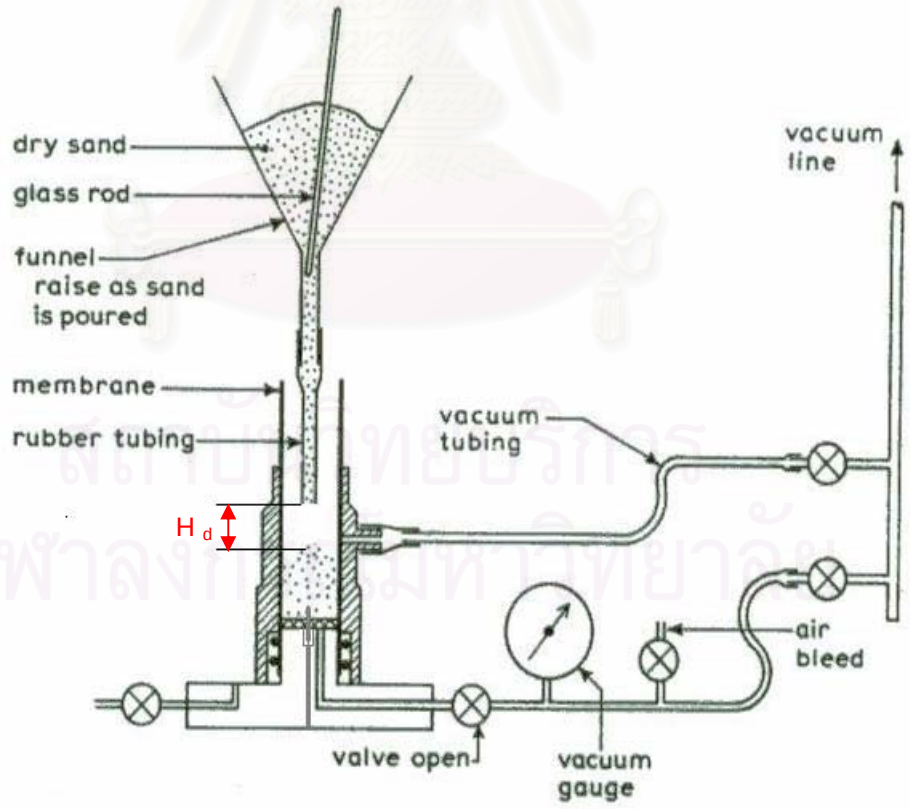

Figure 3.4: Specimen preparation by air-pluviation method (Head, K.H. 1982)

3.4.2. Saturation of Specimens

The triaxial specimens for CU and CD test must be fully saturated before being isotropically or anisotropically consolidated and sheared. The saturation is tested by closing the drainage system, by applying a small increase $\Delta\sigma_3$ in confining pressure, and by measuring the resulting change in pore pressure Δu. The sample is fully saturated when the coefficient $B = \frac{\Delta u}{\Delta\sigma_3} = 1$, and partially saturated when $B < 1$. For CU tests, complete saturation ($B \geq 99.5\%$) is required to generate meaningful pore pressure. Otherwise, partial saturation would result in erroneous pore pressure and undrained shear strength. The degree of saturation can be increased by increasing the backpressure and confining pressure simultaneously so that the soil effective stress and differential pressure across the sample membrane do not change. For CD tests, saturation is not as critical as for CU tests because it is used only to measure volume change. Partial saturation leads only to underestimating the volume change. $B \geq 95$ % is satisfactory for drained tests.

In this study, the dry sand specimens were saturated by allowing the water in the reservoir at high position to flow slowly through the bottom drainage line of triaxial cell base to the specimen. The top drainage line was open in order to let the air- bubbles go out side by this way. This step would be finished after 12 hours or sometimes overnight to make sure that almost air-bubbles were removed. After that the back and cell pressures were applied gradually until the back pressure 200 Kpa and cell pressure 230 Kpa were reached. Keeping in mind, the difference between cell pressure and back pressure must be equal to the applied initial effective confining pressure 30 Kpa

3.4.3. Consolidation of Specimens

In this study, two kinds of consolidations were performed: isotropic and anisotropic consolidations (K=1, 0.8, and 0.6). The specimen can be consolidated after it has been saturated. For isotropic consolidation, keep the backpressure

constant, and increase the cell pressure until the difference between the cell pressure and backpressure becomes equal to the desired confining pressure. Then open all drainage lines to let the specimen consolidate under applied confining pressure. Record the volume-change at each stress increment of consolidations. The consolidation of sand specimens will be finished within 5 minutes for one stress increment.

In anisotropic consolidation test, an axial load is applied to the specimen during consolidation in order to maintain the ratio of the effective horizontal and vertical principal stresses ($K = \sigma_h^{'} / \sigma_V^{'}$) at constant value. Anisotropic test using axial load may be applied either by a dead-weight hanger or by a triaxial load frame with load measuring device by Head, K.H (1982) as shown in Figure 3.5.

The value of volume change transducer and the axial displacement of the displacement transducer were recorded. The specimen was allowed to consolidate and then it was checked by observing the pore pressure response when drainage lines closed or by observing the value of the volume-change transducer if the value keeping constant that means the consolidation was completed. The consolidation pressure was applied step by step until the final effective stress was reached. When the dissipation of the excess pore water pressure was ensured at the end of each step, the travel time of the shear wave was measured by using bender elements.

a. Dead Weight Loading

The forces acting on the soil specimen are shown diagrammatically in Figure 3.5(a). The net down force *F* applied to the sample top cap is given by the equation:

$$F = \left[\frac{m_h + m + (m_p - m_w)}{1000} \right] \times 9.81 - \frac{\sigma_h a}{1000} \quad N$$

It is assumed bellow that piston is counteracted by the effective mass of the piston and top cap $(m_p - m_w)$.

The axial stress is equal to

$$\sigma_V = \left(\frac{F}{A} \times 1000\right) + \sigma_h \qquad (Kpa)$$

$$\sigma_V = \frac{9.81}{A}(m_h + m) - \sigma_h \times \frac{a}{A} + \sigma_h \qquad (Kpa)$$

If $\sigma_V / \sigma_h = \beta$, *i.e.* $\sigma_V = \beta \sigma_h$, then

$$\sigma_h = \left(\beta - 1 + \frac{a}{A}\right) = \frac{9.81}{A}(m_h + m)$$

Therefore,

$$m = \frac{A}{9.81}\sigma_h\left(\beta - 1 + \frac{a}{A}\right) - m_h \qquad (g)$$

Where, σ_v, σ_h = vertical and horizontal stress, (Kpa)

A = corresponding area of cross section of specimen, (mm^2)

a = corresponding to area of cross section of the piston, (mm^2)

m_h = mass of dead load hanger, (g)

m_p = mass of top cap and piston, (g)

m_w = volume or mass of water displaced by the top cap and submerged part of piston, (cm^3)

m = mass of weight applied to hanger (g)

b. Load Ring Loading

When using a load frame fitted with an external load measuring device, the load or load dial reading, needed to give required principal stress ratio ($\beta = \sigma_V / \sigma_h$) is determined as described below. The symbol are the same as those used above, with addition of force exerted by load ring, P (N) and friction force in cell bushing opposing downward movement of piston, f (N). The forces acting on the specimen indicated in Figure 3.5(b). The net downward force F on the sample top cap is given by the equation:

$$F = P + \frac{(m_p - m_w) \times 9.81}{1000} - \frac{\sigma_h a}{1000} - f \qquad (N)$$

The force due to the effective mass of piston and top cap is represented by *Q*, where

$$Q = \frac{m_p - m_w}{1000} \times 9.81 \qquad (N)$$

Axial stress $$\sigma_V = \left(\frac{F}{A} \times 1000 \right) + \sigma_h$$

$$\sigma_V = \frac{1000}{A}(P + Q) - \sigma_h \times \frac{a}{A} - \frac{1000\, f}{A} + \sigma_h \qquad (Kpa)$$

Putting $\sigma_V = \beta \sigma_h$,

$$\sigma_h \left(\beta - 1 + \frac{a}{A} \right) = \frac{1000}{A}(P + Q - f) \qquad (Kpa)$$

Hence,

$$P = \frac{A}{1000} \times \sigma_h \left(\beta - 1 + \frac{a}{A} \right) - Q + f \qquad (N)$$

Note: the axial load must be kept constant by winding up the machine platen to compensate for axial deformation of the specimen.

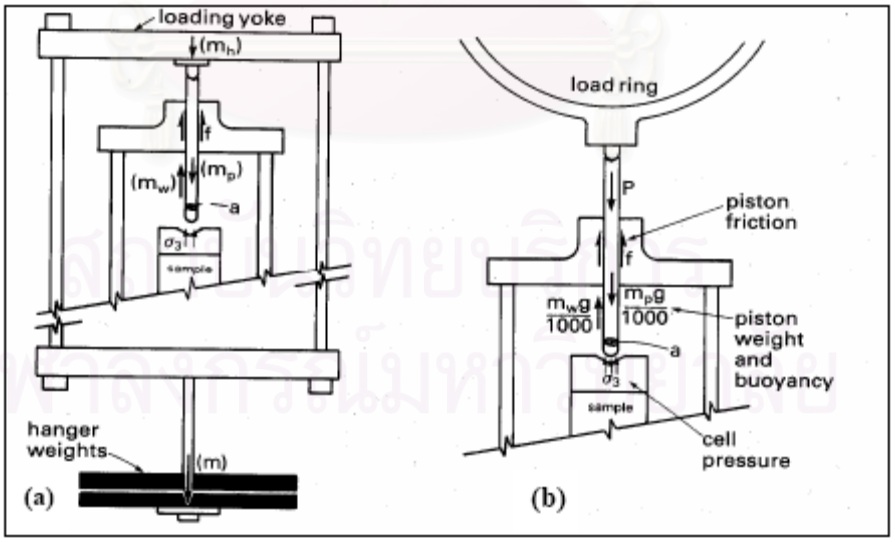

Figure 3.5: Anisotropic consolidation test in triaxial cell, illustrating forces acting on the specimen: (a) using dead weight loading, (b) using a load ring (Head K.H, 1982)

3.4.4. Shearing of Specimens

For drained triaxial test, at the end of consolidation period and final mean effective stress, the drainage valves were opened and the specimen was sheared to failure at an appropriate strain rate (between 0.02 - 0.1 mm/min). The slow rate of strain was used so that the travel time of the shear wave could be accurately measured. The pore pressure readings, the cell pressure readings, the axial force transducer readings, axial displacement reading, and volume-change reading, and travel time readings were recorded at each regular reading, i.e. for the first 2% of strain, take a set of readings about every 0.2% of strain. For the rest of the test, take readings every 0.5% to 1% strain. Continue the test until axial strain of about 20 % was reached. After having completed the axial loading, release the back pressure and decrease the confining pressure to 30 Kpa. Then apply the vacuum of - 30 Kpa through the top specimen drainage line, at the same time that the lower the cell pressure to zero. Drain the chamber water and disassemble the apparatus. Then, sketch the failed specimen. On the sketch, dimension the maximum and minimum diameters, the length of the specimen, and the angle of inclination of the failure plane should be taken if there is one. Alternatively, we can take a photo of the failed specimen.

3.5. Determination of Elastic Shear Modulus

In this study, the measurements of the shear wave velocities were divided into two phases: the measurements of shear wave velocities during consolidation of specimens, and the measurements of shear wave velocities during drained shearing of triaxial compression test. Two types of consolidation were performed, i.e. isotropic and anisotropic consolidations with K =1, 0.8, and 0.6. At each stress increment of consolidations, the travel time of shear wave was determined. The measurement of travel time had been continued until the desired stress increment (final stress increment) was reached. Then, the shearing phase was started at the strain rate of about 0.1 mm/min. During this shearing phase, the travel times of the shear wave were also determined at each regular reading. Continue the test until an axial strain of about 20% was reached.

The shear wave velocity can be determined by measuring the travel time of the shear wave (t) by using bender element test. The measuring method of travel time that suggested by Viggiania & Atkinson (1995) was adopted in this study as shown in Figure 3.6. The shear wave velocity V_S is calculated by using the equation (2.7), i.e. $V_s = L_{tt} / t$. From the shear wave velocity, the shear modulus can be calculated by equation (2.8), i.e. $G_{\max} = \rho V_s^2$ (See section 2.6).

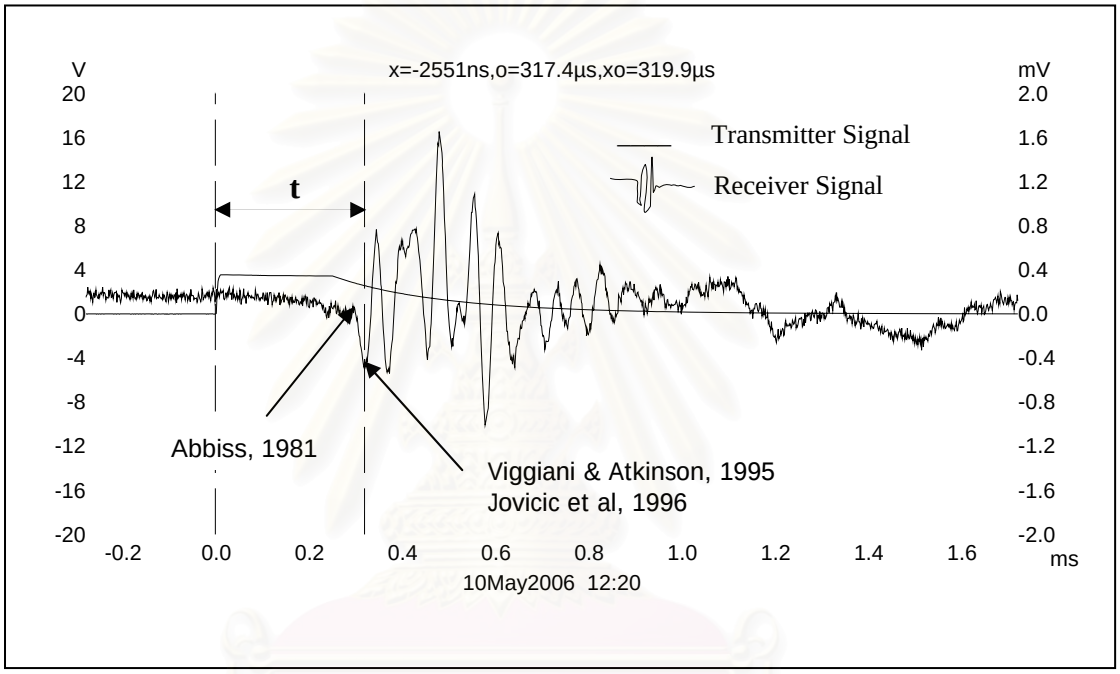

Figure 3.6: Oscilloscope signal from the bender element test with square pulse excitation for this study

3.6. Summary of Testing Program

In this study, the determination of shear modulus was performed in two phases: During consolidation and during shearing. Two conditions of specimens were used, i.e., loose specimens and dense specimens. The test program was summarized in the Table 3.1 below:

Table 3.1 Research testing program

Testing material	Initial conditions	Relative densities	Void ratios	series	$K = \frac{\sigma'_h}{\sigma'_v}$	Quantities	Total	Effective confining stress (Kpa)	Shearing
Ping river sand	Loose	$D_{r0} \approx 30\%$	$e_0 \approx 0.75$	**CID**	1	3	18	30 / 40 / 50 / 60 / 80 / 100	Yes
								30 / 40 / 50 / 100 / 150 / 200	Yes
								30 / 40 / 50 / 100 / 200 / 300	Yes
				CAD	0.8	3		30 / 40 / 50 / 60 / 80 / 100	Yes
								30 / 40 / 50 / 100 / 150 / 200	Yes
								30 / 40 / 50 / 100 / 200 / 300	Yes
					0.6	3		30 / 40 / 50 / 60 / 80 / 100	Yes
								30 / 40 / 50 / 100 / 150 / 200	Yes
								30 / 40 / 50 / 100 / 200 / 300	Yes
	Dense	$D_{r0} \approx 70\%$	$e_0 \approx 0.62$	**CID**	1	3		30 / 40 / 50 / 60 / 80 / 100	Yes
								30 / 40 / 50 / 100 / 150 / 200	Yes
								30 / 40 / 50 / 100 / 200 / 300	Yes
				CAD	0.8	3		30 / 40 / 50 / 60 / 80 / 100	Yes
								30 / 40 / 50 / 100 / 150 / 200	Yes
								30 / 40 / 50 / 100 / 200 / 300	Yes
					0.6	3		30 / 40 / 50 / 60 / 80 / 100	Yes
								30 / 40 / 50 / 100 / 150 / 200	Yes
								30 / 40 / 50 / 100 / 200 / 300	Yes

Considering the subject of the experimental study, the testing procedures can be outlined in the flowchart as shown in Figure 3.7 below:

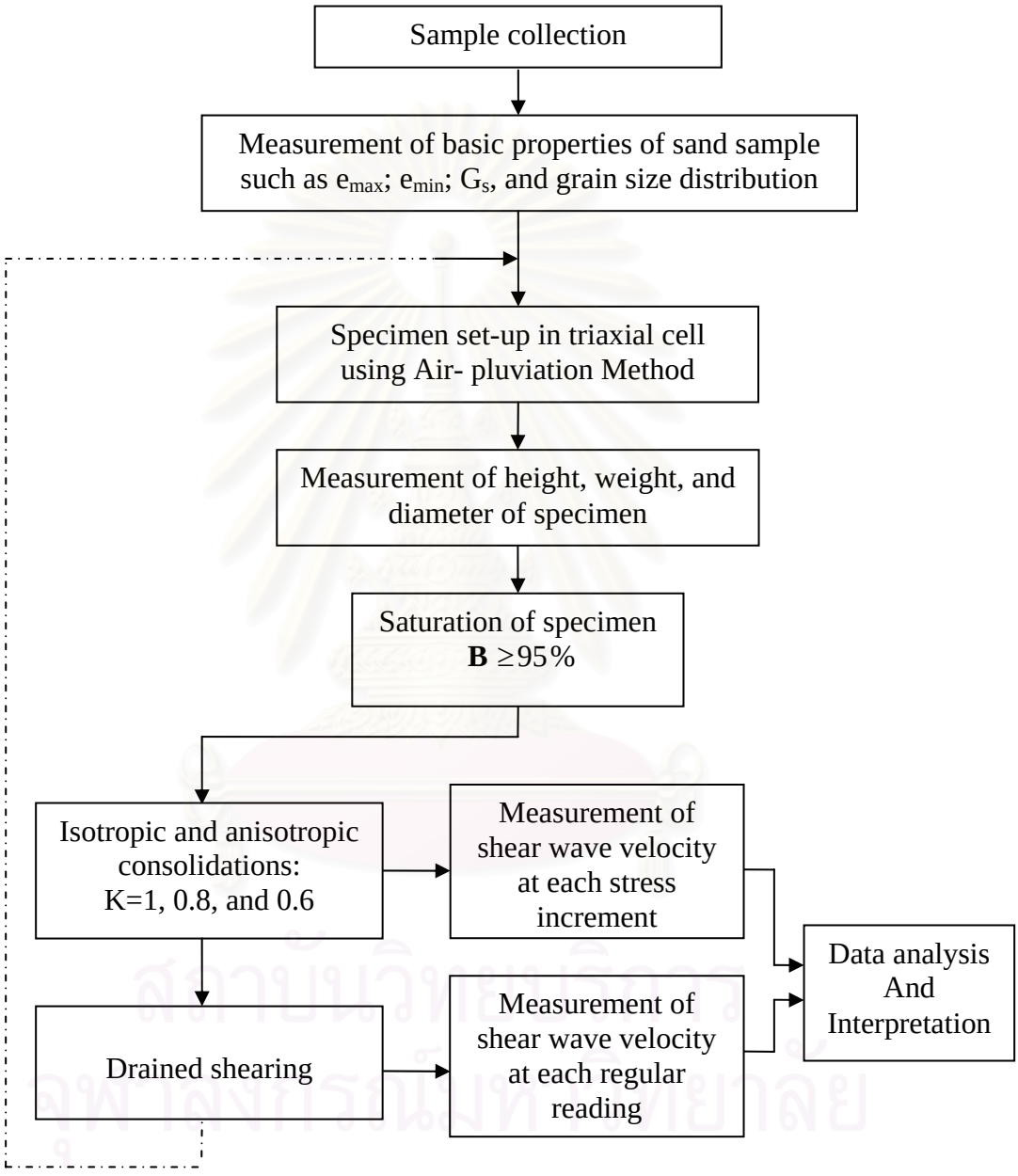

Figure 3.7: Schematic diagram of testing procedure

CHAPTER IV

RESULTS, ANALYSES AND DISCUSSIONS

4.1. Introduction

The results of the laboratory tests performed in this experimental study are presented in this chapter. A series of drained triaxial compression with bender element tests were carried out to determine the elastic shear modulus of saturated sand. Two types of sand specimens were used, i.e. loose and dense specimens. The values of G_{max} were considered during isotropic and anisotropic consolidations of specimens and during drained shearing. In this study, the following factors affecting elastic shear modulus were taken into account: mean effective stress, void ratio, deviator stress. The effect of localization of the specimen was also discussed.

Comparisons were made between the isotropically consolidated specimens and anisotropically consolidated specimens in order to examine the effect of stress - induced anisotropy on elastic shear modulus of saturated sand.

4.2. Physical Properties of Sand

According to the test results, the sand used in this study was poorly graded sand (SP). The physical properties and the grain size distribution curve of this sand are shown in Table 4.1 and Figure 4.1 respectively.

Table 4.1 Physical properties of sand

Sand name	Specific gravity	Diameter coresponding to 50 % finer	Coefficient of gradation	Uniformity coefficient	Miximum void ratio	Minimum void ratio
	G_s	D_{50}	C_z	C_u	e_{max}	e_{min}
Ping river sand	2.65	0.44	1.03	2.86	0.86	0.53

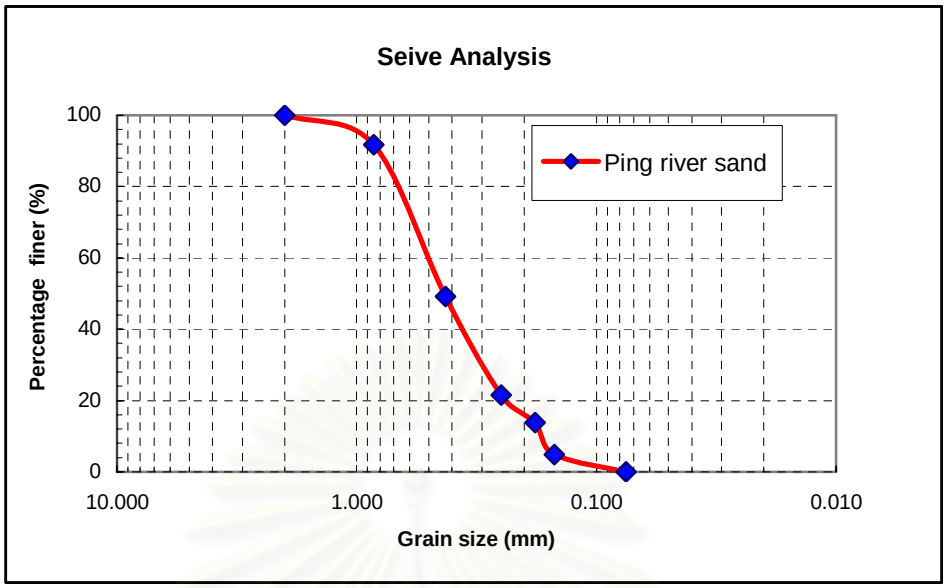

Figure 4.1: Grain size distribution of sand sample

The sand specimens of about 50 mm in diameter and 100 mm in height prepared by Air- pluviation method (as explained in the previous chapter) were used. In this study, there were two conditions of specimens: loose specimens with initial void ratio (e_o) ranging from 0.74 to 0.79, ρ_d from 1.48 – 1.52 g/cm^3, and relative density (D_r) from 20.8% to 35.4%; and medium dense specimens with e_o ranging from 0.60 to 0.63, ρ_d from 1.62 – 1.65 g/cm^3, and D_r from 69.4% to 77.6%. These values are tabulated in Table 4.2 below:

Table 4.2 Initial properties of tested sand specimens

conditions	Initial void ratio	Dry density	Relative density
	e_o	ρ_d	D_{r0}
		(g/cm^3)	(%)
Loose	0.77 ± 0.02	1.50 ± 0.02	28.1 ± 7.3
Dense	0.62 ± 0.01	1.64 ± 0.01	73.5 ± 4.1

4.3. Effect of Mean Effective Stress on Elastic Shear Modulus

According to test results, the elastic shear modulus increases significantly while the mean effective confining stress increases in both isotropic and anisotropic consolidations as shown in Figure 4.2 – 4.3. These results are in good agreement with previous researches such as Hardin & Richart, 1963; Hardin & Black, 1968; Koshuko, 1980; Jovicic & Coop, 1998; Zhou & Chen, 2005; and others.

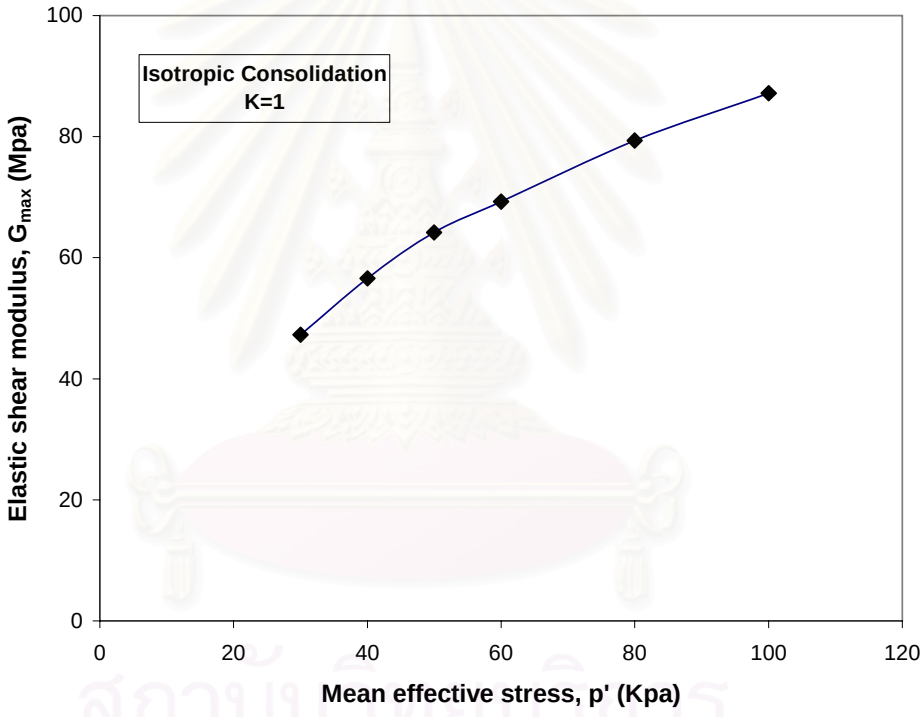

Figure 4.2: Effect of mean effective stress on shear modulus of sand during isotropic consolidation.

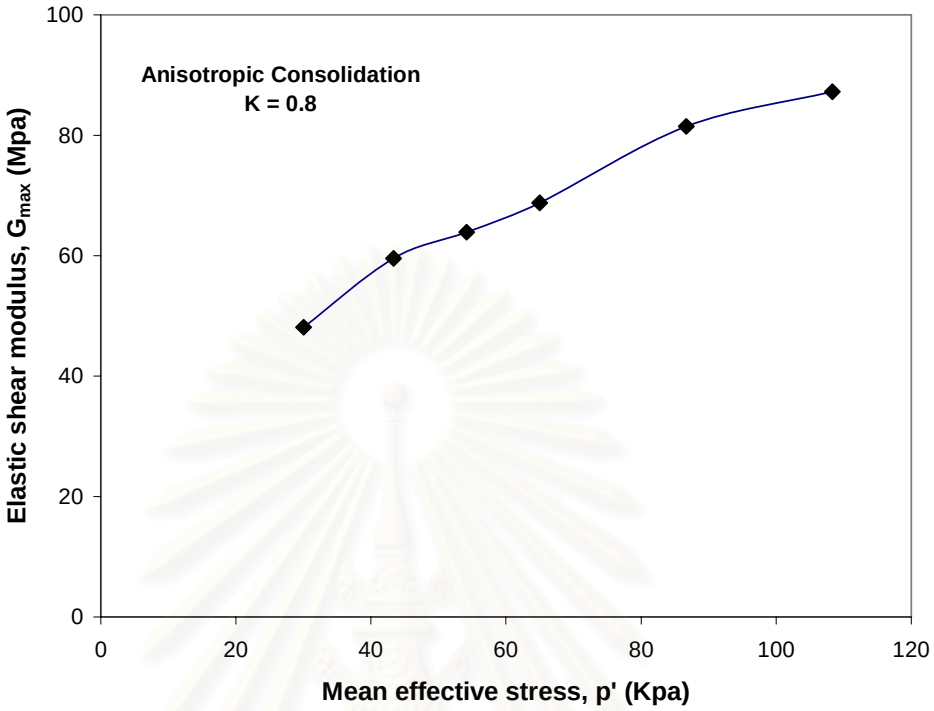

Figure 4.3: Effect of mean effective stress on shear modulus of sand during anisotropic consolidation.

4.4. Variation of Elastic Shear Modulus during Consolidations

In this study, to examine the effect of stress-induced anisotropy on elastic shear modulus of sands, a number of tests under isotropic and anisotropic consolidations with consolidation stress ratio $K = \sigma_h^{'} / \sigma_v^{'}$ were carried out. The values of *K* studied were 1, 0.8, 0.6; and the specimens used were loose and medium dense. The original test data of G_{max} against the mean effective stress of both isotropic and anisotropic tests were plotted. Moreover, to eliminate the effect of void ratio non-uniformity, G_{max} was further divided by void ratio function F (e). The results of the tests were plotted in Figure 4.4 – 4.9 for loose specimens, and Figure 4.10 – 4.15 for dense specimens.

Based on the findings in Figure 4.4 – 4.15, the data show that the value of G_{max} increases almost linearly when the mean effective stress increases in both isotropic and anisotropic tests. This behavior is the same for loose and dense specimens. However, at the same mean effective stress, the value of G_{max} measured in the dense specimens is larger than the one in loose specimens. This is due to the different initial densities.

To investigate the effect of consolidation stress ratio, the data from isotropic and anisotropic consolidation tests were plotted in the same graph as shown in Figure 4.4 – 4.15. The observation indicates that at the same value of mean effective stress the value of G_{max} trend to decrease very slightly when the value of *K* decreases, i.e. $G_{max} : K = 1 > G_{max} : K = 0.8 > G_{max} : 0.6$. This trend agrees with the previous studies by Yu & Richart (1984); and also Bellotti *et al* (1996). However, Yu & Richart (1984); and Bellotti *et al* (1996) had concluded that the reduction of G_{max} can be observed when $K < 0.5$ *or* $K > 2$ compression and extension consolidation stress paths respectively. There is no effect of consolidation stress ratio if $K > 0.5$.

.

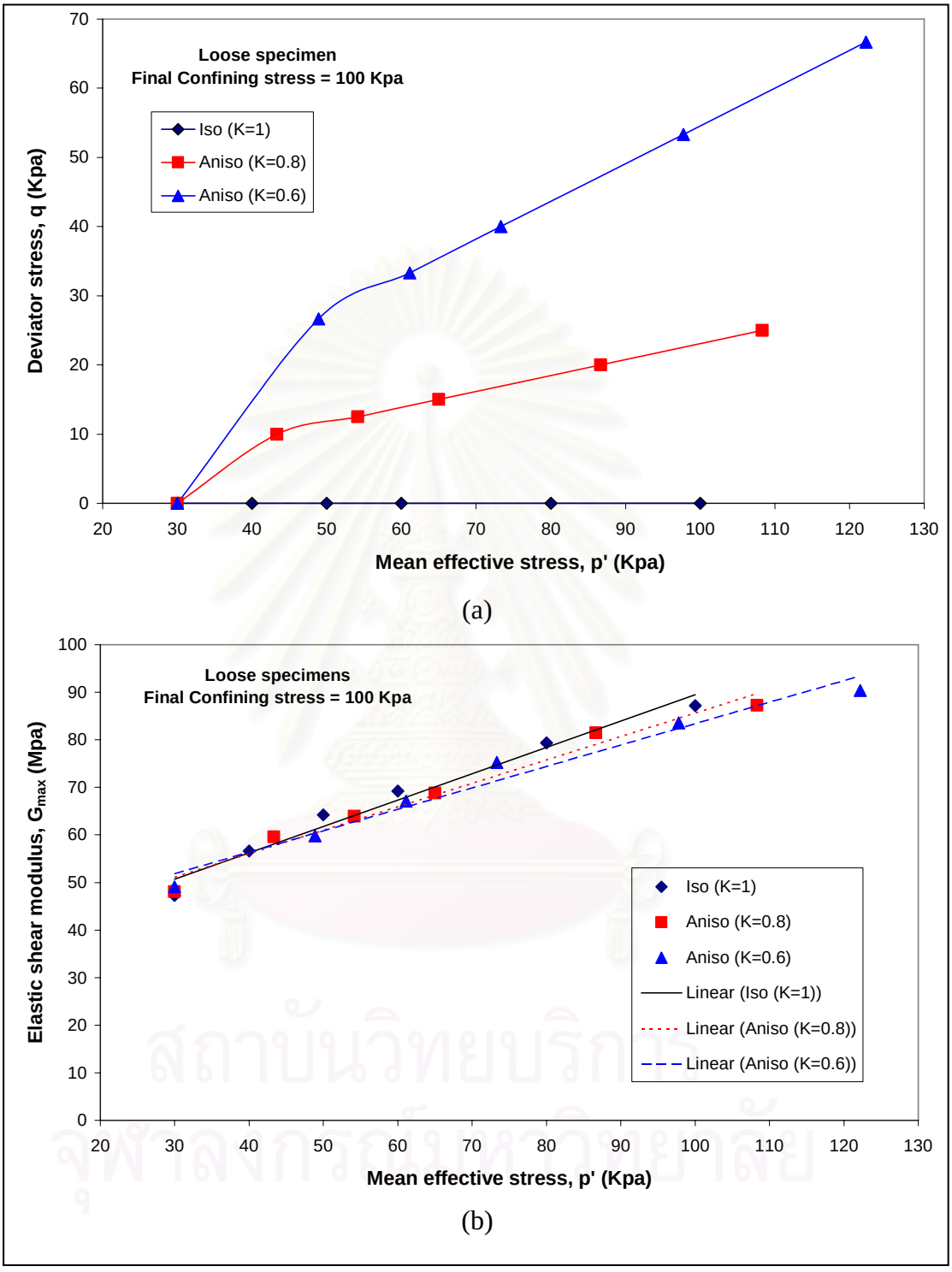

Figure 4.4: (a) Effective stress paths at which bender element tests were performed

(b) Variation of G_{max} during consolidations against P' with different consolidation stress ratio for loose specimens at final confining stress = 100 Kpa

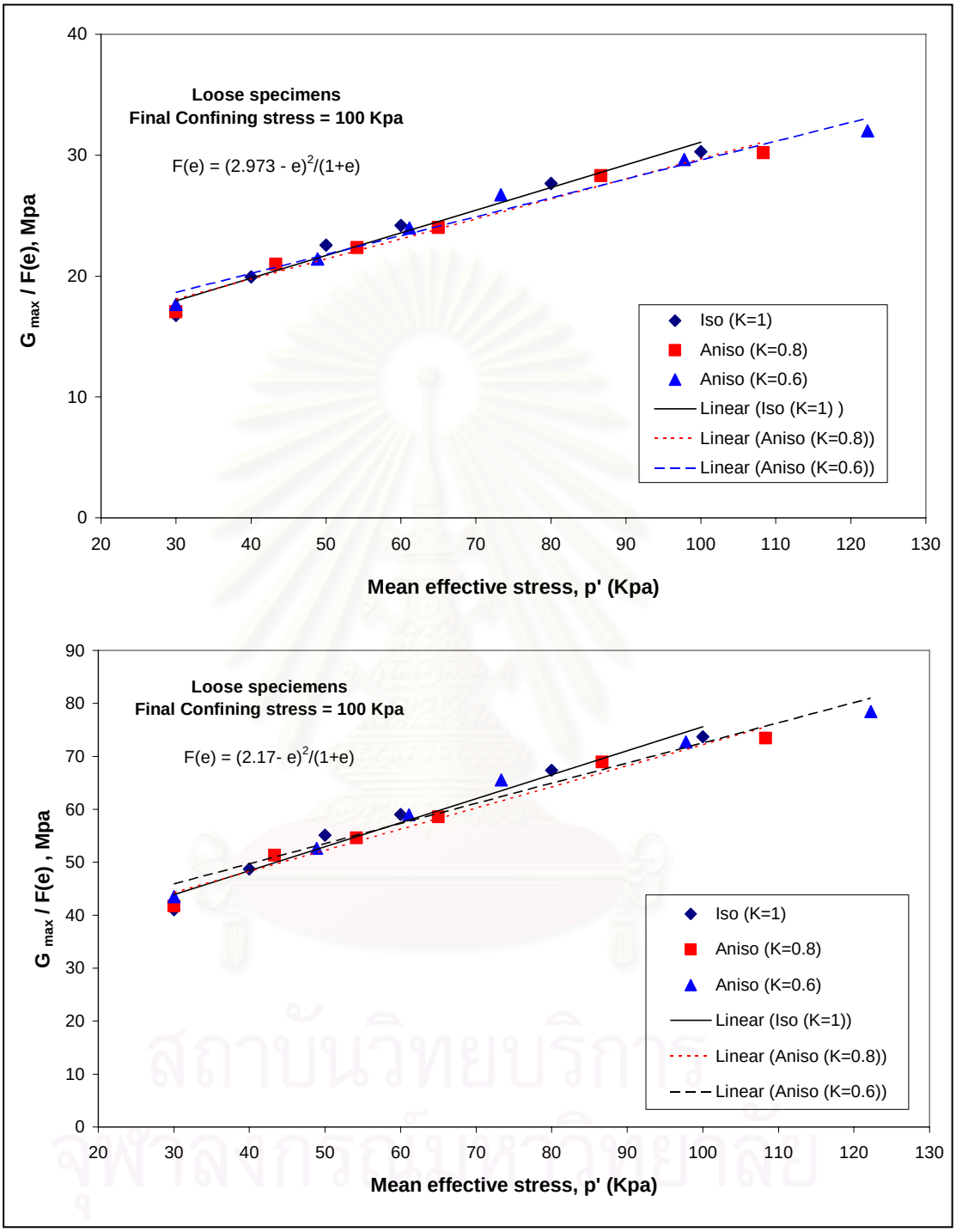

Figure 4.5: Variation of $G_{max} / F(e)$ during consolidations against P' with different consolidation stress ratio for loose specimens at final confining stress = 100 Kpa

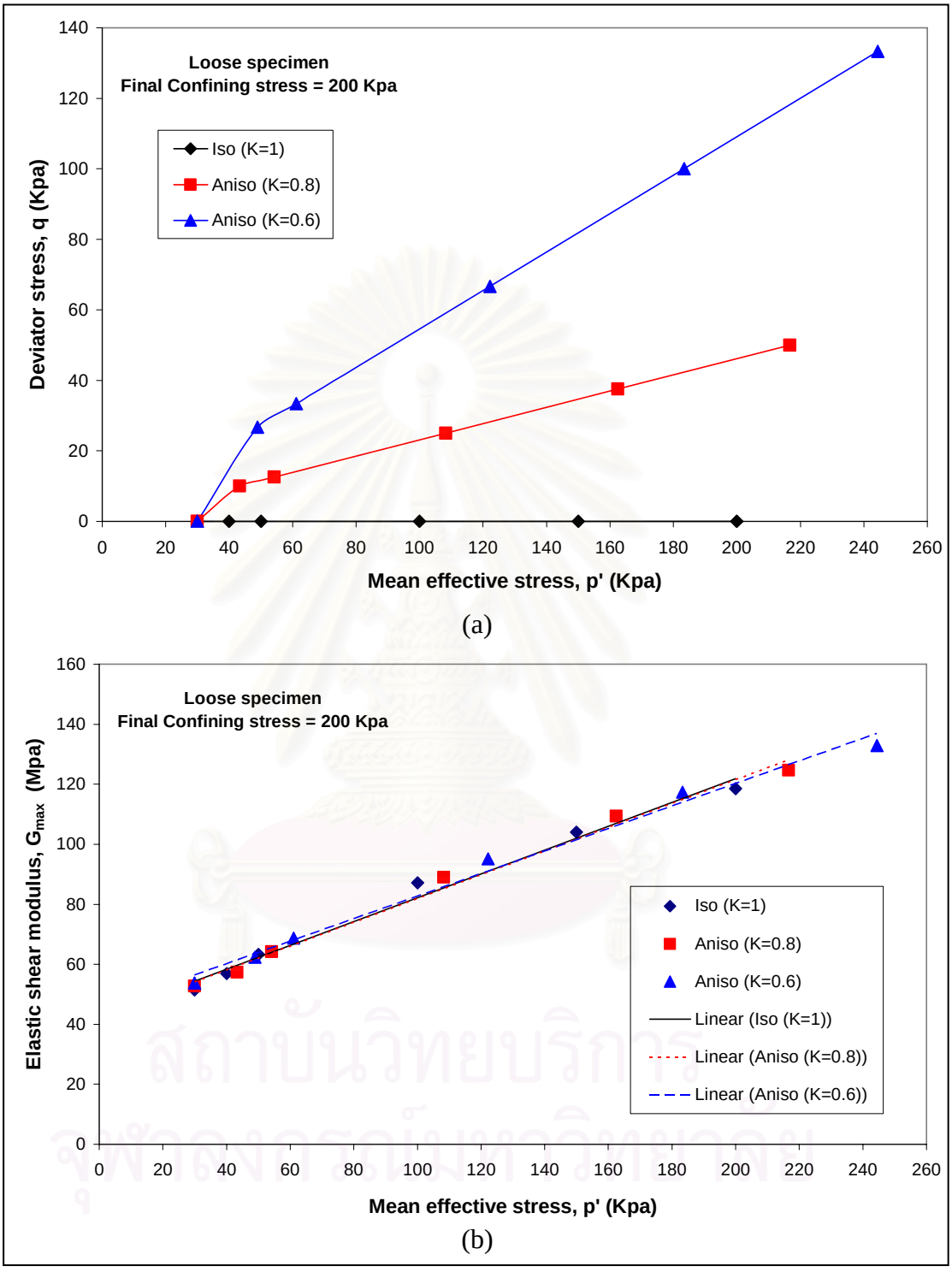

Figure 4.6: (a) Effective stress paths at which bender element tests were performed

(b) Variation of G_{max} during consolidations against P' with different consolidation stress ratio for loose specimens at final confining stress = 200 Kpa

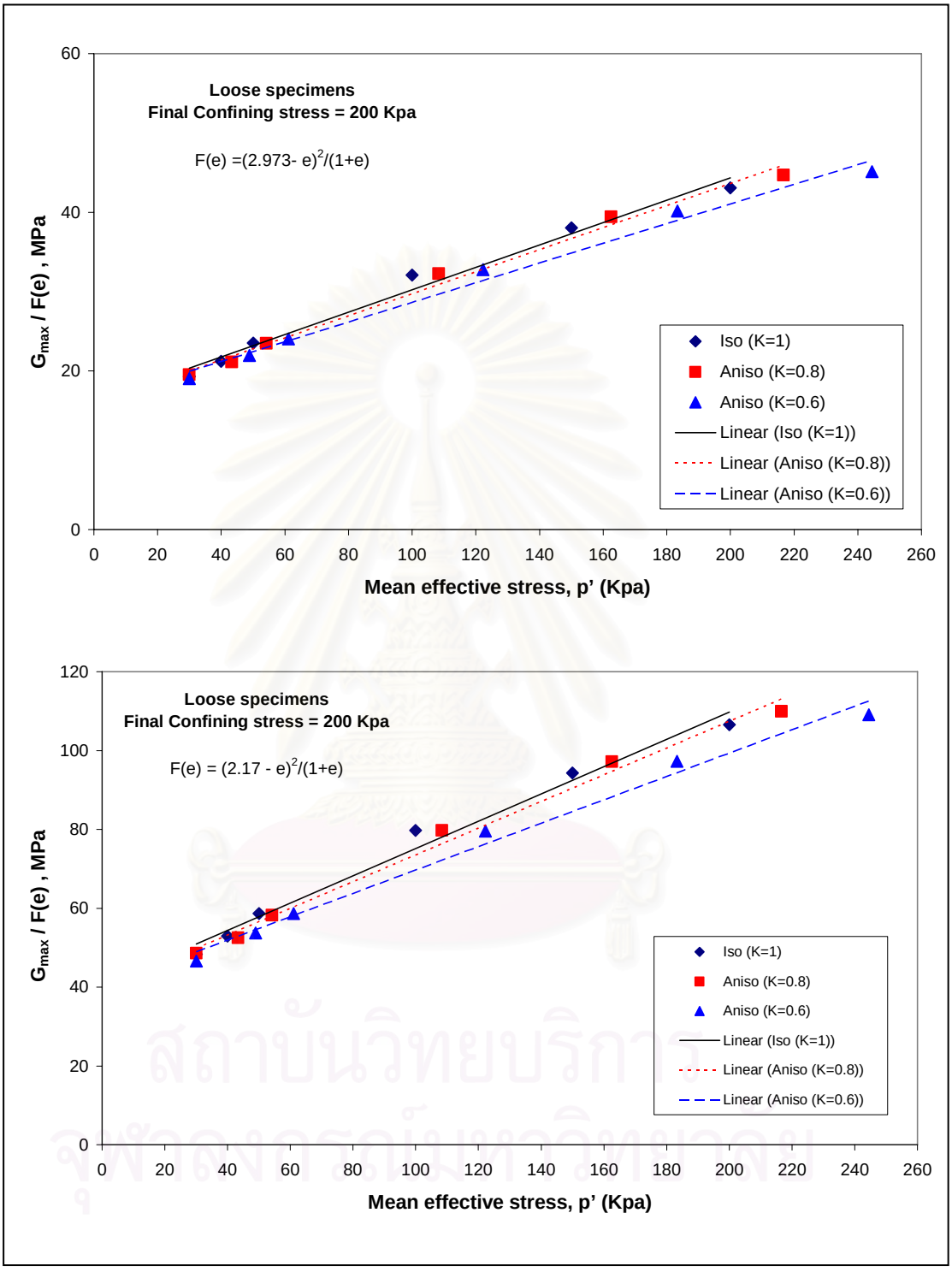

Figure 4.7: Variation of $G_{max} / F(e)$ during consolidations against P' with different consolidation stress ratio for loose specimens at final confining stress = 200 Kpa

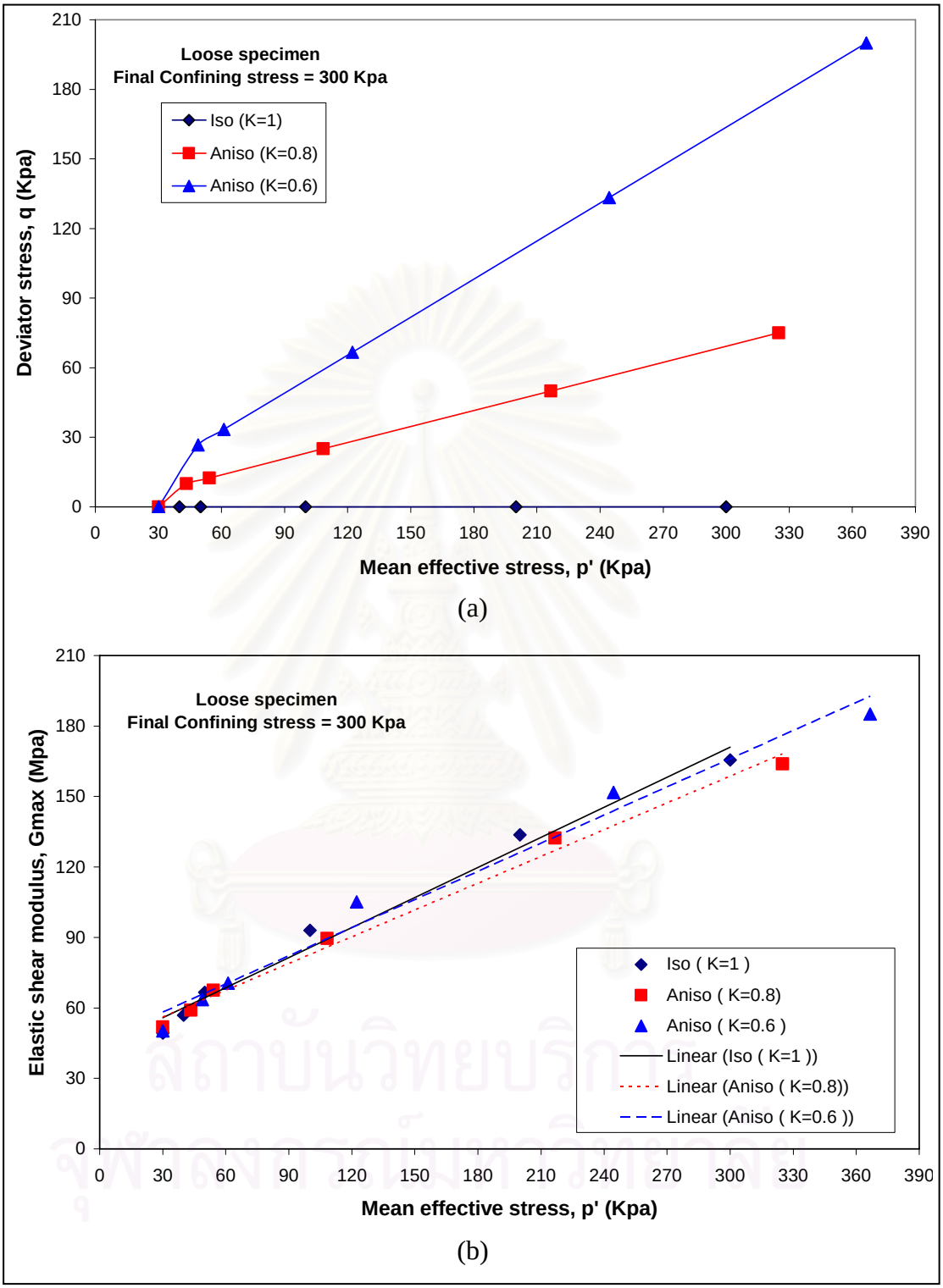

Figure 4.8: (a) Effective stress paths at which bender element tests were performed

(b) Variation of G_{max} during consolidations against P' with different consolidation stress ratio for loose specimens with final confining stress = 300 Kpa

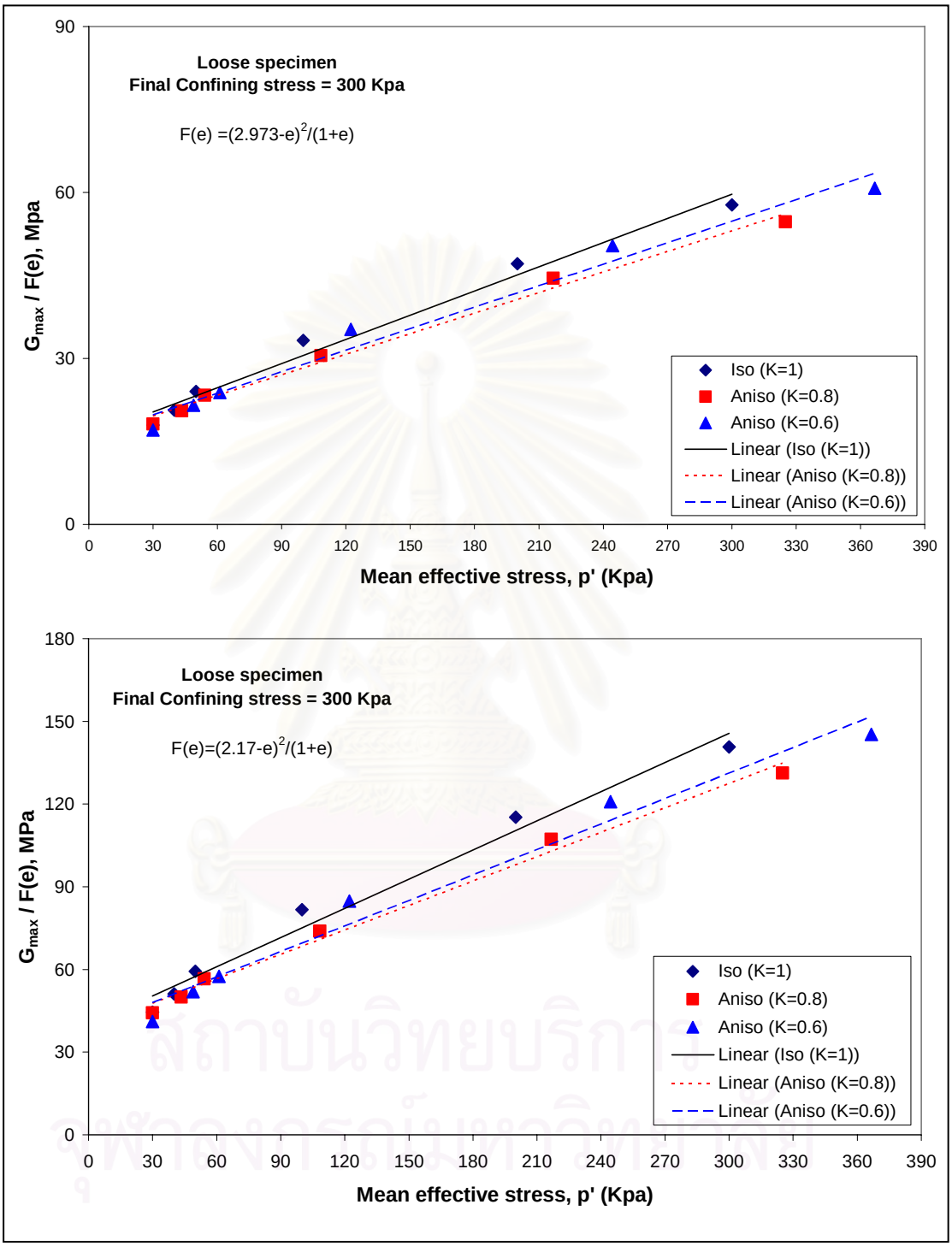

Figure 4.9: Variation of $G_{max} / F(e)$ during consolidations against P' with different consolidation stress ratio for loose specimens with final confining stress = 300 Kpa

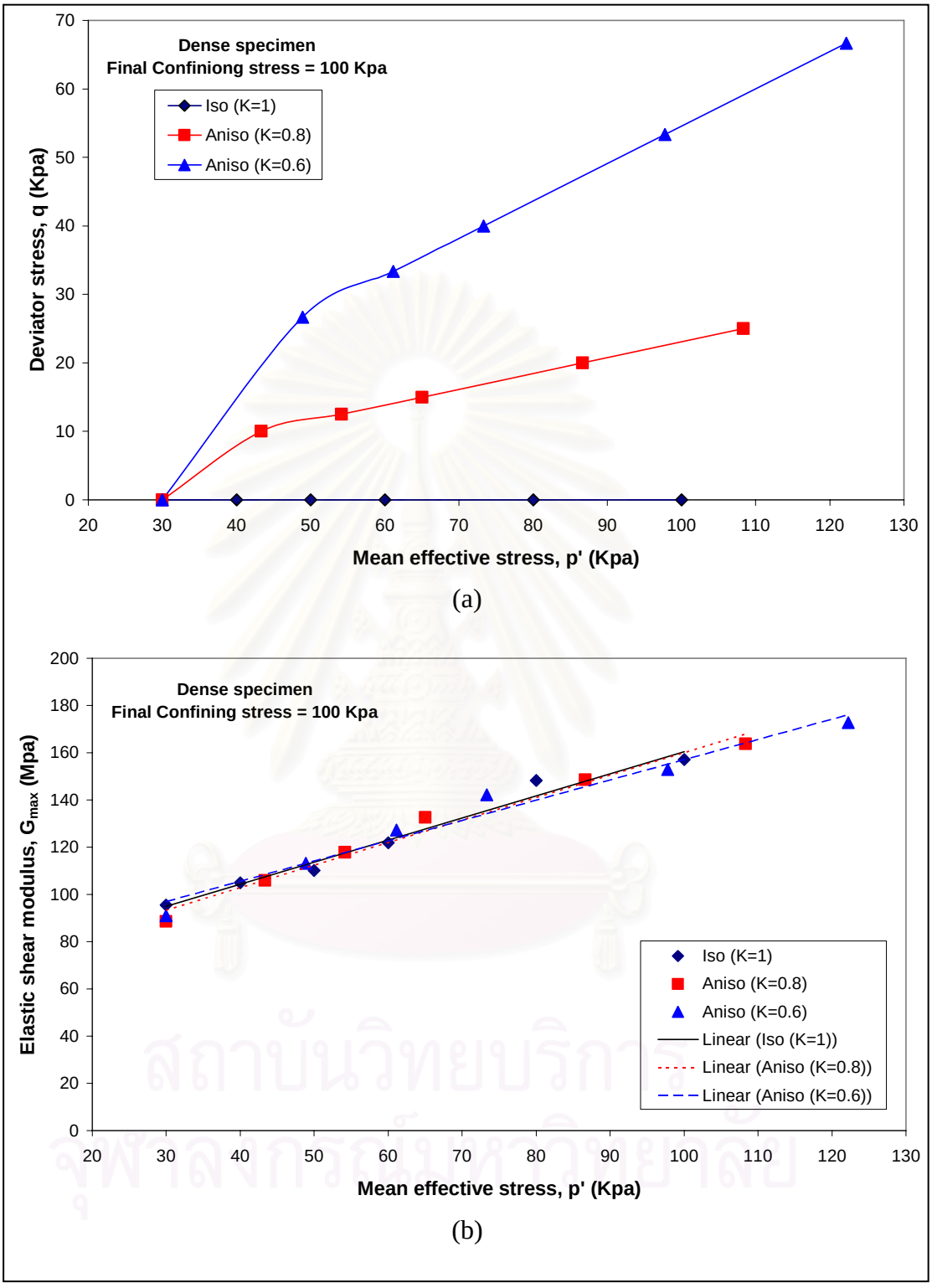

Figure 4.10: (a) Effective stress paths at which bender element tests were performed

(b) Variation of G_{max} during consolidations against P' with different consolidation stress ratio for dense specimens at final confining stress = 100 Kpa

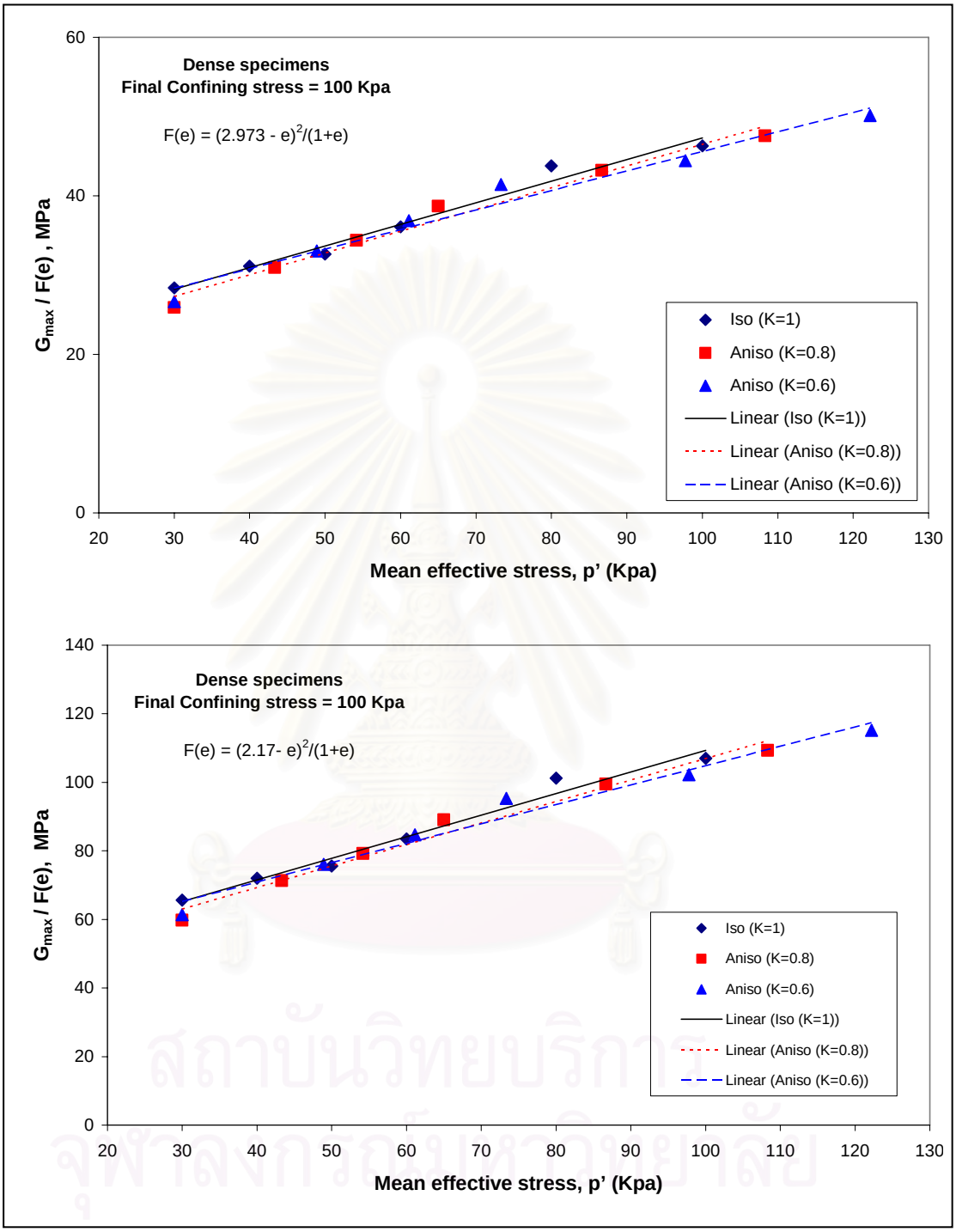

Figure 4.11: Variation of $G_{max} / F(e)$ during consolidations against P' with different consolidation stress ratio for dense specimens at final confining stress = 100 Kpa

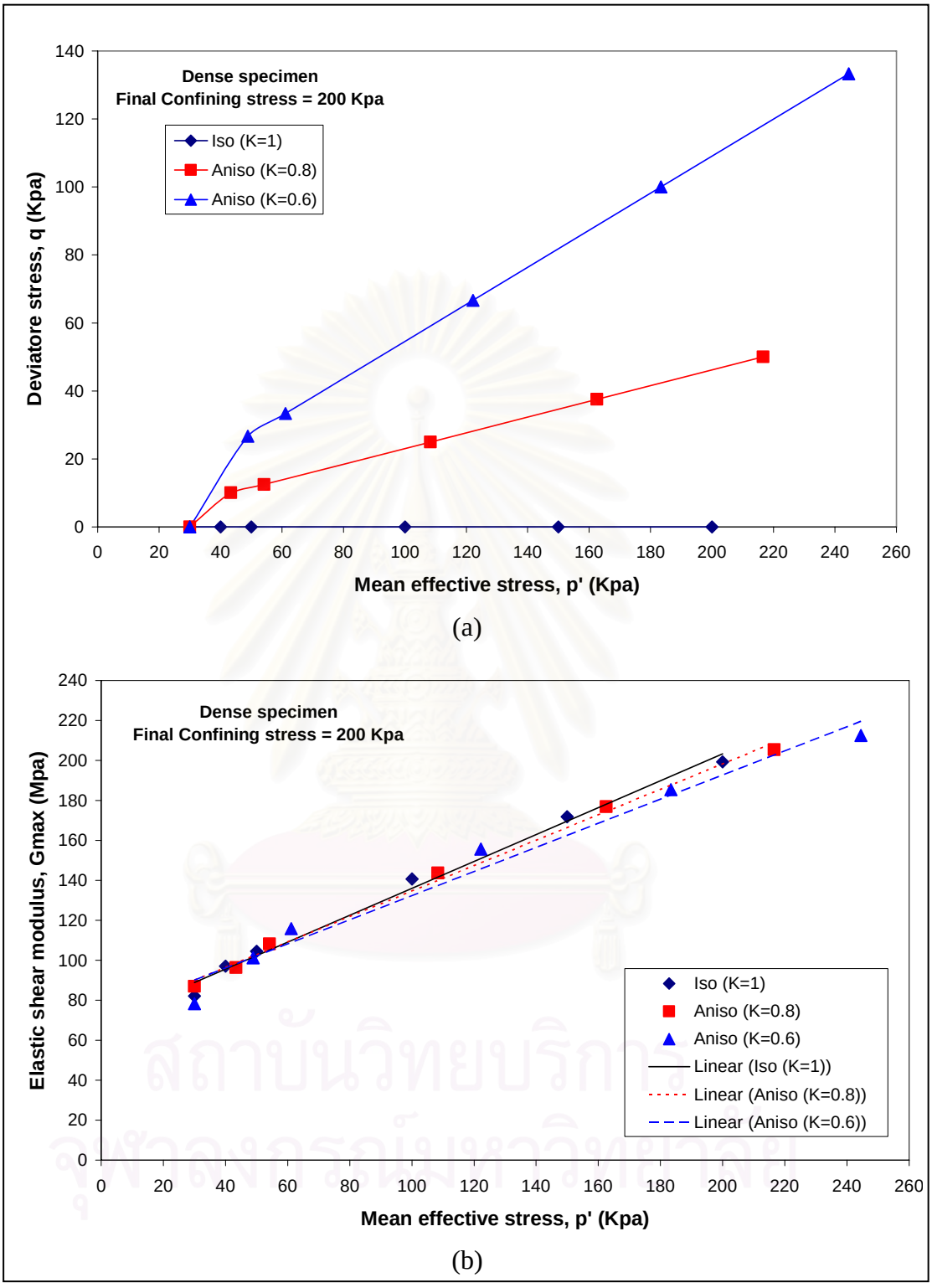

Figure 4.12: (a) Effective stress paths at which bender element tests were performed

(b) Variation of G_{max} during consolidations against P' with different consolidation stress ratio for dense specimens at final confining stress = 200 Kpa

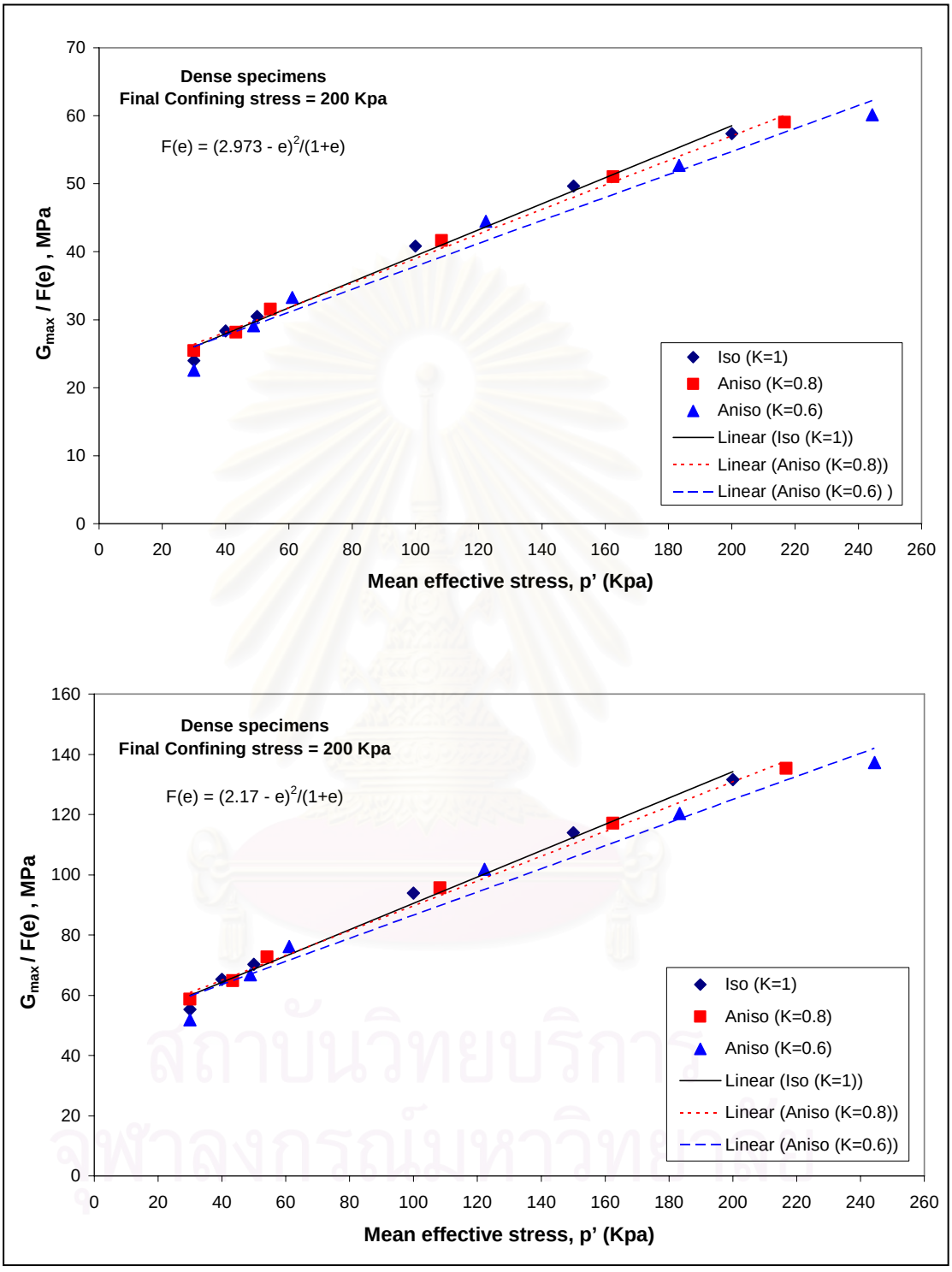

Figure 4.13: Variation of $G_{max} / F(e)$ during consolidations against P' with different consolidation stress ratio for dense specimens at final confining stress = 200 Kpa

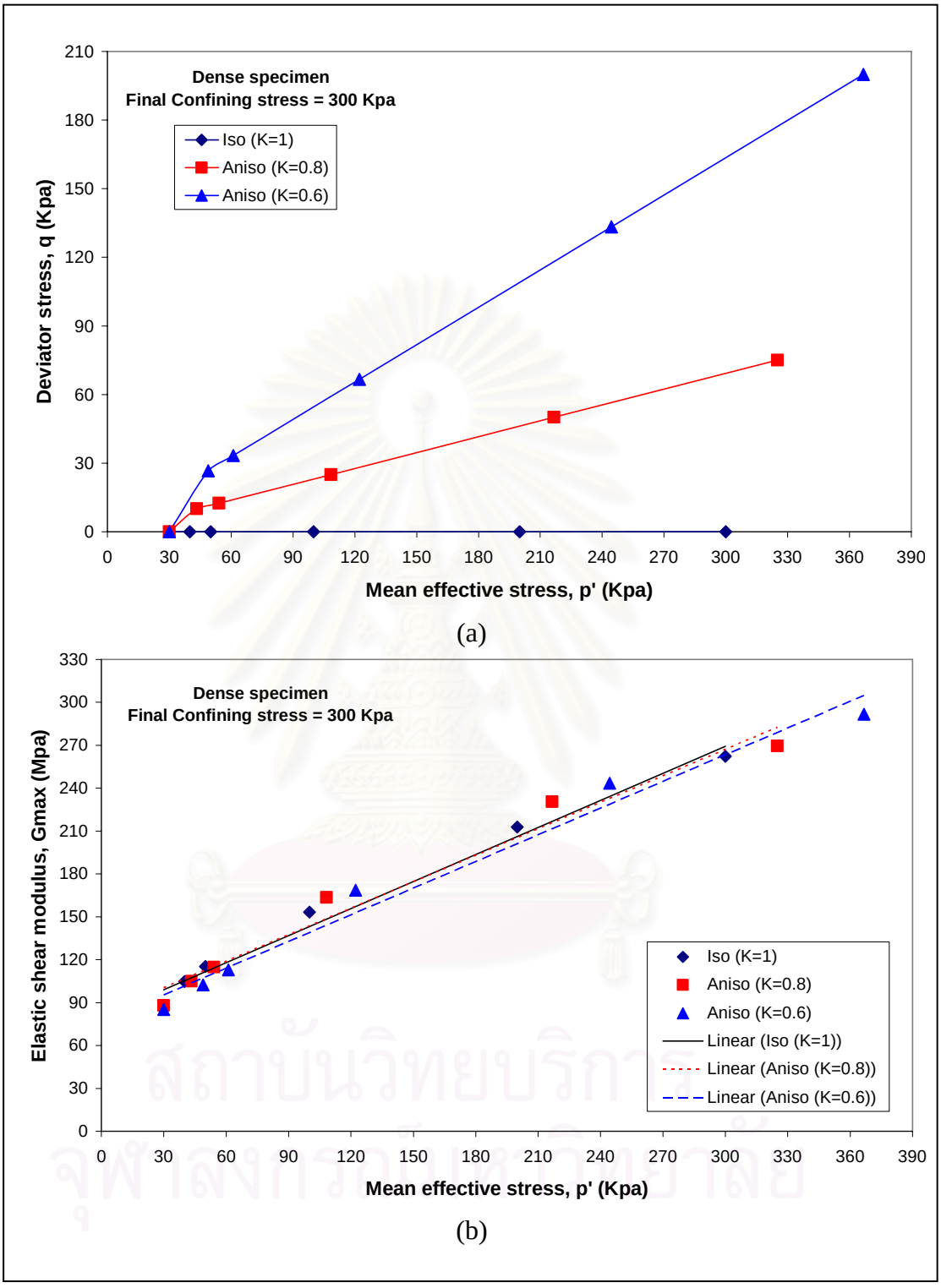

Figure 4.14: (a) Effective stress paths at which bender element tests were performed

(b) Variation of G_{max} during consolidations against P' with different consolidation stress ratio for dense specimens at final confining stress = 300 Kpa

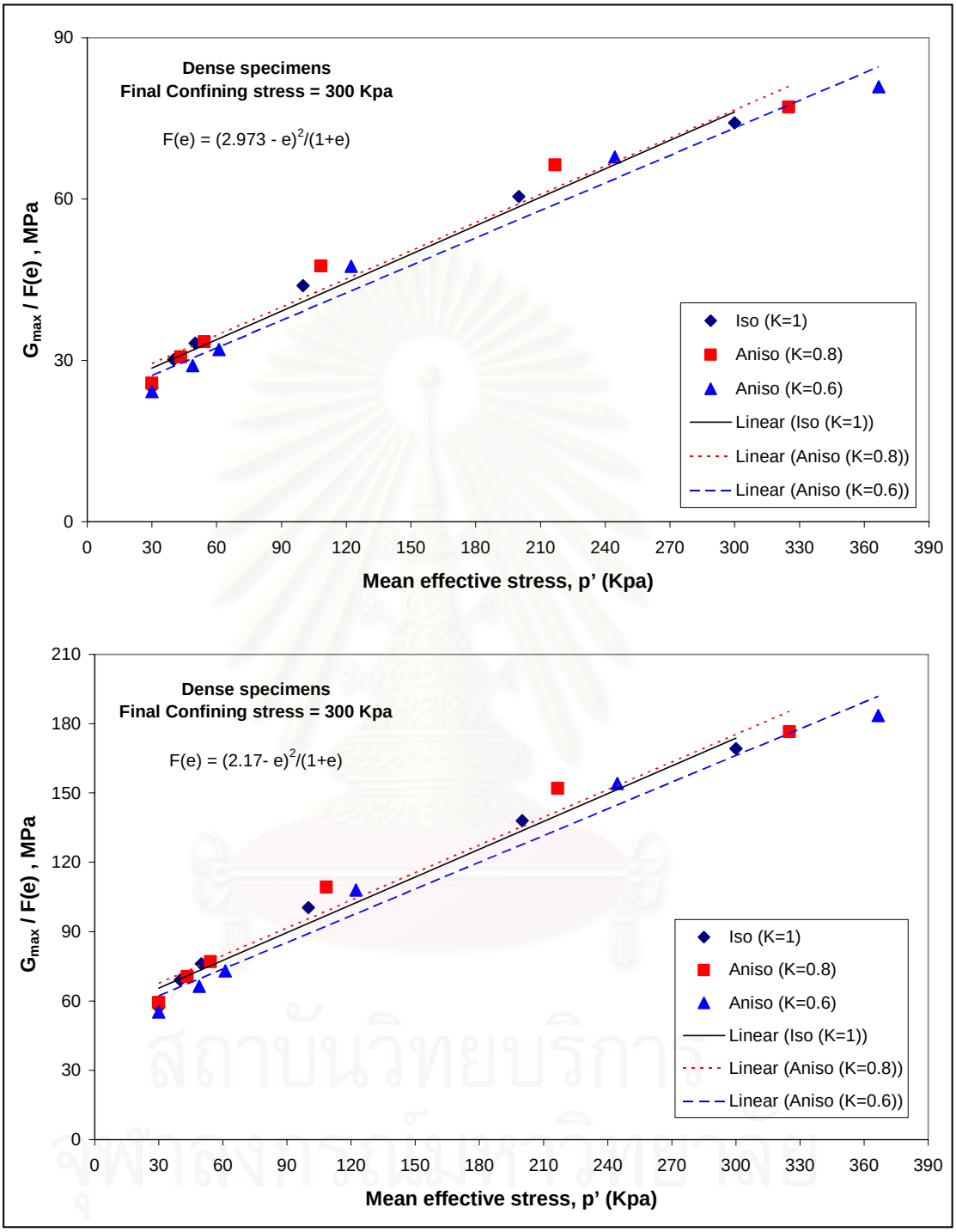

Figure 4.15: Variation of $G_{max} / F(e)$ during consolidations against P' with different consolidation stress ratio for dense specimens at final confining stress = 300 Kpa

4.5. Variation of Elastic Shear Modulus during Shearing

In this study, the drained triaxial compression tests on sand were performed. After the consolidation phase had been finished, the sand specimens were sheared under drained condition, i.e. all drainage valves were opened during shearing. In this shearing phase, the travel times of the shear wave were determined at each regular reading of triaxial compression test (see section 3.5 for details), and each of the tests was continued until an axial strain of about 20% attained.

Like mentioned before, in this experimental study two conditions of specimens were used: loose and medium dense specimens. These specimens were consolidated under different consolidation stress ratios (K=1, 0.8, and 0.6), and were sheared at different final confining stresses (100; 200; and 300 Kpa). Then the data of these tests were presented by plotting the values of G_{max} against mean effective stress p' as shown in Figure 4.16 – 4.27. These figures consist of the graph showing the effective stress paths [$q = \sigma_1^{'} - \sigma_3^{'}$ versus $p' = (\sigma_1^{'} + 2\sigma_3^{'})/3$] which bender element tests were performed and corresponding values of G_{max} against p' during consolidations and shearing phases. In p'–q plots, the solid lines and hollow lines represent the p'–q stress paths during consolidations and during shearing, respectively. On the other hand, in the $G_{max} - p'$ plots, the solid lines represent the $G_{max} - p'$ paths during consolidations and hollow lines represent $G_{max} - p'$ paths during drained triaxial compression tests on sand.

Figure 4.16 – 4.21 show the variation of G_{max} under different consolidation stress ratios, but shearing at the same final confining stresses. It can be seen that the variation of G_{max} obtained during isotropic and anisotropic shearing are almost similar. However, some of the tests as in Figure 4.18 and Figure 4.20 have shown that the values of G_{max} that obtained from anisotropic tests tend to decrease a little bit. These data also show that the paths of elastic shear modulus during drained shearing phase almost follow the paths of elastic shear modulus obtained during consolidations

phase. It means that the effect of the deviator stress, *q*, on elastic shear modulus is relatively small.

Figure 4.22 – 4.27 show the variation of G_{max} under the same consolidation stress ratio, but the final confining stresses were varied from 100, 200, and 300 Kpa. Based on observation, the values of G_{max} increase with an increase of mean effective stress in both isotropic and anisotropic tests. Also the $G_{max} - p'$ paths during drained shearing phase almost follow those achieved during consolidations phase as well.

This behavior is clearly shown in Figure 4.28. It shows the data from all of the specimens tested in this experimental study. In this figure, it should be noted that the reduction of G_{max} from all tests can be observed obviously when the deviator stress, *q*, approaches its peak value. This behavior was also stated in previous researches by Viggiani & Atkinson (1995), and Teachavorasinskun & Amornwithayalax (2002). This matter will be explained in details in section 4.6 later.

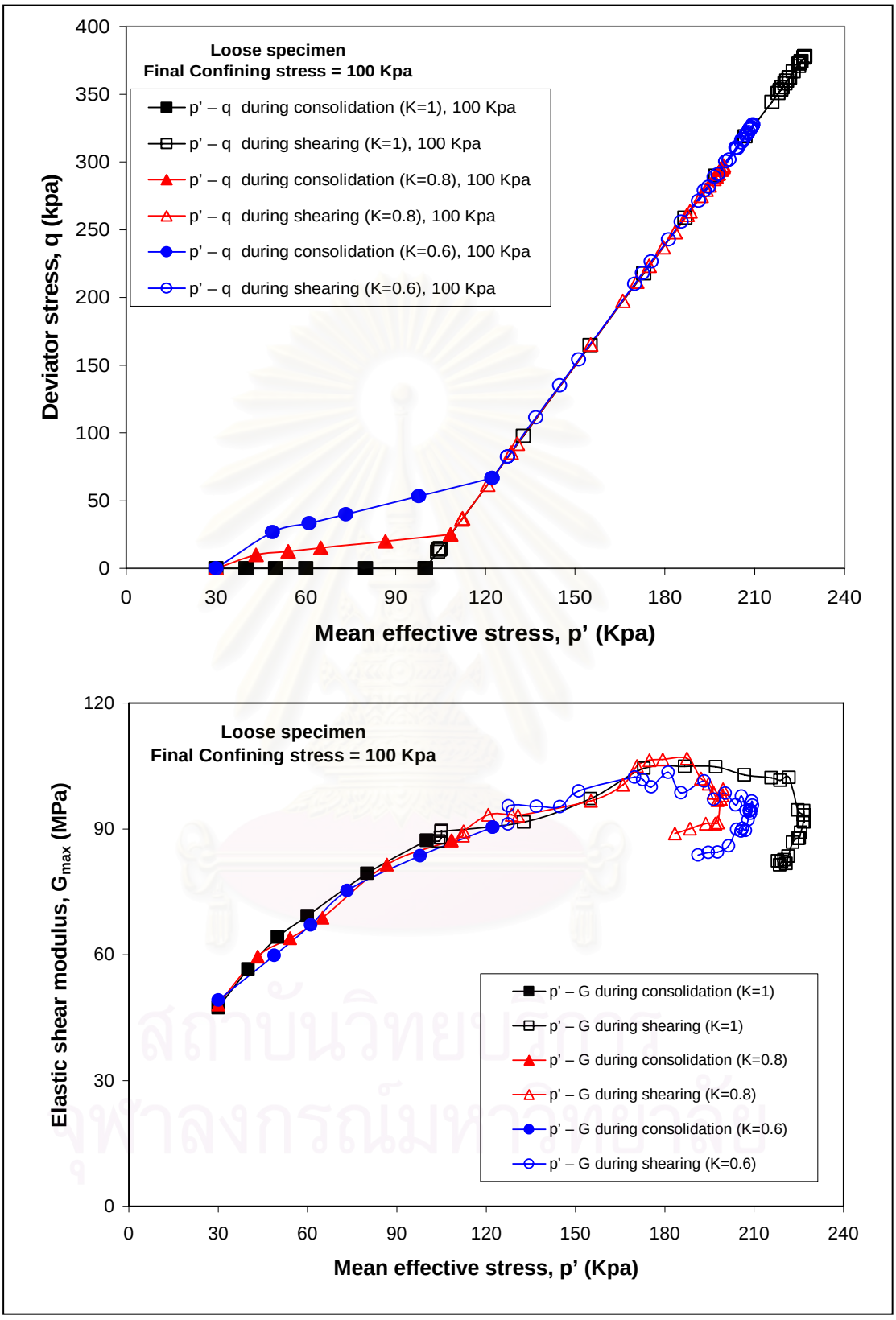

Figure 4.16: Variation of G_{max} against P' during consolidations and drained shearing at final confining stress = 100 Kpa for loose specimens (K=1; 0.8; and 0.6)

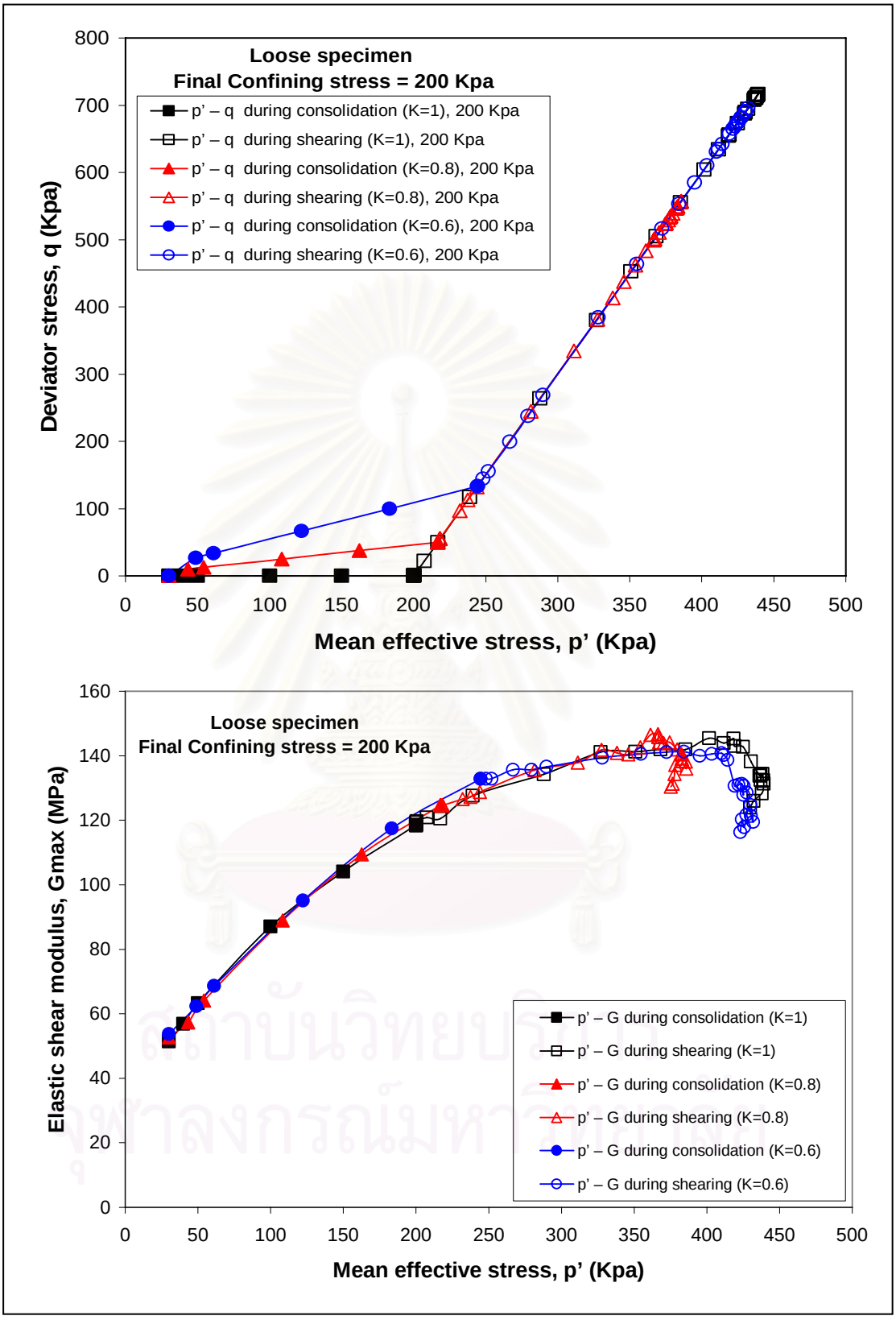

Figure 4.17: Variation of G_{max} against P' during consolidations and drained shearing at final confining stress = 200 Kpa for loose specimens (K=1; 0.8; and 0.6)

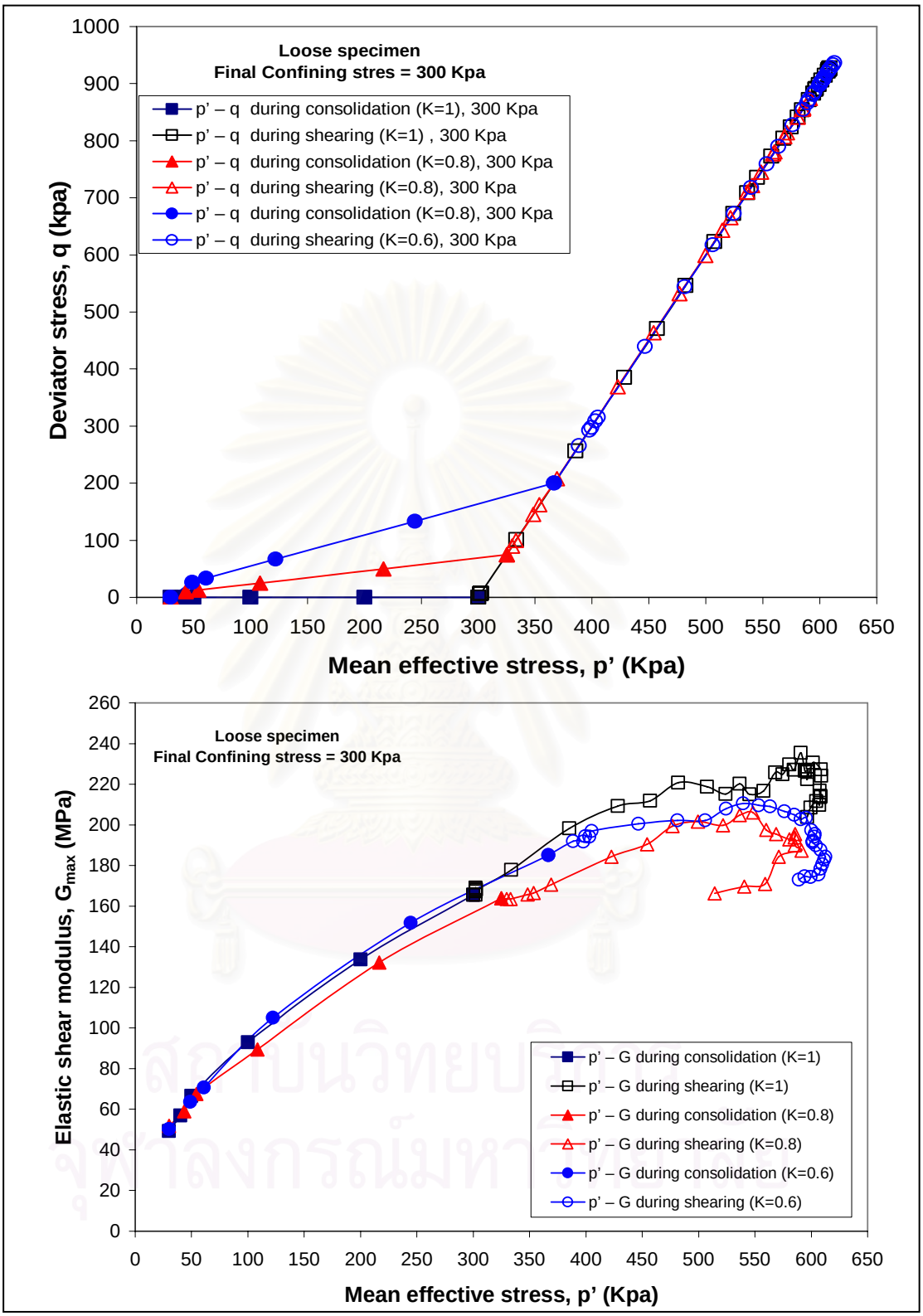

Figure 4.18: Variation of G_{max} against P' during consolidations and drained shearing at final confining stress = 300 Kpa for loose specimens (K=1; 0.8; and 0.6)

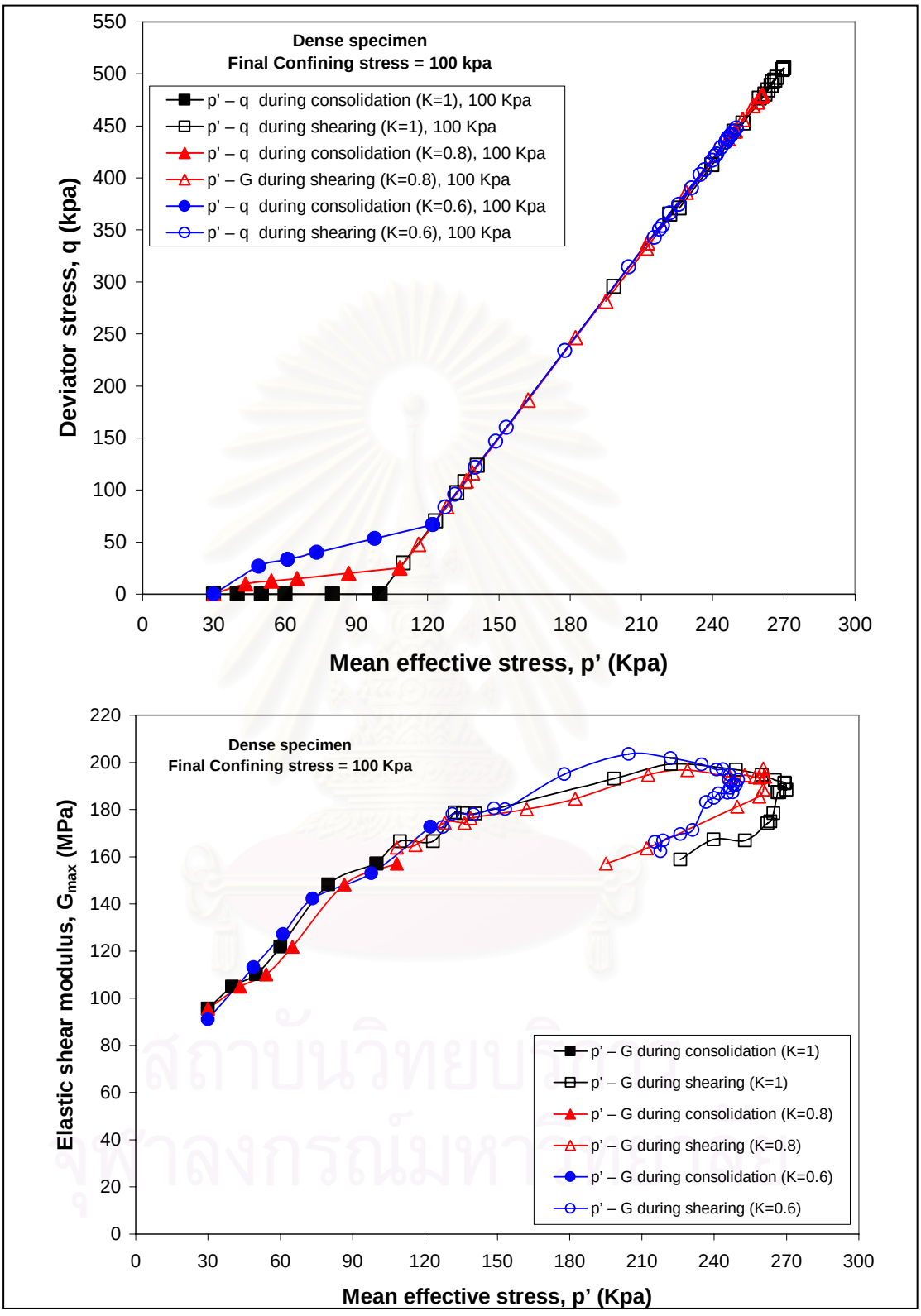

Figure 4.19: Variation of G_{max} against P' during consolidations and drained shearing at final confining stress = 100 Kpa for dense specimens (K=1; 0.8; and 0.6)

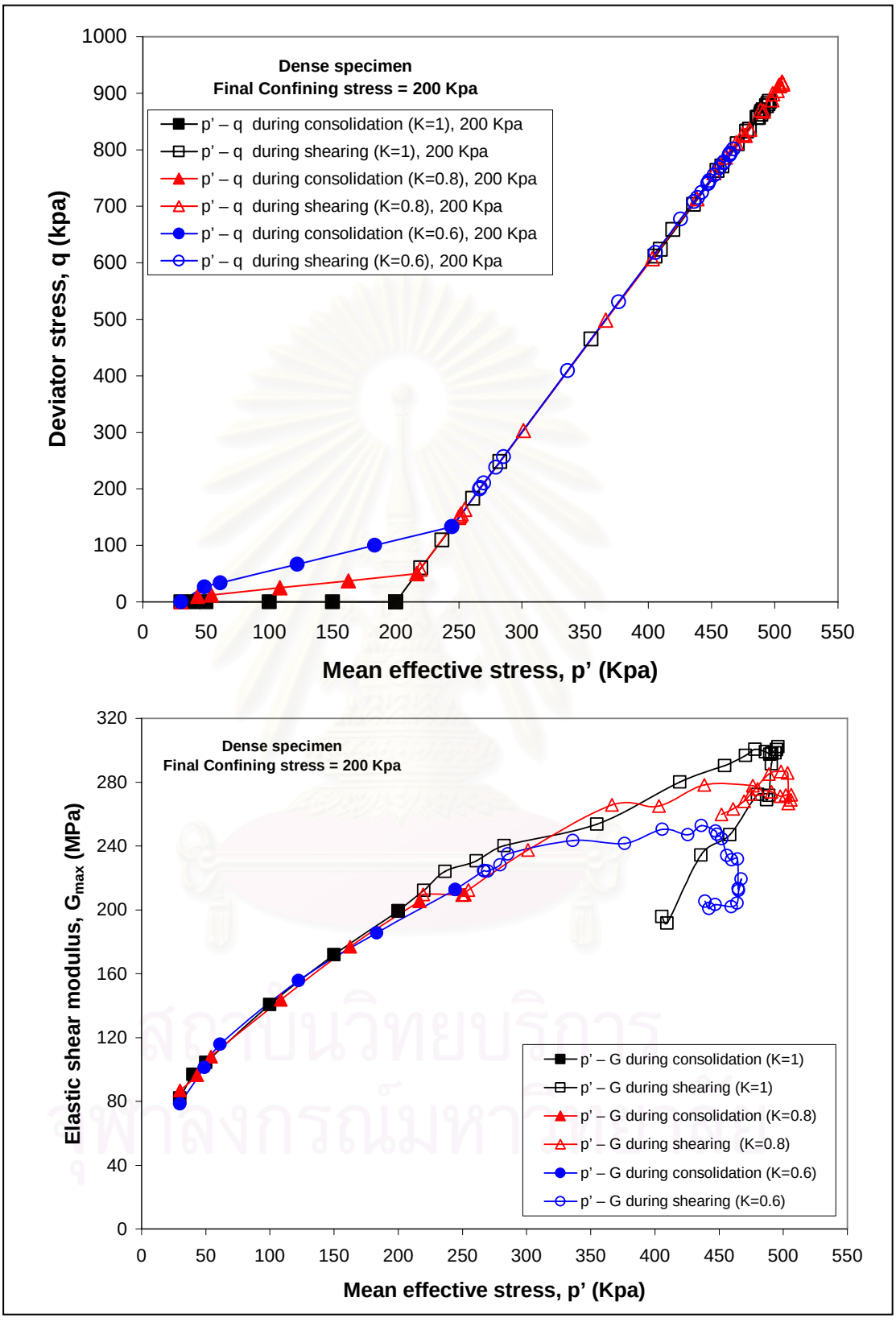

Figure 4.20: Variation of G_{max} against P' during consolidations and drained shearing at final confining stress = 200 Kpa for dense specimens (K=1; 0.8; and 0.6)

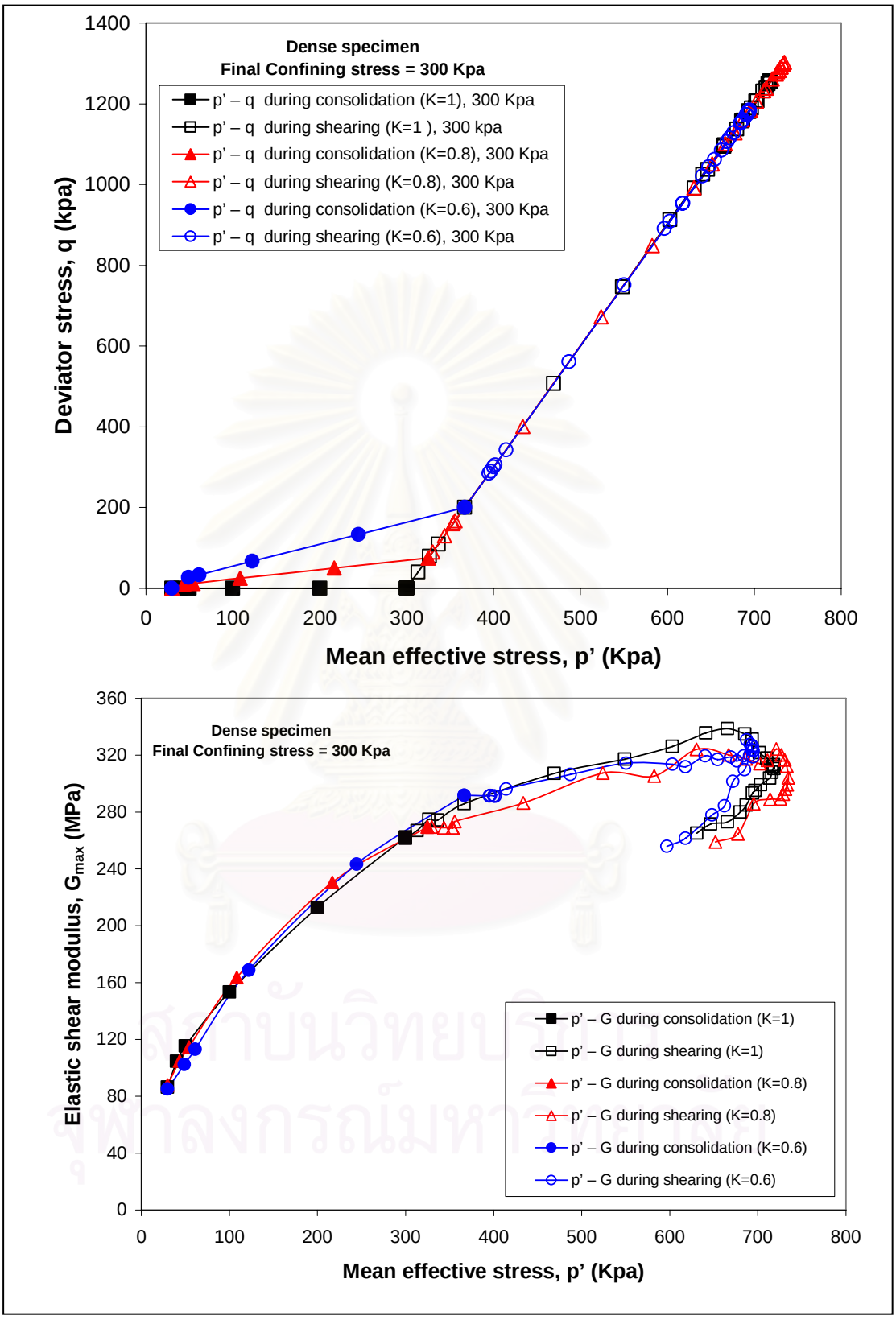

Figure 4.21: Variation of G_{max} against P' during consolidations and drained shearing at final confining stress = 300 Kpa for dense specimens (K=1; 0.8; and 0.6)

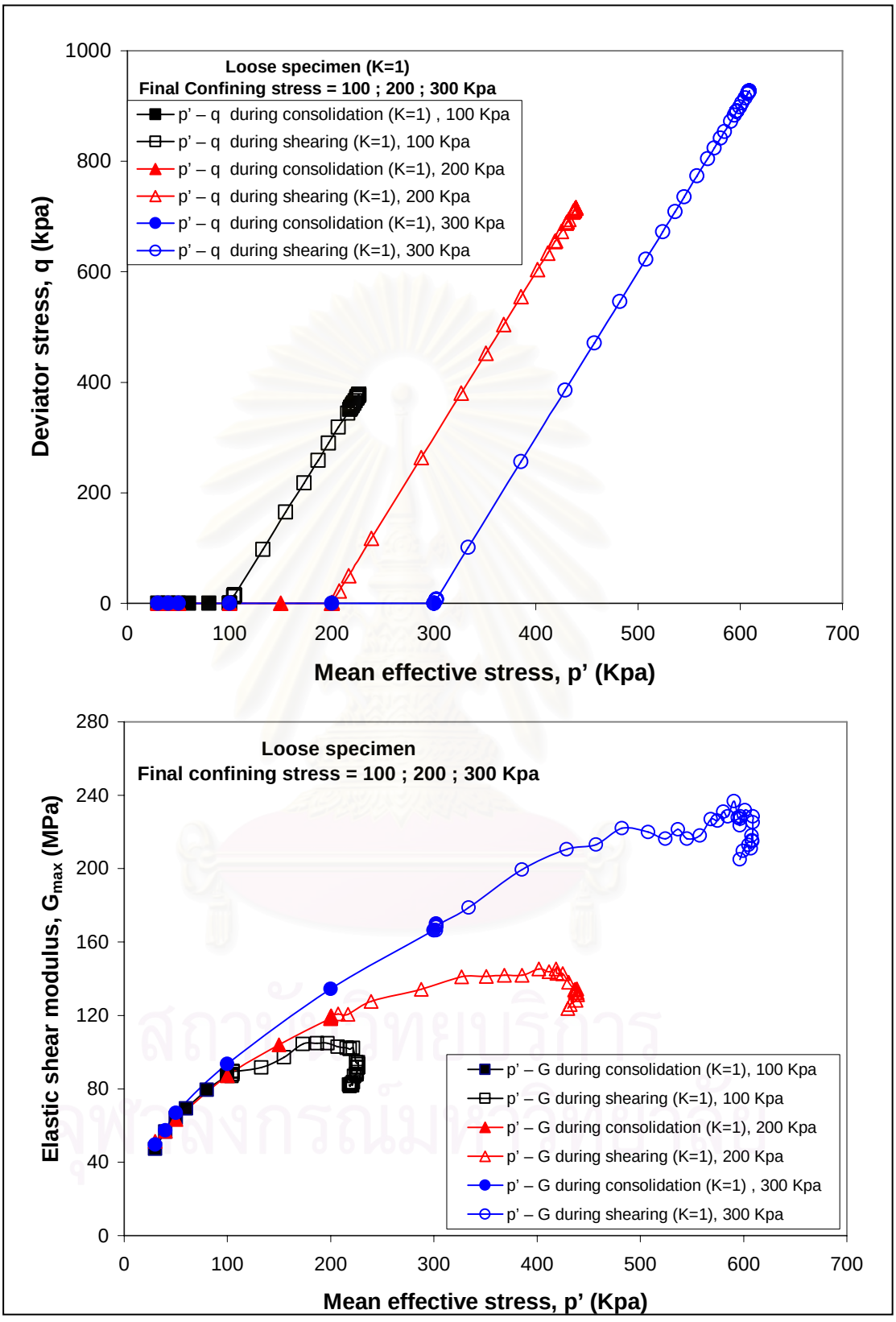

Figure 4.22: Variation of G_{max} against P' during consolidations and drained shearing at final confining stress = 100; 200; 300 Kpa for loose specimens (K=1)

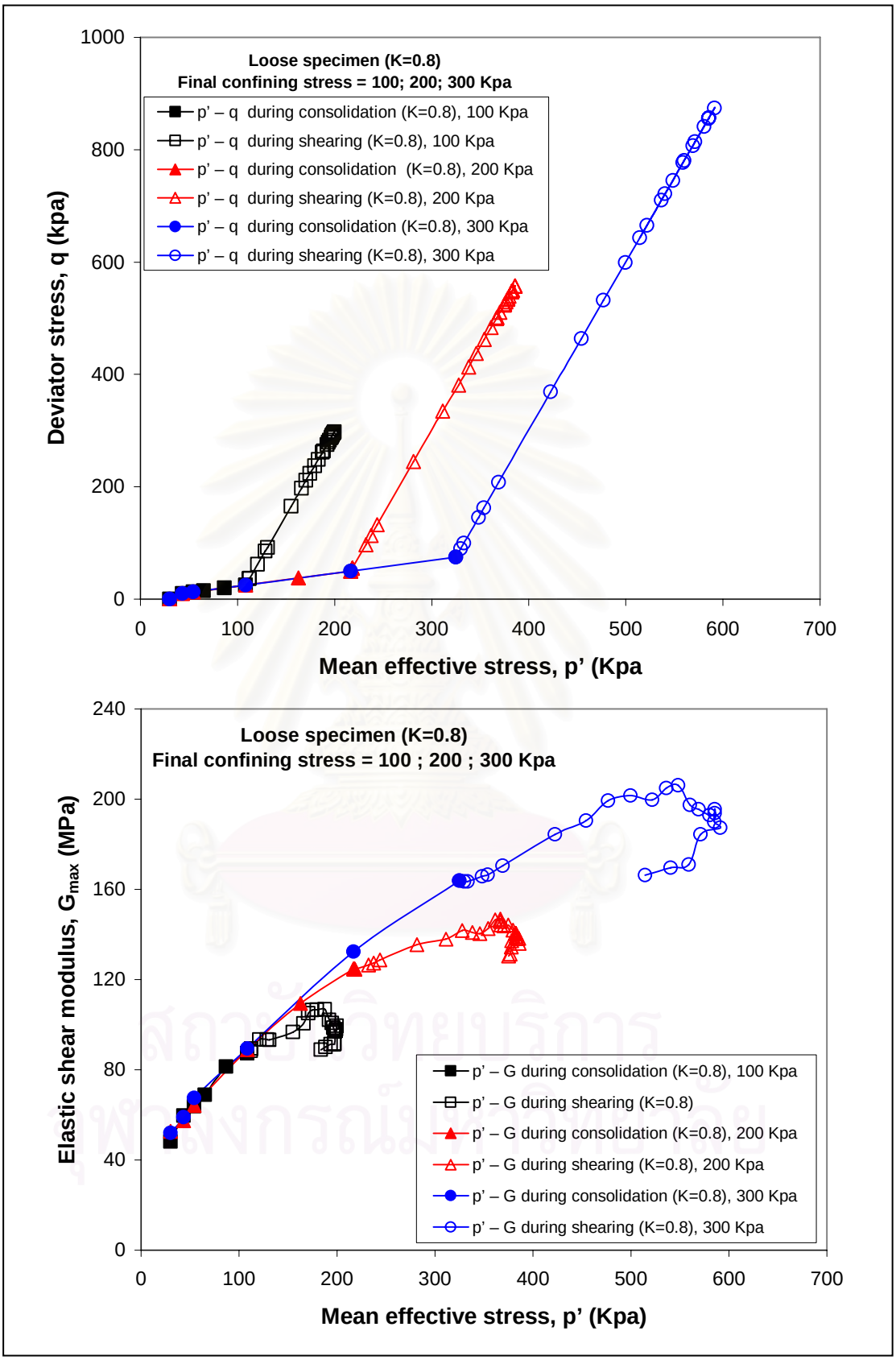

Figure 4.23: Variation of G_{max} against P' during consolidations and drained shearing at final confining stress =100; 200, 300 Kpa for loose specimens (K=0.8)

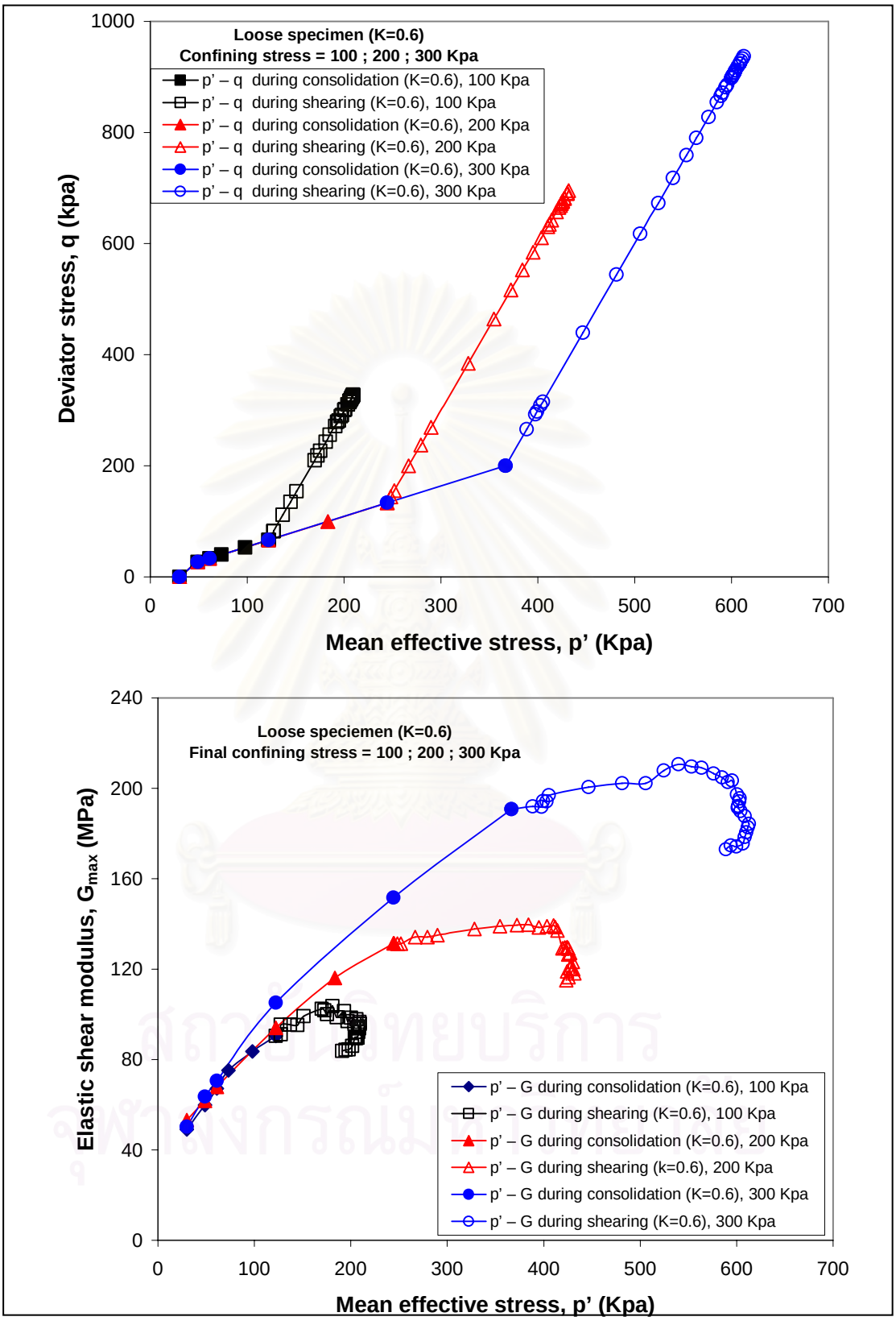

Figure 4.24: Variation of G_{max} against P' during consolidations and drained shearing at final confining stress =100; 200; 300 Kpa for loose specimens (K=0.6)

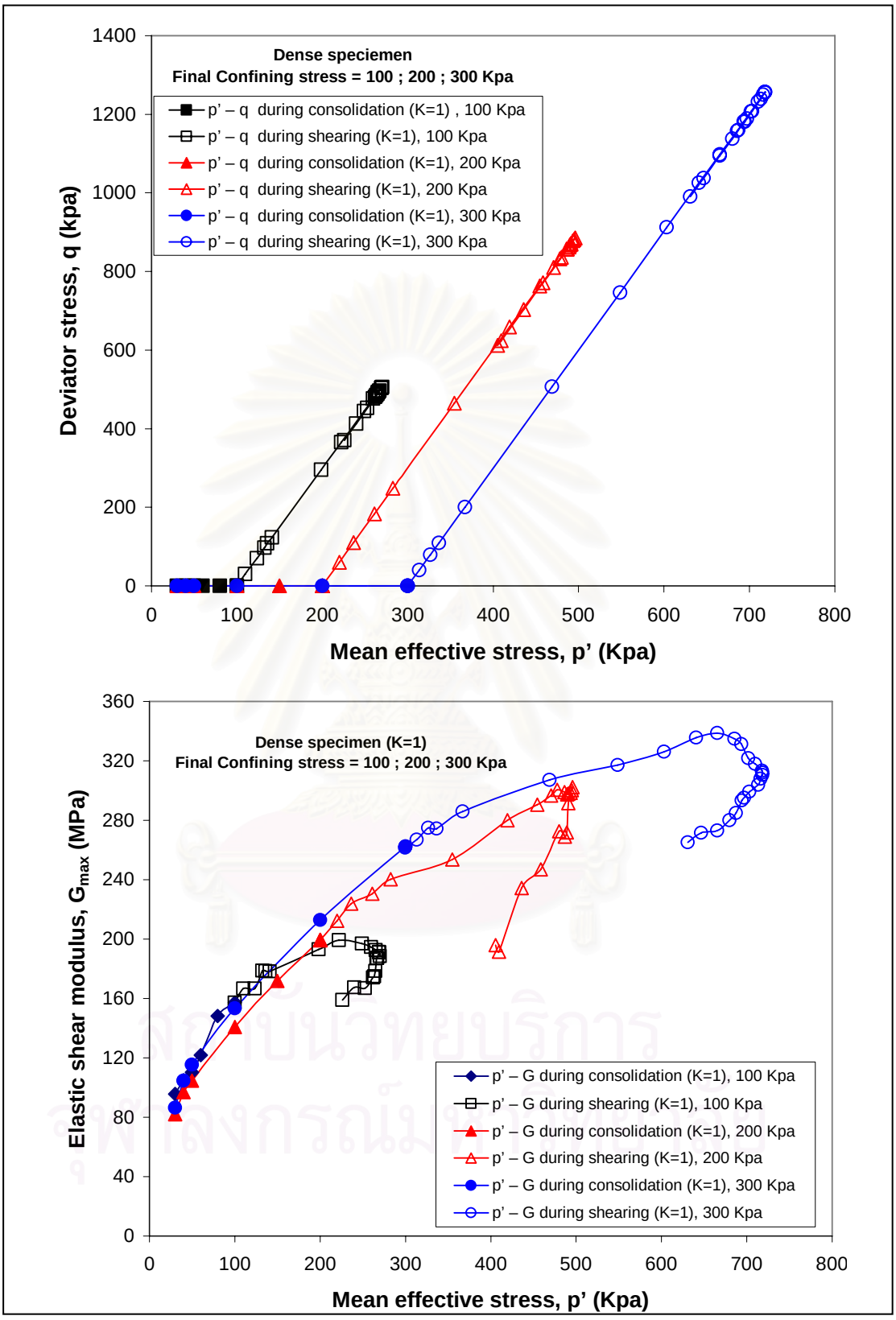

Figure 4.25: Variation of G_{max} against P' during consolidations and drained shearing at final confining stress = 100; 200; 300 Kpa for dense specimens (K=1)

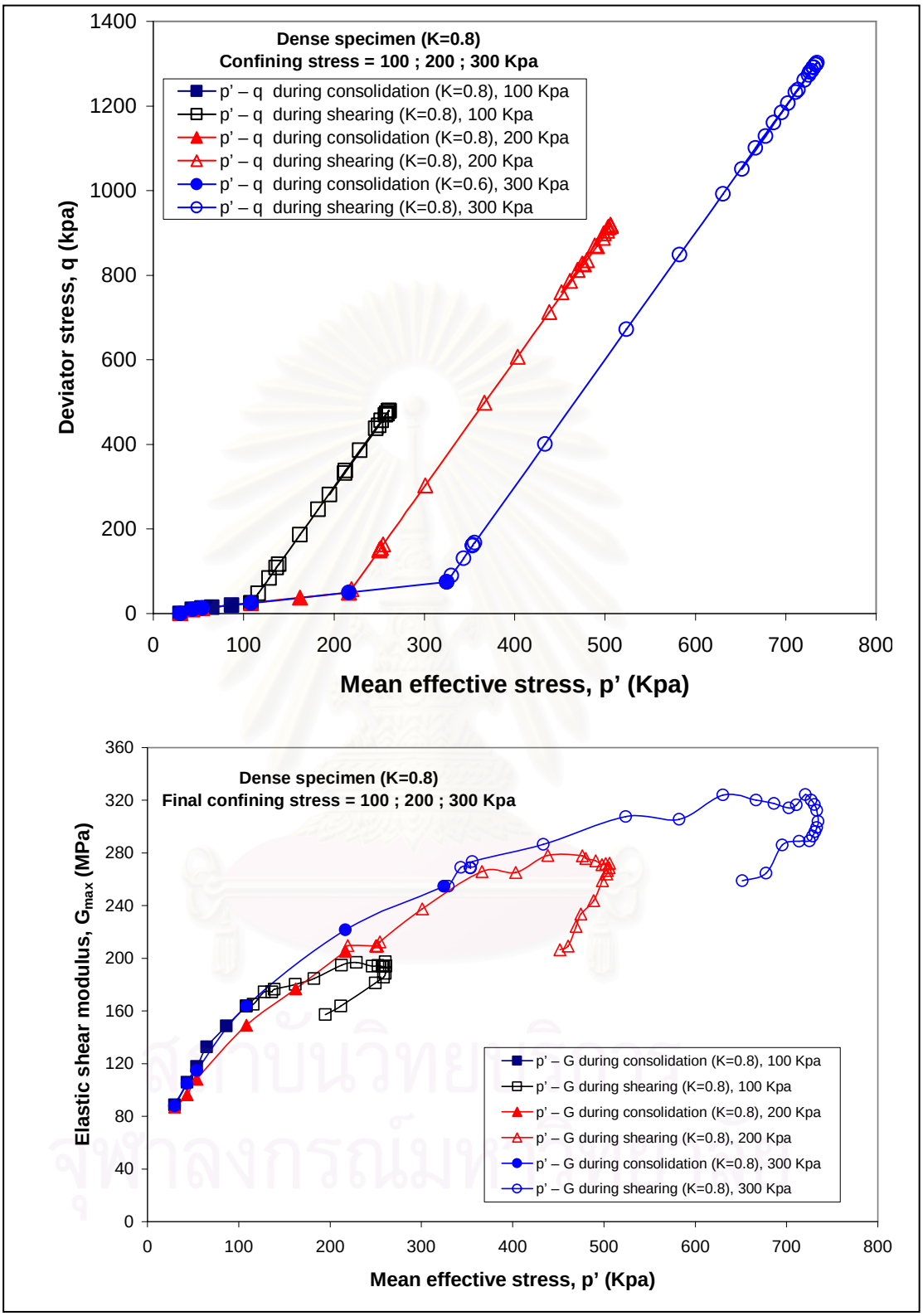

Figure 4.26: Variation of G_{max} against P' during consolidations and drained shearing at final confining stress =100;200; 300 Kpa for dense specimens (K=0.8)

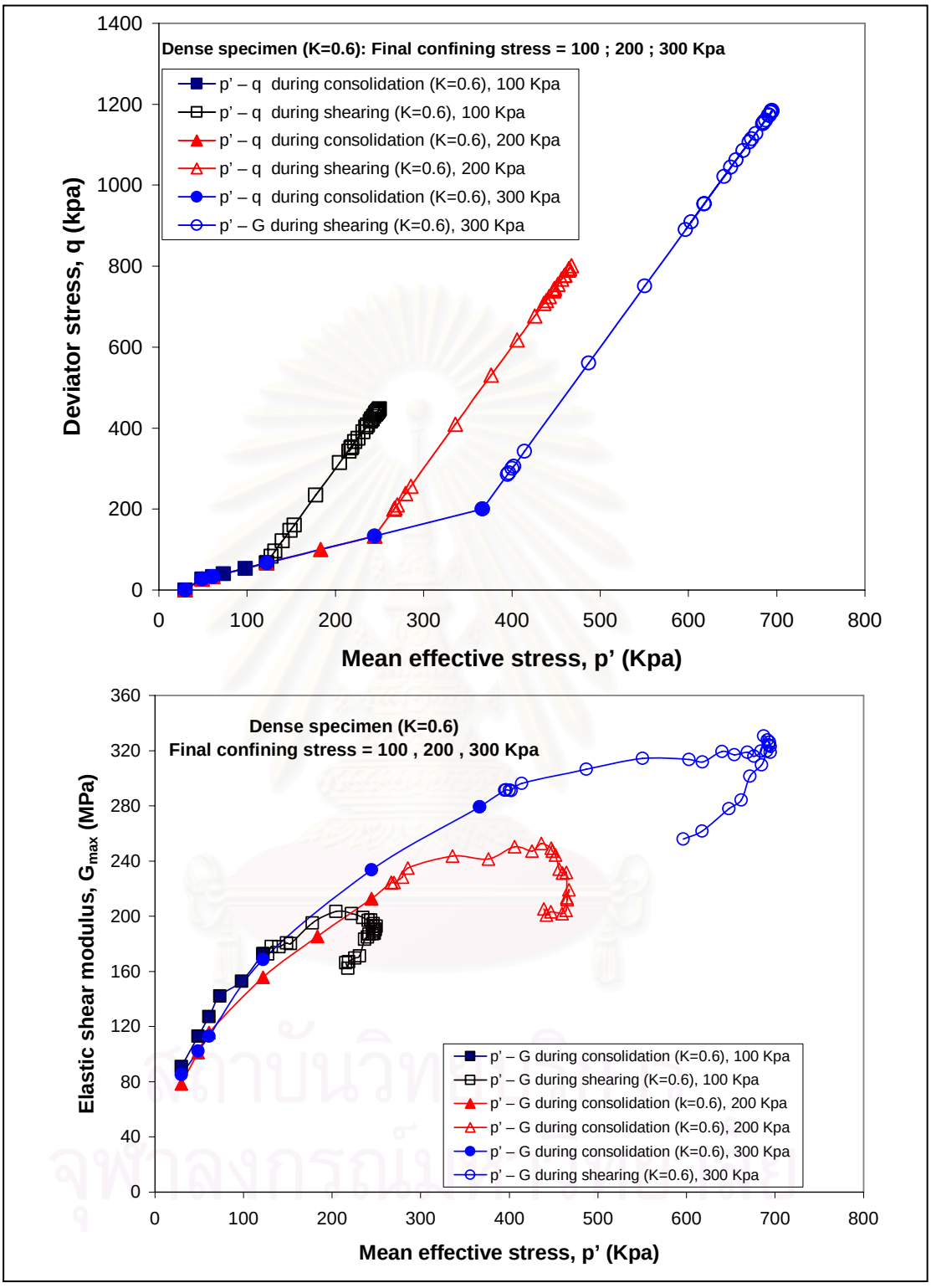

Figure 4.27: Variation of G_{max} against P' during consolidations and drained shearing at final confining stress =100; 200;300 Kpa for dense specimens (K=0.6)

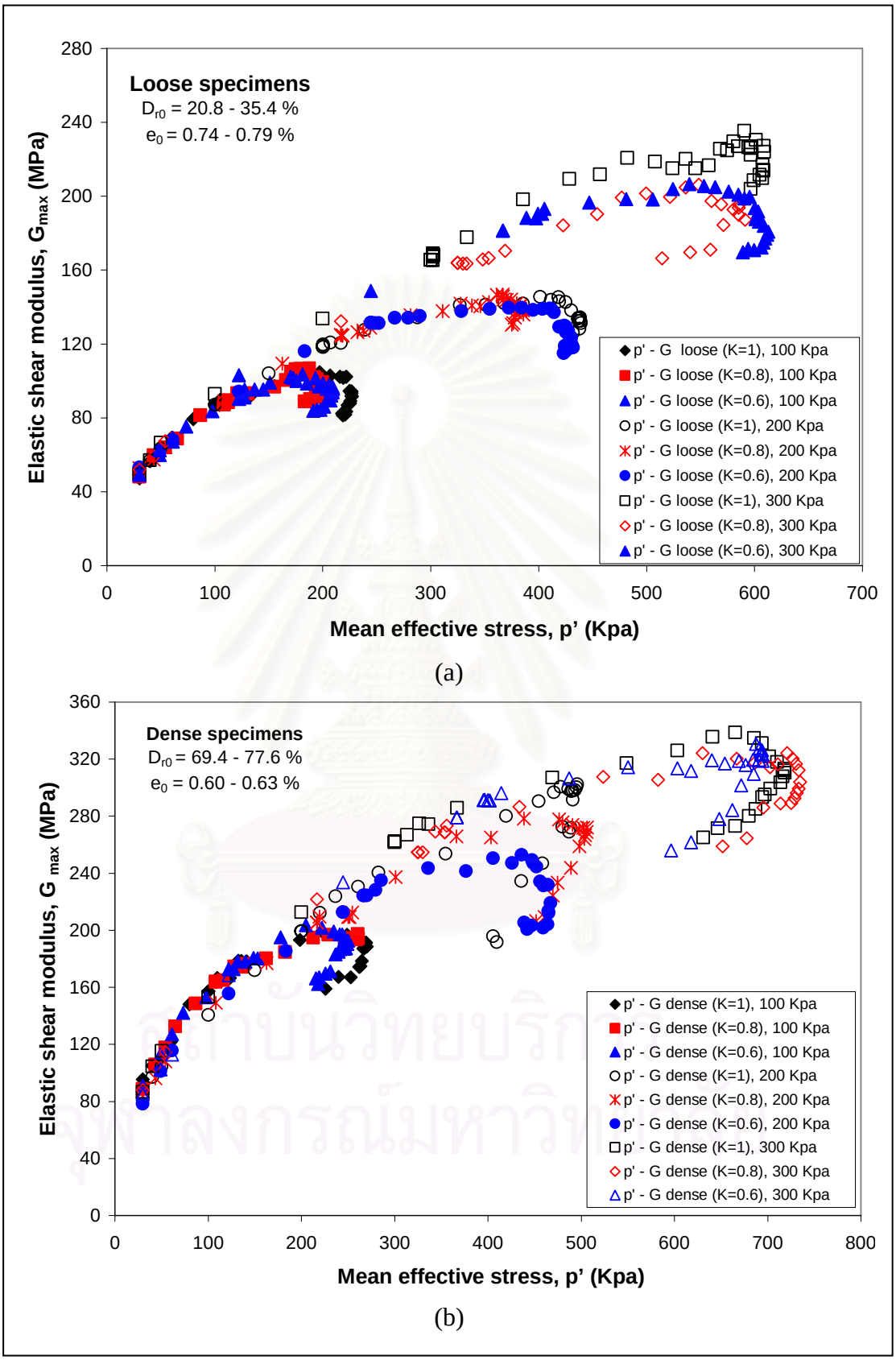

Figure 4.28: Variation of G_{max} against P' during consolidations and drained shearing for all tests: (a) Loose specimens (b) Dense specimens

4.6. Effect of Localization on Elastic Shear Modulus

As mentioned before, the $G_{max} - p'$ paths during shearing almost followed the one obtained during consolidations as long as the specimens were still in the contracting domain. However, when the deviator stresses attained its peak values, the specimens started to dilate. At this time, a decrease of the elastic shear modulus could be observed clearly. This behavior could be seen for all specimens tested. It was believed that the reduction of the elastic shear modulus was caused by the loose zone that occurred at the shearing slip plane of the specimen. The slip plane usually occurs at the angle of $45° + \frac{\phi'}{2}$ with the horizontal plane as shown in Figure 4.29 and Figure 4.30. This loose zone is also known as localization which may be the main factor that slows down the arrival of the shear wave. Therefore, a sudden drop in elastic shear modulus can be noticed obviously. This behavior was also proposed in the previous study by Teachavorasinskun & Amornwithayalax (2002), and Teachavorasinskun & Akkakakun (2004).

When considering the shear wave velocity in the loose zone, it had been shown that the value of shear wave velocity decreased around 50 % of intact zone at the same mean effective stress, or it could be said that whatever the maximal axial strain might be, the reduction of elastic shear modulus was located between 15 % and 25 % from the value of the one before the failure of the specimen under the same mean effective stress. This is because of the shearing phase induced an obvious fabric change inside the specimens.

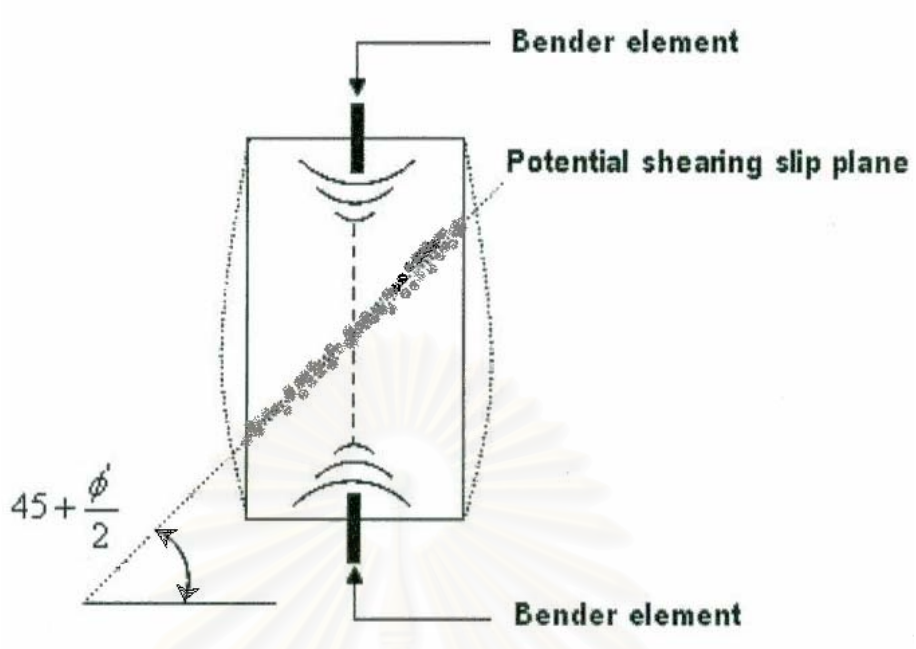

Figure 4.29: Potential failure plane of specimen during shearing

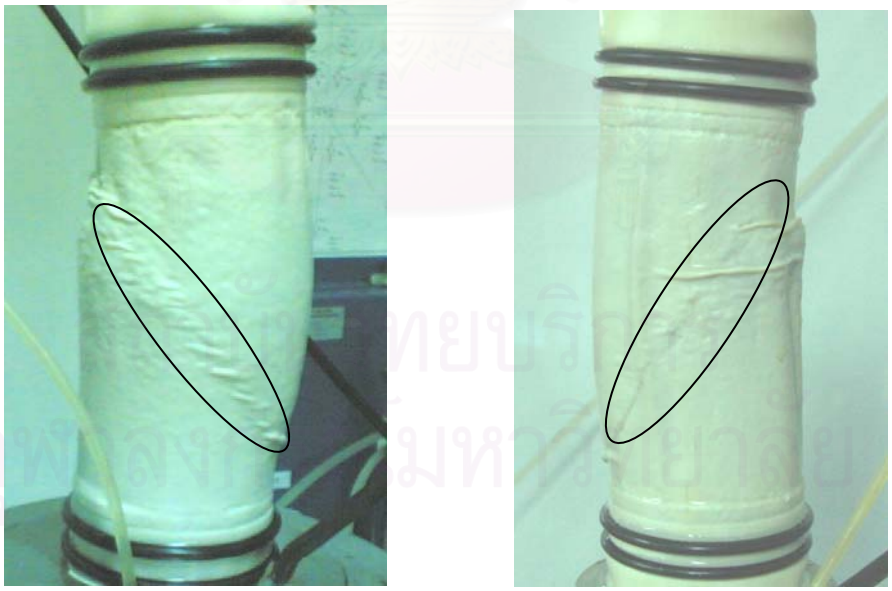

Figure 4.30: The localization (loose zone) in the failed specimens

4.7. Empirical Equations

As explained before in the literature review, it has been recognized that the elastic shear modulus of sand mainly depends on void ratio and effective principal stresses $\sigma_1^{'}$ and $\sigma_3^{'}$. However, during triaxial compression test, the horizontal principal stress is kept constant. Consequently, the elastic shear modulus is expressed as a function of void ratio and mean effective stress $P^{'} = (\sigma_1^{'} + 2\sigma_3^{'})/3$. The void ratio function has been established by many researchers. However, the well known void ratio function suggested by Hardin & Richart (1963) was adopted in this study because it provided the best fitting relationship for the data obtained from this experiment.

The linear regression analysis was used to analyze the available data for establishing the formula of elastic shear modulus. The aim was to create the formula that can represent the variation of elastic shear modulus during consolidation and during shearing before the occurrence of failure plane. Figure 4.32 shows the variation of $G_{\max} / F(e)$ against P' during consolidation together with the data during shearing before specimen failure (contracting domain) for all of the tests in this experimental study. These data were plotted in a logarithmic scale to fit them linearly. The function of void ratio used here was $F(e) = (2.17 - e)^2 /(1 + e)$ because it provided the best fitting of the data. It can be seen that all of the data points fall closely to the straight line. Based on these results, the proposed empirical equation to express the relationship between elastic shear modulus, void ratio and mean effective stress were established as shown below:

$$G_{\max} = 11.03\ F(e)\ (p')^{0.44} \qquad (4.1)$$

where, $G_{\max}$ = elastic shear modulus (Mpa)

p' = mean effective stress (Kpa)

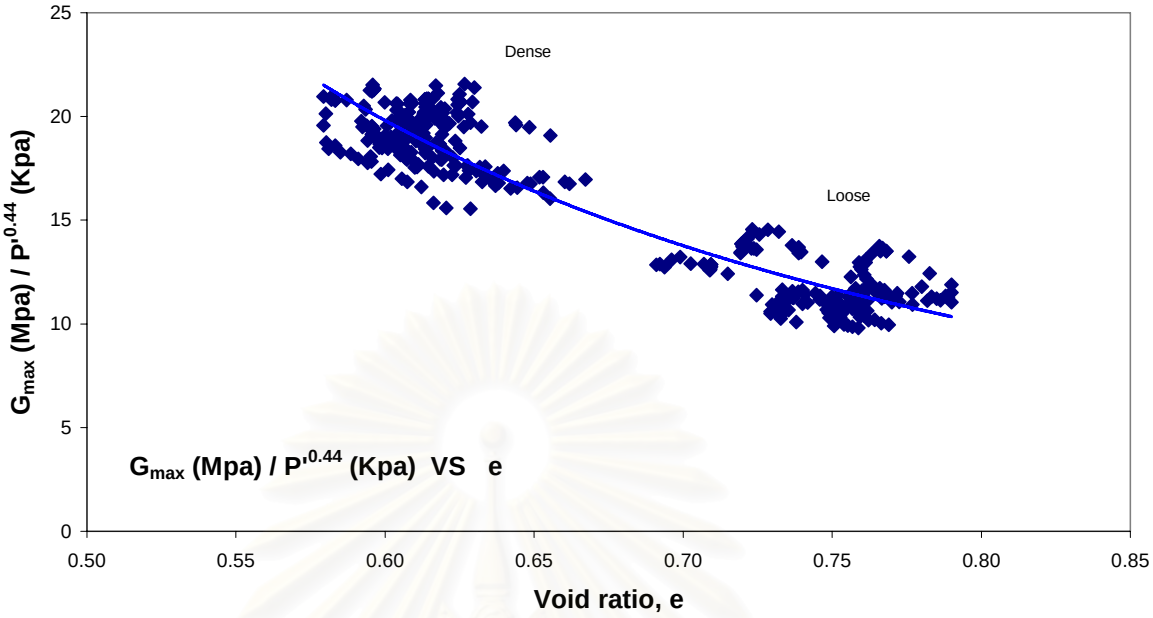

Figure 4.31: Normalized elastic shear modulus versus void ratio

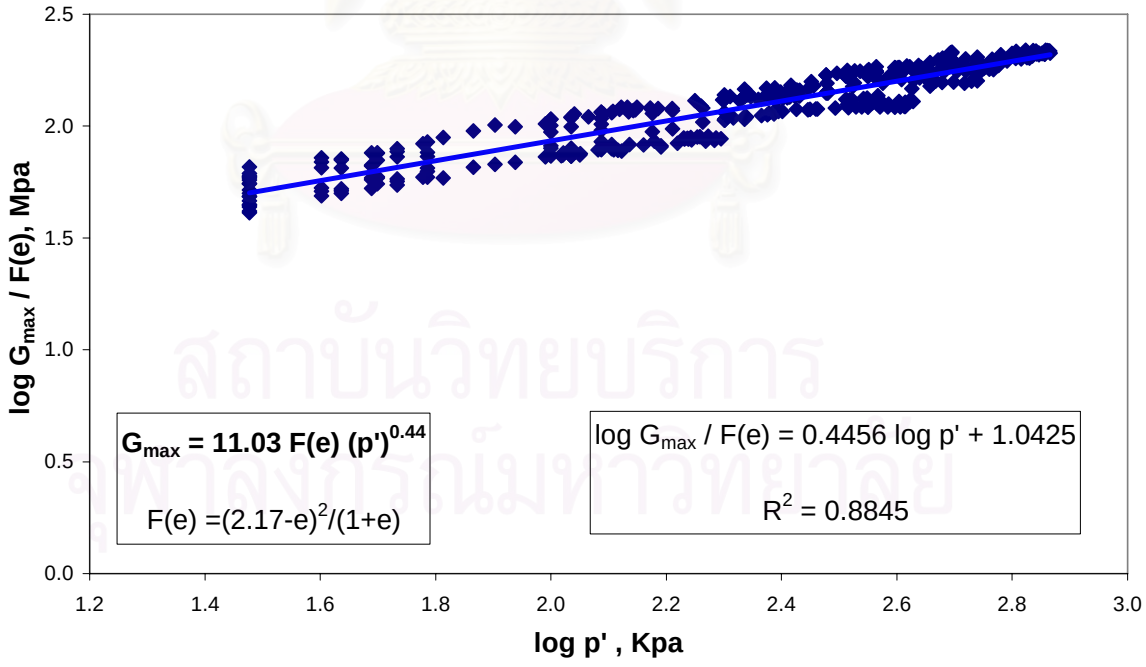

Figure 4.32: Linear regression analysis for developing formula of G_{max} during consolidation and shearing

Figure 4.33 shows a comparison between the values of G_{max} obtained from the measurement of the tests and those obtained from the calculation using empirical equation (4.1). In general, good agreement is seen between measured and predicted G_{max} values. The difference between the values of measured elastic shear modulus and predicted elastic shear modulus is about 7 % for this dataset. It means that this empirical equation is reliable.

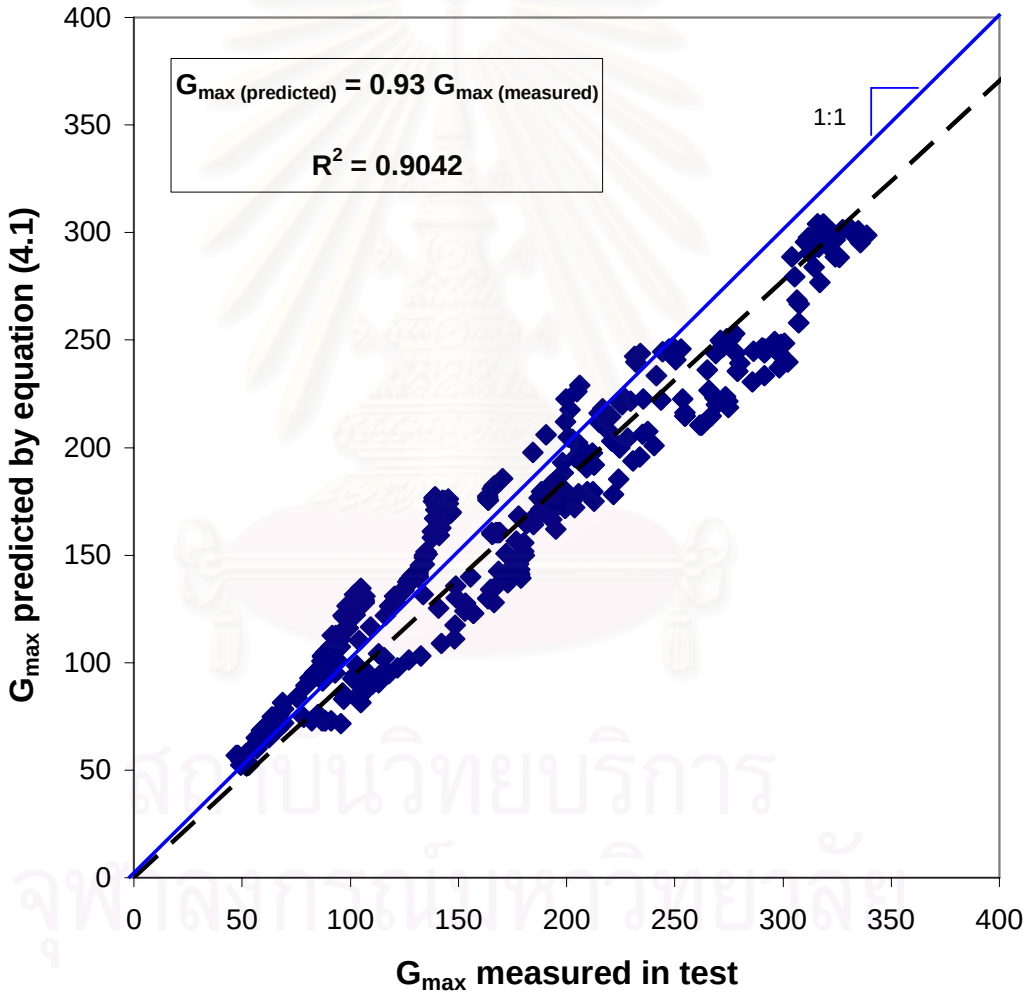

Figure 4.33: Comparison between computed elastic shear modulus using empirical equation and measured elastic shear modulus obtained from laboratory

CHAPTER V

SUMMARY, CONCLUSIONS AND RECOMMENDATIONS

5.1. Summary and Conclusions

The stiffness of soil at very small strain, G_{max}, also known as elastic shear modulus is a useful parameter in geotechnical engineering problems. It is a required parameter for soil dynamic and soil-structure interaction analyses such as earthquake respond analysis, and designs of geotechnical structures subjected to seismic loading. There are many methods to determine G_{max}, whether they are applied in the field or in the laboratory. However, the lab-technique called bender element test was adopted throughout this experimental study because it is non-destructive and relatively easy to use.

The sand sample tested was the poorly graded sand having the maximum void ratio $e_{max} = 0.86$, minimum void ratio $e_{min} = 0.53$, and specific gravity $G_s = 2.65$. In this study, two conditions of specimens were used, i.e. loose specimens with initial void ratio ranging from 0.74 to 0.79, and dense specimens with initial void ratio ranging from 0.60 to 0.63. These specimens were prepared by air-pluviation method.

This research focuses on the performance of bender elements to investigate the effect of the different stress states of consolidations (stress-induced anisotropy) on elastic shear modulus of sands. A number of the isotropically and anisotropically consolidated drained triaxial compression tests were carried out. The results obtained from different tests were compared and the following conclusions were made:

(a) The elastic shear modulus of sand mainly depends on mean effective stress and void ratio. When mean effective stress increase the elastic shear modulus also increase almost linearly.

(b) The variation of elastic shear modulus during consolidation under different consolidation stress ratios shows that the effect of stress-induced anisotropy on elastic shear modulus of sands is available. However, this effect is relatively small.

(c) The paths of elastic shear modulus during drained shearing phase in both isotropically and anisotropically consolidated specimens typically follow the one obtained during consolidation phase. It may be concluded that the effect of deviator stress, q, is also small.

(d) The value of elastic shear modulus still increase during drained triaxial compression test, but just in the contracting domain. When the deviator stress (shear stress) reaches the maximum value (peak), then the specimen start to dilate, and causes the value of shear modulus to decrease significantly. It is believed that this reduction results from localization that occurs at the failure plane of the specimens. It can be said that whatever the maximal axial strain might be, the reduction of elastic shear modulus was located between 15 % and 25 % from the one before the failure of the specimen under the same mean effective stress.

(e) The empirical equation was established based on the experimental results to express the relationship of the elastic shear modulus, mean effective stress, and void ratio of Ping river sand taken from the northern part of Thailand as shown below:

$$G_{max} = 11.03\, F(e)(p')^{0.44}$$

where, G_{max} = elastic shear modulus (Mpa)

p' = mean effective stress (Kpa)

(f) The findings of this experimental study are generally in good agreement with the previous researchers namely Hardin & Richart (1963); Iwasaki., Tatsuoka., and Takagi (1978); Koshuko (1980); Bellotti *et al* (1996); Teachavorasinskun & Amornwithayalax (2002); and Teachavorasinskun & Akkarakun (2004).

5.2. Recommendations

Based on the experience of doing this work the following recommendations can be brought out:

(a) It is suggested that in bender element test, preparation and set-up bender elements with the apparatus is a very crucial step. If this process is not properly done, many problems will happen such as leaking, unclear signal and so on.

(b) It is recognized that the main difficulty in estimating the initial shear modulus is to find the exact travel time of shear wave through the specimen. This difficulty can be minimized by using a modern digital oscilloscope. Therefore, to obtain more accurate estimation of the initial shear modulus, the use of high resolution digital oscilloscope is recommended.

(c) It is recommended to perform the test under different consolidation stress states by using undisturbed sand specimen and Air-pluviated specimen to compare the differences.

(d) It is suggested to perform the triaxial extension test both in isotropic and anisotropic test using the bender elements with varying mean effective stress so that effect of deviator stress could be more clearly evaluated.

(e) It is recommended to measure elastic shear modulus in the vertical and horizontal direction to evaluate the effect of inherent anisotropic on sands

REFERENCES

Amornwithayalak, T. Shear wave velocity in clay during triaxial compression using bender elements. Master's thesis, Civil Engineering, Chulalongkorn University, 2000.

Atkinson, J. H. An introduction to the mechanics of soils and foundations through critical state soil mechanics. England: McGraw-Hill, 1993.

Atkinson, J. H., and Sallfors, G. Experimental determination of stress-strain-time characteristics in laboratory and in-situ tests. Pro. 10th Eur. Conf. Soil Mech., Florence 3, (1991): 915 – 956.

Bates, C. R. Dynamic soil properties measurements during triaxial testing. Geotechnique, 39, 4 (1989).

Bellotti, R., Jamiolkowski, M., Lo Presti, D., and O'Neil, D. Anisotropy of small strain stiffness in Ticino sand. Geotechnique, 46, 1 (1996): 115-131.

Berland. Small is beautiful – the stiffness a small strain. Ninth Laurits Bjerrum memorial lecture, Canadian Geotechnical Journal, 26, (1989): 69 – 76.

Bishop, A. W., and Henkel, D. J. The measurement of soil properties in triaxial test. 2 nd ed. London: Edward Arnold (Publishers) LTD, 1982.

Blewett, J., Blewett, I. J., and Woodword, P. K. Phase and amplitude responses associated with the measurement of shear wave velocity in sand by bender elements. Canadian Geotechnical Journal, 37 (2000): 1348 - 1357.

Callisto, L., and Rampello, S. Shear strain at small strain stiffness of a natural clay under general stress conditions. Geotechnique, 52, 8 (2002): 547 – 560.

Dano, C., and Hicher, P.Y. (2002), Evaluation of elastic shear modulus in granular materials along isotropic and deviatoric stress paths. 15th ASCE Engineering Mechanics Conference, 2002.

Dano, C., Hareb, H., and Hicher, P. Y. Characterization of Loire river sand in the small strain domain using new bender-extender elements. 16th ASCE Engineering Mechanics Conference, 2003.

Dyvik, R., and Madshus, C. Laboratory measurements of G_{max} using bender elements. Proc. Am. Soc. Civ. Engrs Convention, Detroit. New York: American Society of Civil Engineers, 1985.

Hardin, B. O., and Richart, F. E. Elastic wave velocities in granular soils. Journal of the Geotechnical Engineering Division, ASCE, 89, 1(1963): 33 – 65.

Head, K. H. Manual of soil laboratory testing. vol. 3: Effective stress tests. London: Pentech press. (1982): 1013 – 1016.

Holt, R. M. Theoretical Acoustic Anisotropy in Rocks. Lecture notes NTNU, Trodheim, 2000.

Iwasaki, T., Tatsuoka, F., and Takagi, Y. Shear moduli of sands under cyclic torsional shear loading. Soil and Foundations, 18, 1 (1978): 39 – 56.

Jovicic, V., Coop, M.R., and Sicmic, M. Objective criteria for determining G_{max} from bender element tests. Geotechnique, 46, 2 (1996): 357-367.

Jovicic, V., and Coop, M.R. The measurement of stiffness anisotropy in clays with bender element tests in the triaxial apparatus. Geotechnical Testing Journal , GTJODJ, 21, 1 (1998): 3 -10.

Kokusho, T. Cyclic triaxial test of dynamic soil properties for wide strain range. Soil and foundations, 20, 2 (1980): 45 - 60.

Kuwano, R., and Jardine, R. J. On the applicability of cross-anisotropic elasticity to granular materials at very small strains. Geotechnique, 52, 10 (2002): 727 – 749.

Leong, E. C., Yoe, S. H., and Rahardjo, H. Measuring Shear Wave velocity Using Bender Elements. Geotechnical Testing Journal, 28, 5 (2005): 488 - 498.

Lings, M. L., and Greening, P. D. A novel bender/extender element for soil testing. Geotechnique, 51, 8 (2001): 713 - 717.

Mair, R. J. Developments in Geotechnical research: Application to tunnels and deep excavations. Proc. Instn. Civ. Engrs. London , 3 (1993): 27 – 41.

Ng, C. W. W., Leung, E. H. Y., and Lau, C. K. Inherent anisotropic stiffness weathered geomaterial and its influence on ground deformations around deep excavations. Canadian Geotechnical Journal, 41 (2004): 12 – 24.

Roesler, S. Anisotropic Shear Modulus due to Stress Anisotropy. Journal of Geotechnical Engineering Division, ASCE, 105, GT7 (1979): 871 - 880.

Shirley, D.J., and Hampton, L.D. Shear wave measurements in laboratory sediments. Journal of the Acoustic Society of American, 63, 5 (1977): 607 – 613.

Sumaryono. Effect of stress-induced anisotropy on stiffness of clays using bender elements. Master's thesis, Civil Engineering, Chulalongkorn University, 2004.

Teachavorinsinskun, S., and Amornwithayalax, T. Elastic shear modulus of Bangkok clay during undrained triaxial compression. Geotechnique, 52, 7 (2002): 537-540.

Teachavorinsinskun, S., and Akkarun, T. Paths of elastic shear modulus of clays. Geotechnique, 54, 5 (2004): 331 - 333.

Viggiani, G., Akinson, J. H. Interpretation of bender element tests. Geotechnique, 45, 1 (1995): 145 - 154.

Viggiani, G., Akinson, J. H. Stiffness of fine-grained soil at very small strains. Geotechnique, 45, 2 (1995): 249 – 265.

Yamashita, S., and Suzuki, T. Effect of Fabric Anisotropy of a Sand Specimen on Small Strain Stiffness Measured by the Bender element Method. Advanced Laboratory Stress-Strain testing of Geomaterials, ISBN 90 2651 8439 (2001): 317 - 322.

Yu, P., and Richart, F.E. Jr. Stress ratio effects on shear modulus of dry sands. Journal of Geotechnical Engineering Division, ASCE, 110, GT3 (1984): 331 - 345.

Zeng, X., and Ni, B. Stress-Induced Anisotropic G_{max} of Sands and Its Measurements. Journal of Geotechnical and Geoenvironmental Engineering, 125, 9 (1999): 741 – 749.

Zhou, Y.-g., and Chen, Y.-m. Influence of Seismic Cyclic Loading History on Small Strain Shear Modulus of Saturated Sands. Soil Dynamic and Earthquake Engineering, 25 (2005): 341 - 353.

APPENDICES

Soil Testing Laboratory
Grain - Size Analysis

Sample No.	K 1	Project No.	Master Thesis
Location	Chiang Mai Province	Boring No.	
Depth		Date of Test	30/05/2006
Description of Soil	Ping river sand	State of Specimen	
Tested by	Alitking Anongphouth		

[A] Seive Analysis

(1) Mass of total air-dried sample = 1190.50 g
(2) Mass of fraction retained on No.10 seive = 0 g
(3) Percentage of sample retained on No.10 seive = 0 %
(4) Percentage of sample passing No.10 seive = 100 %

Seive size No.	Seive opening (mm)	Mass of seive (g)	Mass of seive+soil (g)	Mass retained (g)	Mass passing (g)	Percent finer by weight (%)
10	2.000	464.92	464.92	0.00	1189.66	99.93
20	0.850	427.64	526.10	98.46	1091.20	91.66
40	0.425	385.52	891.22	505.70	585.50	49.18
60	0.250	366.78	695.89	329.11	256.39	21.54
80	0.180	415.38	506.75	91.37	165.02	13.86
100	0.150	209.12	316.26	107.14	57.88	4.86
200	0.075	342.20	399.53	57.33	0.55	0.05
Pan	-	268.65	269.20	0.55	0.00	0.00

Total mass M_{tot} = 1189.66 g

D_{10} = 0.175 mm C_u = 2.86
D_{30} = 0.3 mm C_z = 1.03
D_{60} = 0.5 mm C_u < 6

USCS: Poorly graded sand

(Medium sand)

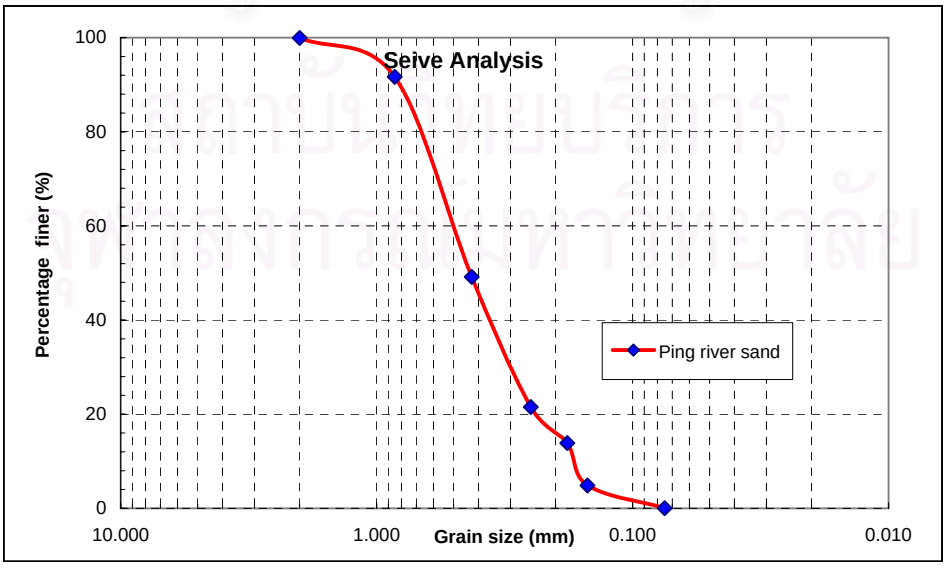

Soil Testing Laboratory
Specific Gravity Determination

Sample No.	K 1	Project No.	Master Thesis
Location	Chiang Mai Province	Boring No.	
Depth		Date of Test	14/06/2006
Description of Soil	Ping river sand	State of Specimen	
Tested by	Alitking Anongphouth		

[A] Calibration Pycnometer

(1) Mass of dry, clean pycnometer, M_p = 173.56 g
(2) Mass of pycnometer + water, M_{pw} = 670.7 g
(3) Observed temperature of water, T_i = 29 °c

[B] Specific Gravity Determination

Test Method used: Oven - dried speciemens
Maximum particle size of test specimen: No. 10 (2 mm)

Determination No.		1	2	3
Mass of pycnometer + soil + water, M_{pws}	(g)	732.85	732.78	
Temperature, T_x	(°c)	29	29.5	
Mass of pycnometer + water at T_x , M_{pw} *	(g)	670.70	670.62	
Evaporating dish No.		1A	1B	
Mass of evaporating dish, M_d	(g)	33.21	33.08	
Mass of evaporating dish + oven - dried soil, M_{ds}	(g)	132.79	132.74	
Mass of solids, M_s	(g)	99.58	99.66	
Conversion factor, K		0.9977	0.9976	
Specific gravity of soil, $G_s = \frac{KM_s}{M_s + M_{pw}(at\,T_x) - M_{pws}}$		2.65	2.65	
	Average	**2.65**		

$$* M_{pw}(at\,T_x) = \frac{\rho_w(at\,T_x)}{\rho_w(at\,T_i)}[M_{pw}(at\,T_i) - M_p] + M_p$$
$$= \frac{0.99582}{0.99597}[670.70 - 173.56] + 173.56$$
$$= 670.62$$

Soil Testing Laboratory
Minimum Index Density and Unit Weight of Solids and Calculation of Relative Density

Sample No.	K 1	Project No.	Master Thesis
Location	Chiang Mai Province	Boring No.	
Depth		Date of Test	17/06/2006
Description of Soil	Ping river sand	State of Specimen	
Tested by	Alitking Anongphouth		

[A] Calibration Mold

(1) Thickness of surcharge base plate, T_p = 1.459 cm
(2) Diameter of the mold, D_m = 15.240 cm
(3) Height of the mold , H_m = 15.519 cm
(4) Volume of the mold, V_m = 2830.894 cm

[B] Minimum Index Density Determination

	Units	Specimen 1	Specimen 2	Specimen 3
Mass of empty mold, M_m	(g)	3505.00	3507.00	3508.00
Mass of mold + soil, M_{m+s}	(g)	7559.00	7524.00	7517.00
Mass of soil, M_s	(g)	4054.00	4017.00	4009.00
Minimum index density, $\rho_{d\,min}$	(g/cm^3)	1.43	1.42	1.42
Average value of $\rho_{d\,min}$	(g/cm^3)	1.42		
Specific gravity of soil, G_s	-	2.65	2.65	2.65
Density of water at 20°c	(g/cm^3)	0.99821	0.99821	0.99821
Maximum index void ratio, e_{max}	-	0.86		

Soil Testing Laboratory
Maximum Index Density and Unit Weight of Solids and Calculation of Relative Density

Sample No.	K 1	Project No.	Master Thesis
Location	Chiang Mai Province	Boring No.	
Depth		Date of Test	17/06/2006
Description of Soil	Ping rever sand	State of Specimen	
Tested by	Alitking Anongphouth		

[A] Calibration Mold

(1) Thickness of surcharge base plate, T_p = 1.459 cm
(2) Diameter of the mold, D_m = 15.240 cm
(3) Height of the mold , H_m = 15.519 cm
(4) Volume of the mold, V_m = 2830.894 cm

[B] Maximum Index Density Determination

This test used dry method and vibratory table (ASTM D 4253)

	Units	Specimen 1	Specimen 2	Specimen 3
Mass of empty mold, M_m	(g)	3505.00	3507.00	3508.00
Mass of mold + soil, M_{m+s}	(g)	7559.00	7524.00	7517.00
Mass of soil, M_s	(g)	4054.00	4017.00	4009.00
Difference in elevation between top surfaces of mold and soil (Bottom surface of surcharge base plate), H	(cm)	2.50	2.74	3.08
Volume of the dry soil, V_s	(cm^3)	2375.22	2331.26	2269.97
Maximum index density, $\rho_{d\,max}$	(g/cm^3)	1.71	1.72	1.77
Average value of $\rho_{d\,max}$	(g/cm^3)	1.73		
Specific gravity of soil, G_s	-	2.65	2.65	2.65
Density of water at 20°c	(g/cm^3)	0.99821	0.99821	0.99821
Minimum index void ratio, e_{min}	-	0.53		

BIOGRAPHY

Alitking Anongphouth was born in Vangviang district, Vientiane province, Lao P.D.R., in 1982. He received his B.Eng in Civil Engineering from National University of Laos, Vientiane Lao P.D.R. in 2004. He continued his Master's Degree in Civil Engineering, Chulalongkorn University, Bangkok, Thailand in 2004 under AUN SEED Net – JICA scholarship. His research is Geotechnical Engineering.